A MATHEMATICAL ANALYSIS OF THE SUBSIDENCE IN THE LONG BEACH - SAN PEDRO AREA

by

G. D. McCann

Professor of Electrical Engineering

and

C. H. Wilts

Assistant Professor of Applied Mechanics

California Institute of Technology
Pasadena, California
November 1951

Charles R. Dickens

A MATHEMATICAL ANALYSIS OF THE SUBSIDENCE IN THE LONG BEACH - SAN PEDRO AREA

by

G. D. McCann

Professor of Electrical Engineering

and

C. H. Wilts

Assistant Professor of Applied Mechanics

California Institute of Technology
Pasadena, California
November 1951

TABLE OF CONTENTS

LIST OF FIGURES

List of Figures

List of Figures

List of Figures

List of Figures

LIST OF TABLES

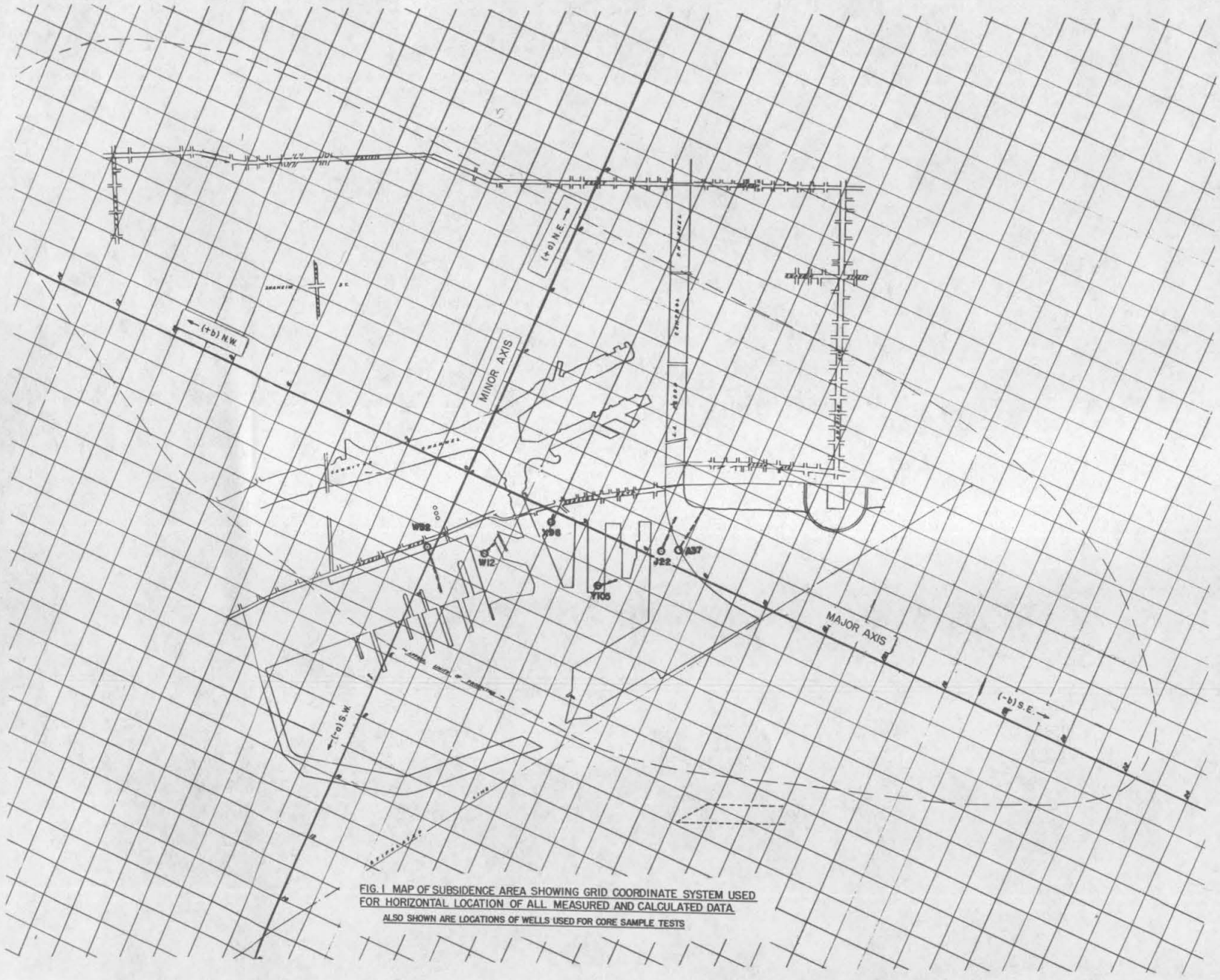

FIG. 1 MAP OF SUBSIDENCE AREA SHOWING GRID COORDINATE SYSTEM USED FOR HORIZONTAL LOCATION OF ALL MEASURED AND CALCULATED DATA.

ALSO SHOWN ARE LOCATIONS OF WELLS USED FOR CORE SAMPLE TESTS

SUMMARY

This report presents the significant results from a mathematical study of the subsidence in the Long Beach area. The work, begun in December 1949 at the request of Mr. M. D. Hughes, Chief Petroleum Engineer, the Petroleum Division of the Long Beach Harbor Department, has been in progress for two years. During this period a large volume of physical data pertinent to the subsidence phenomena has been made available and analyzed. Additional tests suggested by the mathematical analysis have been instigated by the Petroleum Division so that a well integrated program of research has been brought to bear upon this problem.

The important results of the mathematical study are contained in the five sections of the main body of the report. They are summarized here to emphasize the points of greatest interest.

The Introduction lists the physical data available for the analysis including the subsidence measurements, the geological structure and the oil pumping time history. To provide a method of identifying all points in the subsidence bowl, a coordinate system has been established which is shown in Figure 1.

The next section, The Mathematical Model, discusses the basis for choosing a three dimensional semi-infinite, uniform, isotropic elastic medium for the model. This study has resulted in the development of a new computing technique whereby solutions can be obtained for the motions and stresses developed in such a medium under the action of perfectly general distributions of subsurface disturbance forces designated as "tension centers" and "vertical pincers". New analytical formulae were derived for single sets of these symmetrical disturbance forces. The derivations are given in Appendix I and the equations are summarized in Figures 3 and 4. General solutions to these equations are contained in Figures 5 through 9. The machine computing technique developed for integrating general distributions of such disturbance forces, to represent actual conditions in the subsidence area, is discussed in Appendix II.

In the third section, Use of Models to Fit Surface Motion, are described preliminary studies on the properties of solutions using arbitrary distributions of disturbance forces to fit the measured surface motion. Here it is pointed out that many solutions could be found which would provide a perfect fit to the vertical motion at only one plane, such as the surface. The validity of any one model solution must be determined from the accuracy with which it also fits other parts of the motion and such stress conditions as can be determined. The "vertical pincers" model was developed to satisfy some of the concepts of Prof. Grant who envisioned the phenomena as subsidence of an elastic plate through the compaction of the underlying oil bearing sands which were considered by him as incapable of supporting shear stress. The manner in which distributions of the two types of forces, as chosen to accurately fit the vertical surface motion, also fit the horizontal surface motion, vertical motion at the bottom of the overburden and the conditions of shear failures in certain limited regions is studied in detail. It is found that in this

respect the "tension center" model fits all such data to the accuracy with which they can be measured while the "vertical pincers" model fits none of them. The more important results of this are contained in Figures 15 through 20 which lead to the conclusion that only the "tension center" model should be given further consideration.

In this phase of the study the need for obtaining data on average elastic parameters for the earth and soil shear resistances was emphasized and such data were obtained from a core sample test program set up by the Petroleum Division.

To provide a final method of testing the model and a basis for predicting future conditions from a knowledge of proposed future oil pumping schedules, it is essential to be able to determine a proper distribution of the disturbance forces from a knowledge of the conditions in the oil sands. This is discussed in the section Direct Calculations from the Pressure Drop in the Oil Bearing Sands. The only comprehensive data so far available on oil sand conditions are their location, thickness and the oil pressure drop time history. A method of directly converting the distribution throughout the region of the product of the oil sand thickness and oil well pressure drops (ΔPxT) into an appropriate distribution of "tension centers" is derived in Appendix II and used in this section for a general study of results for the years 1945 through 1951. Many calculations were made at numerous points throughout the bowl of subsidence with the very significant results summarized in Figures 25 through 28. Here it is seen that actual subsidence is related to the supposed source of the subsidence, by an essentially single valued function. Although there is a non-linear relationship whose source is not yet adequately established, a reasonable method of directly calculating expected motions and stresses from a given (ΔPxT) distribution is thereby provided.

The remarkable correlation (as shown in Figures 29 through 38) between the actual subsidence measurements so far made and those calculated from the respective (ΔPxT) distributions leaves little doubt but that the extraction of oil is the major cause of the subsidence.

This phase of the program is subject to further study which requires certain additional physical data. In lieu of this the method has been tentatively used to investigate the expected results from certain proposed future pumping schedules in the last section of the report, Study of the Effects of Future Pumping Schedules. These include possible additional well shear failures and excessive surface stress conditions which might develop as early as 1951 and 1952 and the general results to be expected from two proposed ultimate pumping schedules. A complete and concise summary of these results is contained in Figures 39 through 66 for expected vertical and horizontal surface motion, horizontal shear stresses and their expected consequences. Examination of Figures 55 through 66 shows that by 1951 and 1952 danger areas are developing to the northeast along the minor axis where well shear failures can be expected. This has now been confirmed by actual failures in this region. The proposed ultimate pumping schedules indicate a marked extension of these danger areas to the southeast where a serious problem of well failure and surface stress conditions is indicated.

The ability to correlate such a comprehensive mathematical analysis with the important physical measurements being conducted by the Harbor

Department has opened up many new concepts of the subsidence problem. Certain of these are as yet incomplete and not fully understood. Further physical data must be obtained and correlated with mathematical studies. In this connection it is considered particularly important to pursue the following types of physical studies.

(1) The vertical surface motion measurements should, of course, be continued and correlated with the model calculations.

(2) It is of particular importance to make every practical effort to obtain more accurate horizontal surface motion measurements to provide further verification of the mathematical model.

(3) A continuation of the "collar count" measurements would also provide further checks on the model through the oil bearing sand compaction data which it provides. In this connection it is important to conduct a thorough mathematical investigation of the effect of the lower terminal zone.

(4) More data are needed on the physical properties of the over burden including its elastic parameters and horizontal shear resistances.

(5) Similar data are required on the oil bearing sands for which very little is now known.

It is only through a determined effort to thoroughly correlate such physical measurements with the mathematical model that the reliability of such a method for predicting future events can be determined.

INTRODUCTION

In December 1949, at the request of Mr. Hughes, an initial study was instigated to determine whether or not it would be feasible to set up a practical method of mathematical analysis as an additional approach to the study of the subsidence problem and its related effects. At that time it was not known what degree of complexity was required for the mathematical treatment in order to produce meaningful results. It was not clear whether sufficient data were available on the motion in the subsidence area and on the physical properties of the soil in regions of importance. Other questions to be answered pertained to the type of information that might be gained from such analyses. Would the calculations be limited to surface motions only or could a method of solution be developed which would permit calculation of the subsurface motions and stresses?

The subsidence constitutes a serious problem for three reasons. Vertical subsidence at the surface is lowering large areas to an elevation well below the mean high tide level; thus requiring diking and rendering uncertain the proper elevation for the harbor docks. Horizontal surface motion gives rise to stresses and in some cases failures of such surface structures as pipelines, railroads, and building foundations. Internal soil shear stresses have resulted in failure or local slippage along horizontal planes which renders existing oil wells inoperative. Thus the physical data of greatest interest are the surface motion (both horizontal and vertical) and the horizontal shear stresses within the earth. Since some approximate data exists on compaction in the oil bearing sands, subsurface vertical motion is also of interest.

The information initially available for this study consisted of the following:

(1) Detailed measurements of the vertical surface subsidence from 1945 to the present. Since the subsidence has become a serious problem, very comprehensive surveys to measure surface motion have been initiated. It is unfortunate but to be expected that few accurate bench marks would be available that antedate the subsidence. As a result of this, the recent data is most accurate with respect to differential motion rather than total motion. Nevertheless, great care had been taken to provide the best estimates of total subsidence over the entire region for the years 1945, 1947, 1949 and subsequently for 1950 and 1951.

(2) Horizontal motion data for a very limited number of points. This number is unfortunately so small that it is impossible to form a complete picture of motion in the entire subsidence region.

(3) Detailed information on the general character of the geological structure of the region involved; the location and dimensions of the oil bearing strata being pumped; the location of all natural faults and recent local faults directly attributable to the subsidence.

(4) Oil well collar counting studies have provided important information regarding subsurface compaction. These studies involve systematic measurements of the lengths of pipe sections by means of electromagnetic instruments lowered into wells on the end of a cable. If the pipe has been "seized" by the soil, compaction of the surrounding earth results in compression of the pipe. Inasmuch as the pipe will resist compression, and may be imperfectly bound to the soil, these measurements indicate lower limits for the actual soil compaction. It is possible that the compaction exceeds the amount indicated by these studies. In any case these studies have shown conclusively that substantial compaction has taken place in certain oil-bearing sands, and that very little can be observed elsewhere.
(5) The time history of the pressure drops in the oil-producing zones with the progressing pumping schedule gave some promise of providing the additional information required for directly calculating the magnitude of the subsidence phenomena from the supposed source producing the disturbance forces.

No data were initially available on the physical properties of the subsoils. The magnitudes of the necessary soil parameters required for direct numerical calculations of actual motions and stresses to be expected from given disturbance forces were not known. It was thus apparent that the initial analytical studies would have to consist of a series of trial fits to the measured surface motions for a range of assumed physical properties of the subsoil and some arbitrarily chosen disturbance forces.

DESCRIPTION OF THE SUBSIDENCE REGION

To provide an accurate basis for correlating all calculations with the physical measurements in the subsidence area, the coordinate system shown in Fig. 1 was established. This figure shows a coordinate, or grid system superimposed on a map of the subsidence area. Since the subsidence has a form approximating an ellipse it was natural to establish the coordinate system with its origin at the center of subsidence and the two coordinate axes along the major and minor axes of the ellipse. As shown in Fig. 1, the coordinates have been marked off in 1000 foot grids with distances parallel to the minor axis designated by the coordinate (a) and those parallel to the major axis by the coordinate (b). Positive (a) is to the northeast and positive (b) to the northwest. Thus a point located 4000 feet northeast (parallel to the minor axis) and 6000 feet southeast (parallel to the major axis) would be defined as the point (a = +4, b = -6) on the grid.

Also shown in Fig. 1 are the locations of the wells from which core samples were taken for the tests made by Prof. Converse and which will be discussed later.

This coordinate system serves to locate all points on any horizontal plane. The two planes of greatest interest are the surface (where it is desired to define the surface vertical and horizontal motions) and an arbitrary

plane in the central region of the oil bearing sands which will be used for defining the location of the analytical "disturbance forces" used in the calculations and the data pertinent to the oil bearing zones which must be correlated with them. As will be discussed later, the coordinate grid is also used to locate the points at which the horizontal shear calculations have been made at various depths below the surface together with such related measurements as were obtained from the core sample tests and to locate the observed failures resulting from the actual stresses.

LOCATION OF THE OIL BEARING SANDS

Fig. 2 shows a cross-section of the geological structure as taken along the minor axis of Fig. 1. This single profile is sufficiently typical to describe the important features pertinent to the development of a mathematical model. The principle oil bearing sands involved in the pumping schedule lie in the Tar, Ranger, Upper Terminal and Lower Terminal Zones shown in this figure. From the well collar counting measurements which have been conducted it has been ascertained that practically all of the compaction associated with the subsidence has occurred in the Tar, Ranger, and Upper Terminal Zones. This indicates that the primary source of the disturbance centers in these three zones although some very small compaction is indicated in the Lower Terminal Zone. For this reason it was considered desirable to study the two general regions separately and to first concentrate on calculations which would assume the upper three zones as the source of the disturbance. Referring to Fig. 2 it is therefore seen that the compaction is occurring in a region whose vertical dimension is about 1200-1400 feet centered at a depth of about 3000 feet. Within this region the actual thickness of the oil bearing sands amounts to a total maximum of about 600 feet near the center of subsidence and tapers off in all directions from the center. Approximate thickness of the oil bearing sands is given in Table I.

THE MATHEMATICAL MODEL

The computation of earth motion due to known forces is very difficult for two principal reasons, the boundary conditions are difficult to handle mathematically and the earth does not behave precisely like an elastic medium. A further difficulty is encountered when motion over a physically large region is involved, for in addition lack of uniformity is encountered. This lack of uniformity arises in some cases because of the existence of strata with different composition, and also because the properties of a given material vary with the consolidation pressure which in turn increases with depth. The most serious of these difficulties is the failure of the earth to behave like an elastic material, for this failure defies accurate analytical description.

Extensive consideration was given to the expected physical properties of the soil both by the authors alone and in consultation with engineers of the Long Beach Harbor Department and with various soil mechanics and applied mechanics experts including Professors Frankel, Housner, Hudson, Converse and MacNeal. This led to the definite conclusion that the only physical model which could logically describe the general properties of the soil and be amenable to mathematical solution was one of an elastic material of semi-infinite extent (i.e. extending from the earth's surface downward). Although in fine detail the soil is very heterogeneous with adjacent strata of widely differing structure, the soil properties in the region involved appeared remarkably uniform in gross character with at least no evidence of significant variation with horizontal location.

This coupled with the general lack of knowledge about the soil mechanics of this particular region led to the conclusion that the mathematical model should be based upon a uniform isotropic elastic medium of semi-infinite extent. The additional idealization implied above is that the elastic properties of the earth do not vary with depth. It is possible that this simplification can be avoided, but it is certain that the solution to the problem would be much more difficult. Even for the uniform case, solutions could not be found in the literature.

The calculations to be presented are also based upon the assumption that in some way the removal of oil from the deep-lying strata gives rise to internal stresses which are responsible for the motion of the surrounding earth. As can be seen in Fig. 2, these strata lie so deep with respect to the extent of the oil-bearing area that one probably cannot regard the problem as the "slumping" of a thin cover plate as material is removed from below. It is reasonable to expect that only a complete 3-dimensional analysis can give results which fit the observed facts. Previous and important work by Carrillo in connection with the investigation of the subsidence by the Stanford Research Institute[1] had led to the development of an analytical solution for the surface motion of a uniform, isotropic, semi-infinite elastic medium under the action of a

1 See list at the end of the text for all numbered references.

simple symmetric set of subsurface forces known as a "Tension Center" or "Tension Sphere". This therefore formed a starting point for setting up a mathematical procedure which has now been greatly expanded to the calculation of soil surface and subsurface motions and stresses for not only a variety of such simple symmetrical sets of subsurface forces, but also for a perfectly general distribution of such sub-surface forces as may be required to adequately simulate the actual effects of the oil pumping program.

Only two models for the internal disturbance field have been extensively investigated. One is of course Carrillo's "Tension Center" discussed above. It consists in detail of a spherical region over which the outward pressure is reduced (by virtue of the oil removal). Mathematically speaking, one assumes a spherical boundary over which a uniform tension acts. The second model consists of a pair of equal vertical pressures acting in opposite directions a short distance apart. For mathematical convenience, two colinear opposite forces are postulated an infinitesimal distance apart, but the product of force times separation distance is kept finite. This system of forces has been appropriately called a "vertical pincer". Diagrams of these two systems are shown in Figures 3 and 4.

SYMBOLS FOR MATHEMATICAL TREATMENT

As shown in these figures, a consistent set of symbols is used throughout this report to represent motion and stress within the earth. Vertical motion (subsidence) is denoted by the symbol (w). If this motion is at the surface ($z = 0$), a subscript "zero" is added (w_o). Horizontal motion is represented by the symbol (u), and (u_o) denotes motion at the surface. Generally speaking the symbol for shear stress (τ) should employ two subscripts to denote the inclination and direction, but since the horizontal shear stress is the only one of interest, a single subscript to indicate direction is used when direction is specified. The depth of the disturbance force is designated by (h).

THE SUBSIDENCE EQUATIONS

In the development of the subsidence equations attention was focussed on vertical and horizontal motion and horizontal shear stress, since as was discussed earlier, these were the principle quantities of interest. The detailed derivation of the equations is given in Appendix I. It is sufficient to remark here that all equations were derived by two completely different methods to insure their correctness. Only one of these methods is used in the appendix although the other is briefly described. The equations are rather long and are not reproduced here but are summarized in Figures 3 and 4.

A complete picture of the nature of the solutions is given in Figs. 5 through 9. In the first of these is shown the manner in which

vertical and horizontal surface motion varies with distance from the tension center location. Fig. 7 shows the vertical motion at several depths below the surface. The horizontal shear stress for a tension center is shown in Fig. 8, again for several depths below the surface. It will be noted that the maximum stress increases steadily as depth increases, and that the point of maximum stress becomes closer to the vertical line above the tension center. Similar results for the vertical pincer are shown in Figs. 6 and 9.

PHYSICAL CONCEPTS

It is important to give more consideration to the physical concepts implied by the different mathematical models. One of the first points to observe is that a somewhat unrealistic model for disturbance forces may give useful results. If the oil-bearing region proved to be indescribable by equations of elasticity, a model which fits the facts just above the oil-bearing sands and at the surface can still be used for computations of conditions above the oil-bearing region, even though similar calculations for conditions within the oil-bearing regions may be meaningless. On the other hand it would be highly desirable, if possible, to use a model in which the disturbance forces can be correlated with the physical data in the oil-bearing sands.

The physical model which seems intuitively to be most plausible is the tension center. It is true that in this subsidence problem, the disturbance forces are confined to realively thin strata of large extent, shapes which do not seem similar to the spherical regions used for the tension center model. Nevertheless, such regions can be filled with closely packed tension centers of varying sizes so that one can in the limit obtain a model for such horizontal strata. The mathematical details of this procedure are contained in Appendix II. It is important to realize that one can devise a system of tension centers to represent the effect of pressure reduction in any number of strata.

When the effects of several tension centers are superimposed, it is tacitly assumed that in spite of the pressure reduction in one region, this region behaves as an elastic material with respect to motion and stresses induced by a pressure reduction in another region. This permits superposition of the effects of a large number of centers. Were it not for this assumption, the integration or superposition could not be accomplished.

Another model which other investigators had suggested was one in which the oil bearing sands were incapable of supporting shear stresses, thus giving in effect a thick plate supported by a plastic medium. Although for several reasons this model does not seem plausible, it was felt that the actual behavior might lie between that of such a system and the tension center model. Since such a "thick plate" model cannot be described mathematically by a 3-dimensional semi-infinite elastic model, the computing

technique developed in this report did not seem to be applicable. As another kind of approximation, the vertical pincer model was established. This is a model in which the shear stress reaches a maximum at a certain depth and then decreases, giving just above the disturbance level, a shear stress practically zero. Although calculations in the disturbance region might be less meaningful, it was felt that calculations above this level would be a very good approximation to the desired model.

USE OF MODELS TO FIT SURFACE MOTION

The initial uses of the mathematical model consisted of studies to determine the accuracy with which the surface motion could be fitted by arbitrary distributions of disturbance forces.

CALCULATIONS EMPLOYING A FEW TENSION CENTERS

The first calculations were made to determine what correlation could be obtained between a mathematical model and the measured surface motion when only a few tension centers are used to represent the disturbance stresses being developed beneath the surface. Carrillo had concluded from his preliminary calculations that a single tension center placed at a depth of about 6000 feet would give a good fit to the observed subsidence as measured along the major axis (Fig. 1). He also believed that three equally spaced and equally weighted tension centers could be placed at a depth of 3000 feet (the center of the compacting region) in such a way as to give a good fit to the observed surface subsidence along the major axis and a reasonable fit along the minor axis.

The total recorded surface motion of February, 1949 was chosen for studying such factors as these. The results of the first calculations are summarized in Figures 10 through 14. It was first verified that the best fit to the major axis subsidence to be made with a single tension center required placing it at a depth of about 6000 feet. The calculations for this condition are compared to the actual vertical subsidence in Fig. 10. It can be seen in this figure that more symmetry exists in the actual subsidence across the major axis than across the minor axis. Use of a tension center strength that produces the proper subsidence at the center provides a very good fit to the northwest but drops off too fast to the southeast. Referring to the minor axis data of Fig. 10 the calculated bowl is seen to be much too broad particularly to the southwest.

In Fig. 11 are shown a portion of the calculations made in an attempt to fit the shape of the actual subsidence profile along the major axis with three equal tension centers placed at a depth of 3000 feet with equal weighting and spacings. It was found that such a combination could not be placed at this depth and give a good fit along the major axis. As shown by Case I of Fig. 11, if they are grouped to fit the region around the center of subsidence much too narrow a bowl of subsidence results. If as in Case II the tension centers are spread farther apart the bowl becomes too broad in the region about the center long before a good fit is obtained near the outer edges.

Finally, after trying numerous combinations it was found that a good fit to the major axis profile could not be obtained without a row of about seven tension centers of unequal weighting and spacing as shown in Fig. 12. However, for such a single row of centers, the subsidence bowl is too narrow in the direction of the minor axis. This is illustrated in Fig. 13. The profile of actual subsidence along the two sides of the minor axis is unsymmetrical and thus (as indicated by Case II of Fig. 13) the use of two or three rows of seven tension centers is indicated. For

these the spacings between tension centers is the same for all rows and the relative weighting factors the same for all rows. Such a model gives a reasonably good fit to all parts of the bowl of subsidence.

HORIZONTAL SURFACE MOTION

It should be emphasized that a precise fit to a given bowl of vertical subsidence can be obtained with an infinite number of types of disturbance forces if given a suitable distribution within such a semi-infinite elastic model as is being considered here. The unique solution cannot be established until it has been made to fit more than just the vertical motion at a single surface. Two other sets of measured motions are available for comparison with the model solutions. One of these is the direction and magnitude of the horizontal surface motion (u_o). The other is the vertical motion at the top of the tar zone as indicated by the collar counting study. In the case of the former very little accurate data are available and in the latter the data are all very approximate. However, comparison of observed and calculated motion for both of these cases is very important.

Fig. 14 shows the horizontal surface motion calculations as made with single rows of both five and seven tension centers or Cases I and II of Fig. 12. These are compared with those available measured values of 1949 which seemed meaningful. In making the (w_o) or vertical motion calculations of Figures 10 through 13, the ratio of the parameter C/G (see Figures 3 and 5) was arbitrarily adjusted to fit the maximum subsidence at the center. However, it is important to note that this same ratio was then used for the (u_o) or horizontal surface motion calculations. Thus the magnitude of the calculated curves in Fig. 14 have not just been arbitrarily fitted to the measured data. The check is remarkably good. This comparison will be discussed later in more detail.

DEVELOPMENT OF THE COMPUTING TECHNIQUE FOR A GENERAL FINE DISTRIBUTION OF DISTURBANCE FORCES.

The calculations discussed above have thus demonstrated that if it is only desired to fit the surface motion, three parallel rows, of seven tension centers each, will give a remarkably close fit to both the vertical and horizontal motion as measured for February, 1949. However, the request was next made that consideration be given to the nature of the horizontal shear stresses resulting from such a model. It was at this time that the basic calculations of Fig. 8 were made giving the shear stresses at different depths for a single tension center. These immediately showed that a much finer distribution of tension centers must be assumed if accurate solutions are to be obtained for the shear stresses at depths below five or six hundred feet. This can be seen from the fact that the curves of Fig. 8 reach a maximum for values of r/h of 0.3 or less for values of z/h greater than 0.4. The peak values are also large compared to those for which r/h differs by only a few tenths. Thus to accurately calculate shear stress for ratios of z/h as high as 0.6 it is necessary to represent the tension distribution at intervals not greater than about 600 feet. This value was used for some of the preliminary shear calculations but a fixed interval of 500 feet was soon chosen for all subsequent calculations. The machine numerical integrating technique was then developed

so that the motions and stresses could be computed for a perfectly arbitrary distribution of tension stress in the oil bearing region.

In the case of tension center theory, the technique of making this more general and much more complex calculation employs the basic solutions of Figs. 3 and 5 for a single tension center. An arbitrary distribution of such tension centers over the entire region beneath the subsidence bowl requires the integration of the effect of the loading on each differential element of area in the disturbance force region to obtain the total value of motion or stress at one given point in the elastic medium or on the surface. In the cases of the horizontal motion or horizontal stress this problem is made even more difficult by the fact that they are vectors and each component parallel to the major and minor axes respectively must be individually calculated by this procedure and then combined into a single vector. This is discussed more completely in Appendix II.

CONSIDERATION OF OTHER POSSIBLE TYPES OF DISTURBANCE FORCES

It was at about this time in the course of the investigation that the question was raised by U. S. Grant regarding the validity of the tension center type of model as compared to the elastic plate model which he favored but for which he could obtain no mathematical solution. One of his reasons for suggesting such a model centered about the fact that most of the shear failures so far observed in the wells occurred at a depth of about 1500 feet or about halfway between the surface and the top of the oil bearing sands. He assumed that the shear failures were the result of maximum stresses developed in this region through the existence of a neutral axis and that the earth above the oil bearing region (the over burden) must be moving in a manner similar to a plate with little or no lateral constraint at its lower surface (the top of the oil bearing region). Thus not only must the shear stresses be zero at the top surface but nearly so also at this lower surface with maximum stresses developing somewhere between. Thin plate theory provides a neutral axis near the center of the plate with maximum shear stresses thus developing at the middle. Grant assumed a similar situation to be accounting for the well failures at the medium depth of 1500 feet. No consideration was given by him to the fact that variations in the shear resistance (or strength) of the earth might be a contributing factor. Converse's core sampling study has provided pertinent data relative to this latter point which will be discussed later.

There is, however, one important characteristic of such a plate which is hard to reconcile with actual conditions. Unless the underlying medium is very plastic and free flowing so that it can flow around the well casings, relative motion between the overburden and underlying medium should still cause well casing failures. It is known that the oil bearing sands do not have this property to a sufficient extent to prevent such failures if the two media were not constrained laterally at their bounding surfaces. The oil bearing sands actually grip casings to a sufficient extent that they can be compressed far beyond the yield point without buckling. So far there has been

no evidence of relative motion at the bottom of the over burden. To date all well failures of this sort have occurred above about 1800 feet with one exception in which failure at 2200 feet occurred along a natural fault.

It was requested that consideration be given to developing a model amenable to mathematical calculation which would provide the important properties sought by Grant in his plate theory together with the above condition of absence of relative motion between the over burden and the top of the oil bearing sands. With this in mind, the concept of the vertical pincer was developed and the general solutions of Figures 3 and 6 derived. It cannot readily be seen from these basic equations that this model (when used to fit the subsidence with a distribution of disturbance functions) satisfies the two important conditions of providing a region of maximum horizontal shear stress near the middle of the over burden and very small stress and no relative motion at the bottom of the over burden. It will, however, become apparent when solutions to actual cases are considered later.

CALCULATIONS WITH GENERAL DISTRIBUTIONS OF TENSION CENTERS AND VERTICAL PINCERS

Having developed a machine computing technique adequate to handle general distributions of both types of disturbance functions, it was considered desirable to make comparable calculations with each model. The 1949 case was again used for this purpose. By a trial and error process the necessary shapes were determined for both the tension center distribution and the vertical pincers distribution in order to provide a very good fit to the actual vertical surface motion (w_o). The profiles of these two disturbance force distributions along both coordinate axes are given in Fig. 15. It will be noted that a much narrower distribution of tension centers is required to fit the surface subsidence than for the case of the vertical pincers. The actual calculations for (w_o) as obtained with the tension center distribution is given in Fig. 16 together with a calculation of the expected subsidence at a depth of 2100 feet which represents the top of the oil bearing sand region. Although this shows a somewhat higher maximum subsidence at this depth than indicated by the collar count study, the difference of less than 3 feet lies within the expected errors of the collar count measurements.

The two sets of distributions described in Fig. 15 were then used to calculate the horizontal surface motion. This motion along the two axes is given in Fig. 17. As seen from this a good fit to the measured motion is provided by the tension center distribution whereas the vertical pincers distribution gives values for the horizontal motion that are only about one-half the measured values. Consideration of the physical properties of the two types of models leads to the general conclusion that this should be so.

The next test of the two models pertained to the character of the horizontal shear stresses which they produce. Figures 18 and 19 give values for the shear stress at various depths along the minor axis calculated for the tension center and vertical pincers distributions of Fig. 15. For these calculations it was necessary to specify more than just the ratio (C/G) as

used in equations 1 and 2 of Fig. 3 for the tension center case, and (M/G) as used in the equations for (w_o) and (u_o) of Fig. 4 for the vertical pincers case. Referring to the horizontal shear equations as given in these two figures, it is seen that C and M must be specified directly, and hence a value for G must be assumed.

Considerations to be discussed later lead to the conclusion that an approximate value for the shear modulus (G) could be specified. The value used for G in Figures 18 and 19 is 100,000 psi. It is quite reasonable to assume a value of 0.25 for Poissons ratio which might vary between 0.2 and 0.4, since even the extreme values would have negligible effect upon the results. Thus the assumed value for G corresponds to 250,000 psi for Young's Modulus (E). The assumed value of G specifies C and M from the ratios of C/G and C/M used to fit the (w_o) data. It can also be seen from the basic equations of Figures 3 and 4 that if some other value is indicated for the shear modulus of elasticity (G) the solutions of Figures 18 and 19 should be adjusted by a factor directly proportional to the change in (G) if the model is to still fit the same magnitude of surface subsidence (w_o).

Comparison of Figures 18 and 19 shows that the vertical pincers model indicates much lower shear stress than the tension center model. Figure 20 provides a further comparison. Here the maximum calculated stress at each depth is plotted as a function of depth. Since the maxima occur at a point on the southwest side of the minor axis these data were taken directly from Figures 18 and 19. A peak horizontal shear stress of only 175 psi that occurs at a depth of 1500 feet is indicated by the vertical pincers model whereas the tension center model shows the shear stress to be continually increasing with depth. It is thus apparent that the vertical pincers model does provide a maximum shear stress near the center of the over burden and low shear stress at the bottom of the over burden.

COMPARISON BETWEEN CALCULATIONS AND CORE SAMPLE TESTS

As mentioned previously, the mathematical analysis had been started without direct information on the basic parameters necessary to mathematically describe the properties of both the over burden and the oil bearing sands. Most important of these is the shear modulus of elasticity (G) and Young's Modulus (E). Data on shear strengths in the over burden are also important. The calculations were indicating definite required ranges for these parameters and it was extremely important to obtain information about them.

Accordingly a program of core sample testing was instigated by Mr. Hughes with the results given by Professor Converse in two reports.[2,3] The locations of the actual wells from which the core samples were taken are shown in Figure 1. This phase of the study is covered completely in the Converse reports and only data directly pertinent to the mathematical analysis will be included here. Although more than one hundred core samples have been tested from six wells located in regions of particular

interest, there are as yet admittedly insufficient data to adequately describe the complete area. However, the correlation between these measurements and the mathematical study is extremely important.

Table II lists the shear modulus measurements together with the type of formation involved. These same data are plotted in Figure 21 as a function of the depth from which the sample was taken. A similar list and plot of all of the shear resistance test data are given in Table III and Figure 22. The shear modulus of elasticity results are remarkably uniform with little average increase with depth indicated for depths in excess of about 1300 feet. For depths of less than a thousand feet values of from 20,000 to 40,000 psi are indicated while for depths greater than 1300 feet most values lie within the range between 80,000 and 120,000 psi. These data formed the basis for the choice of 100,000 psi as an average value for G in the horizontal shear calculations of Figures 18, 19 and 20.

It is evident that there is a most significant correlation between the calculated horizontal shear stresses and the measured shear resistances as summarized in Figures 20 and 22 respectively. Comparing these two figures it is seen that (if a mean value of 100,000 psi is assumed for G) the vertical pincers model produces shear stress too low to expect shear failure from material of shear strength as described by the data in Fig. 22. The tension center model on the other hand provides shear stresses lying in the region of most numerous values of shear strength and provides a variation with depth roughly paralleling that of the shear strength data. In this connection it must be remembered that the shear stress data of Figure 20 represents the maximum to be expected in 1949 and that this maximum exists in a small region on the southwest side of the minor axis. This is the region in which the 1949 shear failures occured and such is predicted by these calculations with the tension center model. The tension center model thus indicates that the depth at which shear failures occur is determined primarily by the variation of shear resistance rather than in the variation of shear stress with depth as suggested by U. S. Grant.

TENSION CENTER MODEL PREFERABLE TO VERTICAL PINCERS MODEL

From the above considerations it is seen that a tension center model distribution of disturbance forces which provides a good fit to the vertical surface subsidence also fits the observed horizontal surface motion and subsidence at the top of the over burden to the accuracy of the measurements. This is not the case, however, for the vertical pincers model. When the best available estimate for an average value of the parameter (G) is used the tension center model places the calculated horizontal shear stresses in just the right range of magnitude to predict shear failure in the limited regions where they occurred whereas the vertical pincers model indicates shear stresses too low for shear failures. The conclusion is therefore drawn that the tension center model is the only one of the two that should be considered further.

DIRECT CALCULATIONS FROM THE PRESSURE DROP IN THE OIL BEARING SANDS

So far consideration has been given to the use of mathematical models for empirically fitting the observed surface motion. If the analyses are to be of use in determining future developments it is necessary to incorporate into the calculations a direct correlation between the magnitude of the tension center forces and the supposed major source of the disturbance (the removal of oil from the oil bearing sands). The data available for this are the thickness and location of the oil bearing sands and the time history of the oil well pressure drops throughout the region.

The conversion of such information into an appropriate distribution of "disturbance forces" is admittedly very uncertain, requiring basic assumptions on the physical properties of the oil bearing sands for which there is as yet inadequate data. As an initial consideration the three upper zones have been considered as the total source of subsidence since practically all of the measured compaction is occurring in these zones. As shown in Table I these have a maximum total oil sand thickness of 600 feet with a mean depth of about 3000 feet. The resulting 3000 feet of overburden, in the unstressed state, requires about 5000 psi (at the top of the oil bearing sands) to support it. Before the oil removal was started the oil pressures were everywhere about 2500 psi and it can be assumed that the remaining half of the support was provided by the compressive forces in the oil bearing sands. Although such a point of view is not completely rigorous, it gives an idea of the orders of magnitude involved in this problem.

The reduction of oil pressure by the removal of oil causes a redistribution of forces, part of the resulting pressure drop being accounted for by added compression in the oil bearing sands as they compact and part by the added tensile forces developed in the overburden as it subsides. The disturbance forces effectively pulling down on the overburden may be considered as the difference between the pressure drop and the increase in oil bearing sand compressive force.

The horizontal distribution throughout the field of the product of the pressure drop (ΔP) in pounds per square inch times the total oilsand thickness (T) in feet at the well location provides a distribution function over the oil field which can be converted to an equivalent distribution of tension centers or other "disturbance forces" if certain assumptions are made regarding the added force borne by the oil bearing sands in this compaction.

It was considered reasonable, as discussed previously, to assume

the overburden to be elastic in its gross behavior. Shear forces are being built up and maintained by the subsidence. However, as an aid to determining one limit of the effect of the pressure drop in the oil bearing sands they might be assumed to be plastic and readily compressible upon the withdrawal of oil. Thus the oil pressure drop is taken up completely by the overburden. The conversion of the (ΔPxT) data to appropriate tension centers for this assumption is given in Appendix II.

At the other extreme, a conservatively high value might be taken for the compressive modulus of the oil bearing sands. The calculations would then distribute the load between the oil sands and the overburden. For this case a trial and error type of solution is required in which a distribution of "disturbance forces" is first assumed and a calculation made of the vertical subsidence at the top of the oil bearing sands. From this the compaction and the resulting load borne by the oil sands can be determined. The compaction force distribution over the area is then subtracted from the original assumed "disturbance force" distribution and the result should be the known oil pressure drop distribution. Such series of calculations must then be carried out for numerous cases until a reasonable fit is obtained to the known pressure drop.

Certain preliminary direct calculations of the types discussed above were made. These placed the average value of the shear modulus of elasticity (G) required for a fit of the observed subsidence rather low but of the same order of magnitude as indicated by the core sample tests. It became apparent, however, that certain additional work had to be done before such complex calculations are justified on a large scale. The two most important of these are a comprehensive core sample study of the oil bearing sands and a general analysis to correlate the important characteristics of the (ΔPxT) distribution with those of the developing bowl of subsidence. The latter is a mathematical analysis which could be made immediately and the following factors were considered to be of particular importance.

(1) A comparison of the time history of the developing bowl of actual subsidence with that as directly calculated from the time history of the (ΔPxT) distribution.

(2) A comparison of the variations between actual subsidence and that indicated by the (ΔPxT) distributions over all parts of the bowl and for each year. This is for the purpose of locating any regions of marked divergence that might result from large changes in the soil properties with location.

(3) A search for evidence of any important non-linear effects.

GENERAL STUDY EMPLOYING THE (ΔPxT) DATA

A study of this type involves a very large number of direct

subsidence calculations from the given (ΔPxT) distributions.

It is however practicable if a definite conversion from the (ΔPxT) data to the tension center distribution is applied. For this purpose it was decided to directly convert all of the pressure drop into a disturbance force by the equations given in Appendix II. Here the volume distribution of the oil bearing sands with their corresponding per unit area pressure drop are directly converted into an equivalent volume distribution of tension centers.

The (ΔPxT) data for the years 1945, 1947, 1949, 1950 and 1951 were available for this purpose. Such information is shown in Tables IV through VIII as originally supplied by the Harbor Department. It was known by the Harbor Department when these tables were prepared that some of the data were uncertain since they could not be obtained directly from their own records. After calculations had been made with the data and certain gross discrepancies appeared for the regions where the data were uncertain, the Harbor Department took additional steps to procure more accurate information and supplied the revised (ΔPxT) data of Tables XII through XV. Also compiled for analysis were tabulations of proposed (ΔPxT) distributions for 1952 and two possible ultimate pumping schedules. These are given in Tables IX, X, XI and XVI.

Profiles of the actual surface subsidence for the years 1945 through 1951 are summarized in Figures 23 and 24. These are taken from the contour plots of the bowls of measured total subsidence for each year.

Using the data of Tables IV through VIII and the conversion formulas of Appendix II, vertical surface subsidence values were calculated for each year for a large number of points throughout the bowl. The number was sufficient to accurately locate contours. A fixed average value for (G) of 100,000 psi was used for this purpose. A complete plot was then made for all locations of the calculated versus the measured subsidence. A small portion of these data (points on the two coordinate axes) are shown in Figures 25 and 26. Here it will be noted that a given symbol applies to one particular location and each of the points with that symbol corresponds to a different year. More points are not plotted here since it then becomes difficult to identify them and no new information is provided by doing so.

It was observed from the complete plot of such points that they are all quite close to the single mean curve shown in the figures except for those locations directly to the northwest of the origin. Since this was the region in which the (ΔPxT) information was questionable, the revised data were obtained by the Harbor Department and the calculations repeated. A portion of these results are shown in Figures 27 and 28. It was then found that all points lay even closer generally to a single mean curve. The maximum deviation is about 25 percent with the majority of the points falling within 10 percent of the curve. This applies to all points calculated and is a most significant fact since it shows that so far, regardless of location or time, there is an essentially single valued relationship between the calculated and measured results as

defined by the single curve which is the same in both Figures 27 and 28.

It is important to note the character of this curve. If it were a straight line a completely linear correlation between calculations and measurements would be indicated. The results are not linear and for measured deflections in the region of six to ten feet, there is a marked increase in the ratio of measured to calculated subsidence regardless of location or time. There are several possible causes for this non-linearity. All of them should be thoroughly studied and more information on the soil properties is required for this purpose. Some of the important non-linearities may be in the compacting oil sands, some may be in the over burden such as the known fact that the effective value for E is decreasing as the net compressive forces in certain portions of the over burden shift toward tensile stresses with the subsidence. Considerable thought has been given to this phase of the problem by the authors but the results are not yet well enough defined to present at this time.

The important conclusions to be drawn from this analysis is that there is a direct correlation between the development of the bowl of subsidence and the increase in the (ΔPxT) distribution which is essentially independent of location throughout the bowl and time. Thus, there is no evidence of marked change in soil properties with horizontal location. If the non-linear character of the phenomena can be adequately specified independently of the empirical method used here which produced the average curve, future developments can be predicted with reasonable certainty. For the present the average curve given in Figures 27 and 28 must be extrapolated from considerations based upon events as they have so far occurred and the probable trend of variation of soil properties with further compaction in the oil sands. As noted in the figures giving the results obtained from the two sets of (ΔPxT) data different average curves were obtained. Since it is now known that the original (ΔPxT) data were in error the curve in Figures 25 and 26 should be ignored.

USE OF THE AVERAGE CURVE AS A DIRECT CONVERSION FACTOR

The single valued nature of the results given in Figures 27 and 28 immediately suggested a method of empirically converting calculations made from (ΔPxT) data into predictions of expected subsidence. The use of the average curves as obtained for both sets of (ΔPxT) for the years 1947 through 1951 are shown by the profile curves of Figures 29 through 38. In these figures are shown the actual subsidences for each year as compared to those calculated from the two sets of (ΔPxT) data. The original (ΔPxT) calculations shown there clearly indicate the discrepancy in the results to the northwest.

The conformability of the calculated to actual subsidence is thus seen to be remarkably good for both cases. The position of the calculated bowls of subsidence with respect to the coordinate axes depends entirely upon the

location of and character of the (ΔPxT) distributions. The fact that the calculated bowls coincide so closely with the actual bowls leaves little doubt but that the reduction of oil pressure in the oil bearing sands is the major cause of the subsidence.

These calculations were made before the presentation to the authors of the actual measured subsidence for 1951, the (ΔPxT) data of that year having been supplied first. Thus the curves of Figures 35 and 36 provided the first test of this model as used for predicting future subsidence from a known development schedule in the oil field. The projection into the future is, of course, only one year but the check is still remarkably good. Complete contour maps comparing the calculated and measured surface subsidence for 1951 were also determined. They are given in Figures 37 and 38 for the two sets of (ΔPxT) data.

This procedure thus offers, for the present, the best method of directly calculating expected motions and stresses from a given set of (ΔPxT) data. In making all future calculations described in this report the following method was therefore employed. Expected bowls of vertical surface motion were first calculated from the (ΔPxT) distribution by the method of Appendix II and adjusted by the average curve in Figures 27 and 28. Having thus obtained an estimate of the vertical subsidence, the necessary tension center distribution required for an accurate direct fit of this subsidence was next determined. This tension center distribution was then used for all calculations of additional motions and stresses, such as the horizontal surface motion and horizontal shear stress. This procedure is justified by the results of the detailed studies conducted first where the accuracy of calculations resulting from the use of a tension center distribution that was fitted to the vertical surface subsidences was investigated in considerable detail.

STUDY OF THE EFFECTS OF FUTURE PUMPING SCHEDULES

Although the validity of the mathematical model is still subject to further study and correlation with desired future core sample testing, it was considered important to investigate at this time the possible effects of certain proposed future pumping schedules. These include the expected (ΔPxT) distribution for 1952 which is given in Table IX and two possible ultimate distributions which are presented in their original form in Tables X and XI. Since the revisions of the (ΔPxT) data only affected values to the northwest of the origin, the change had a negligible effect on solutions to the southeast where the two proposed ultimates are different. This is in the region of the stipulated line. It was thus found unnecessary to recalculate more than one of the ultimate cases and thus the revised (ΔPxT) data for just one of them is given in Table XVI.

The calculations requested by the Harbor Department for these future programs are contained in all of the subsequent figures; figures 39 through 66.

VERTICAL SURFACE MOTION

Figures 39 through 44 give the vertical surface subsidence as calculated for the two proposed ultimates. Calculations for both the original and revised (ΔPxT) distributions are included here since they had been worked up completely. However, the revised data of Figures 39, 40, 43 and 44 supercede the original calculations. Referring to these figures it is seen that the maximum subsidence is estimated to be about 24 feet. A long narrow ridge is developed along the major axis to the southeast in which if the pumping extends beyond the stipulated line subsidences of over 20 feet may develop as far as 8,000 feet to the southeast of the origin. Extension of the pumping schedule beyond the stipulated line has little effect, however, on the maximum expected subsidence.

HORIZONTAL SURFACE MOTION

The calculated horizontal surface motions for the two proposed ultimate pumping schedules are given in Figures 45 and 46. In this case recalculations have not yet been made for the revised (ΔPxT) distributions. However, the results to the southeast of the origin are of most interest and they are little affected by the revision. Here the data are presented in the form of contour lines with the vector direction of the expected motions indicated by arrows. Along the southwest side of the minor axis maximum horizontal motions up to 9.3 feet are to be expected for pumping just to the stipulated line and 9.5 feet for pumping beyond the stipulated line. As the

result of developing the field toward the southeast long narrow ridges of high lateral motion together with high rates of change of lateral motion are expected to develop toward the southeast along axes parallel to the major axis and on both sides of it. It is realized, of course, that the rate of change of horizontal surface motion is a measure of the severity of possible surface stresses which may be developed in such surface structures as bridges, pipelines, and rail lines. In this regard there is no significant difference in the results to be expected from the two possible ultimate pumping schedules. Both indicate severe conditions to both sides of the minor axis which extend southeast as much as 4000 to 5000 feet. A severe situation is indicated to the northwest along the major axis and a somewhat less dangerous situation along the major axis in the region from 0 to 4000 feet southeast and 11,000 to 14,000 feet southeast.

HORIZONTAL SHEAR CALCULATIONS

The subsurface horizontal shear calculations from the year 1950 through the two ultimate schedules are plotted in contour form in Figures 47 through 54. The danger of more oil well failures through the development of excessive shear stresses in the immediate future is of primary concern. It was for this reason that the 1951 and proposed 1952 cases were studied to determine expected increases in such stress within the next year or two. As an aid to interpreting the significance of these data it was suggested by Mr. Hughes that a plot be made for each case of the region in which the calculated shear forces exceed the expected shear strength of the earth. Since a single exact value for either the average shear modulus of elasticity (G) or the shear resistance of the soil at a given depth is not available, it was considered desirable to give ranges of values for these two parameters. For (G), maximum and minimum values of 120,000 psi and 80,000 psi respectively were taken since they represent the range indicated by the core sample tests for depths greater than 1300 feet (see Figure 21). For the shear resistance at each depth values were taken from the dashed and solid curves of Fig. 22 as representing minimum and average values respectively. Taking all four possible combinations of the limiting values at three depths, 1200, 1500, and 1800 feet, produces the 12 sets of data of Figures 55 through 66. For the ultimate program the most pessimistic case of minimum shear strength with maximum (G) was not included since the region of danger is so broad even by the most conservative estimates.

EFFECT OF SLIPPAGES THROUGH SHEAR FAILURES

It is known that in three separate instances, the building up of horizontal shear stress has already caused shear failures in localized regions which have resulted in considerable damage through oil well casing failures. It is important to consider the effects of these on the actual motions and stresses as compared to the calculations which cannot take this factor directly into account. So far the amount of relative motion in each case has been of the order of a few inches to one foot with a total

maximum accumulated motion at any point of about three feet in the worst case. Such slippages have the effect of increasing the vertical surface subsidence and decreasing the horizontal surface motions and subsurface shear stresses in the immediate vicinity. However, due to the limited areas so far involved the integrated effects of this are as yet quite small. Thus it is felt that they modify the subsidence motions by a negligible amount. The shear stresses in the region of the failures are reduced appreciably.

In Figures 55 through 66 large areas are shown in which shear stresses in excess of shear resistance are indicated for the ultimate situations. These areas should be greatly modified by additional failures which should occur on a larger scale as the oil fields are developed toward such ultimates. Thus the danger areas as indicated in these figures for the ultimate case are probably appreciably larger than the area where failure will actually result. The fact that extensive failures over a more limited area will bring this about is, however, a serious consideration.

LIST OF REFERENCES

1. Report on Subsidence in the Long Beach-San Pedro Area, Stanford Research Institute, page 67.

2. F. J. Converse, Tests for Physical Properties of Siltstone, Shale and Sands from Terminal Island Oil Wells. Report of April 24, 1950.

3. F. J. Converse, Tests for Physical Properties of Siltstone, Shale and Sands from Terminal Island Oil Wells. Report of Nov. 3, 1950.

4. J. Boussinesq, "Applications des Potentials", Paris, 1885.

5. A. E. H. Love, "The Mathematical Theory of Elasticity", Cambridge, 1934.

6. K. Terezawa, Jour. Coll. Science, Imperial Univ., Tokyo, 37, 1916.

7. A. E. H. Love, "The Mathematical Theory of Elasticity", Cambridge, 1934.

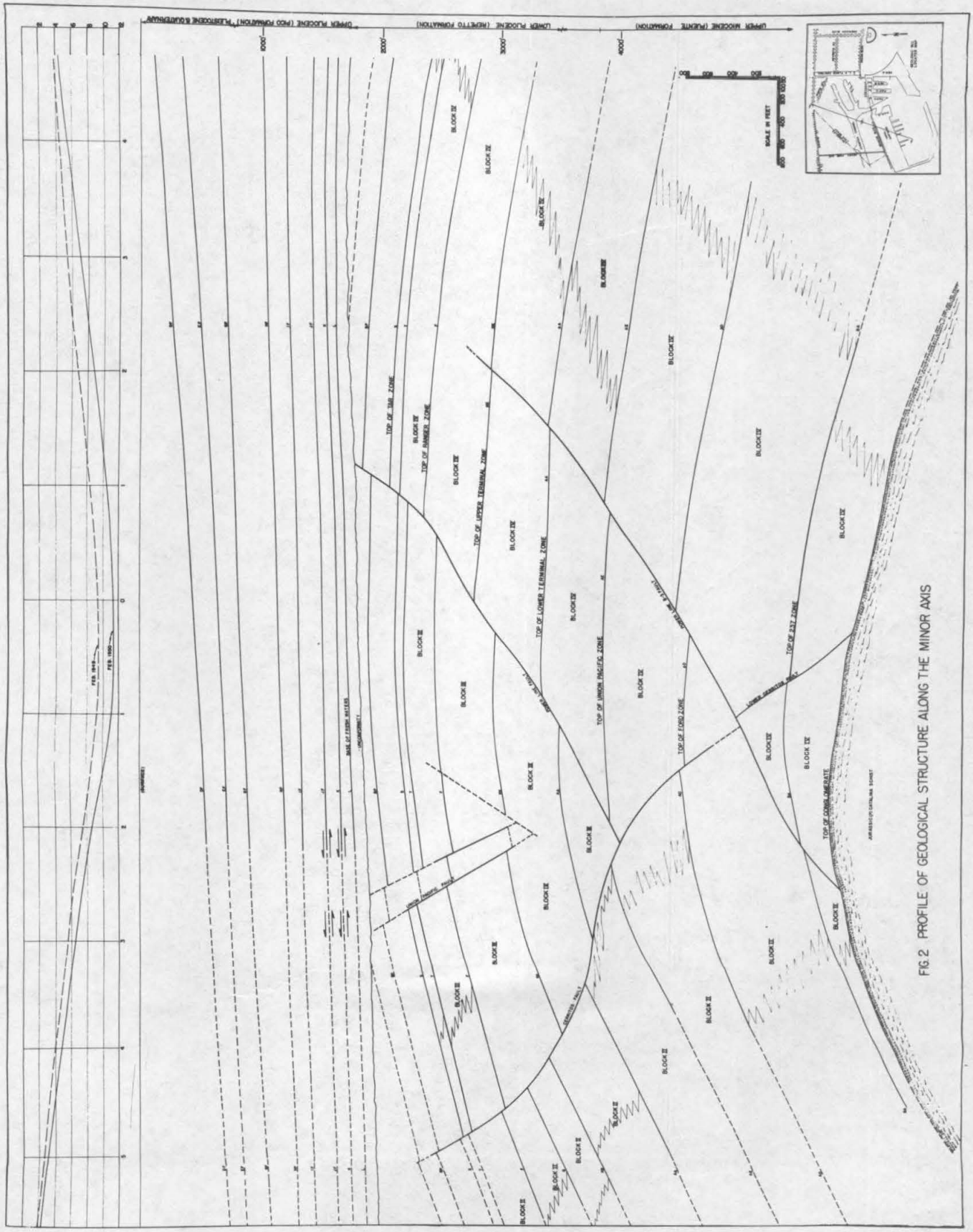

FIG. 2 PROFILE OF GEOLOGICAL STRUCTURE ALONG THE MINOR AXIS

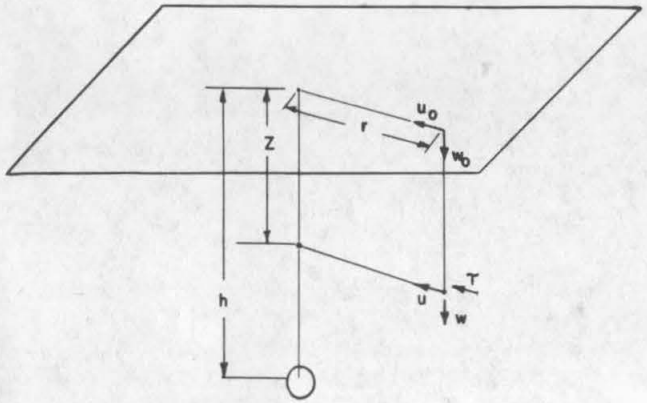

$$w = \frac{C}{2G}\left\{\frac{(h-z)}{[r^2+(h-z)^2]^{3/2}} + \frac{(3-4\nu)(h+z)-2z}{[r^2+(h+z)^2]^{3/2}} + \frac{6z(h+z)}{[r^2+(h+z)^2]^{5/2}}\right\} \quad \cdots (1)$$

$$u = \frac{C}{2G}\left\{\frac{r}{[r^2+(h-z)^2]^{3/2}} + \frac{(3-4\nu)r}{[r^2+(h+z)^2]^{3/2}} - \frac{6rz(h+z)}{[r^2+(h+z)^2]^{5/2}}\right\} \quad \cdots (2)$$

$$\tau = 3C\left\{\frac{r(h-z)}{[r^2+(h-z)^2]^{5/2}} - \frac{r(h+3z)}{[r^2+(h+z)^2]^{5/2}} + \frac{10rz(h+z)}{[r^2+(h+z)^2]^{7/2}}\right\} \quad \cdots (3)$$

AT SURFACE ($z=0$) THESE EQUATIONS REDUCE TO THE FOLLOWING:

$$w_o = \frac{2(1-\nu)C}{G}\,\frac{h}{(r^2+h^2)^{3/2}} \quad \cdots (1a)$$

$$u_o = \frac{2(1-\nu)C}{G}\,\frac{r}{(r^2+h^2)^{3/2}} \quad \cdots (2a)$$

$$\tau_o = 0$$

w = VERTICAL SUBSIDENCE AT DEPTH Z, RADIAL DISTANCE r FROM VERTICAL AXIS.
w_o = VERTICAL SUBSIDENCE AT SURFACE.
u = HORIZONTAL MOTION TOWARD VERTICAL AXIS
u_o = HORIZONTAL MOTION AT SURFACE.
τ = SHEAR STRESS IN HORIZONTAL PLANE.

$G = \frac{E}{2(1+\nu)}$; G = SHEAR MODULUS, E = YOUNG'S MODULUS; ν = POISSON'S RATIO

$C = \frac{t_i a^3}{2}$; t_i = TENSION PER UNIT AREA OVER SURFACE OF TENSION SPHERE; a = RADIUS OF TENSION SPHERE

FIG. 3 SUMMARY OF ANALYTICAL FORMULAS DERIVED IN APPENDIX I FOR A SINGLE TENSION SPHERE BENEATH SURFACE OF A SEMI-INFINITE, UNIFORM, ISOTROPIC ELASTIC MEDIUM.

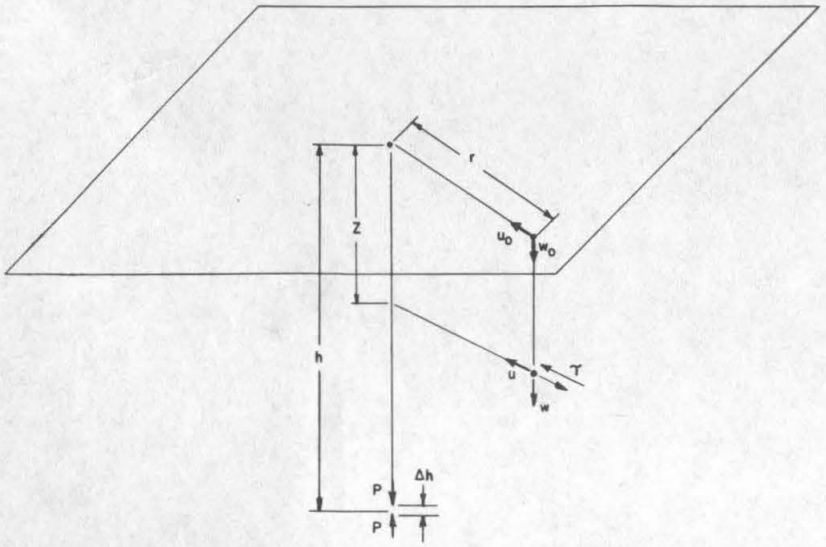

$$w = \frac{M}{8\pi G(1-\nu)}\left\{\frac{2(1-\nu)(h-z)}{[r^2+(h-z)^2]^{3/2}} - \frac{3/2\, r^2(h-z)}{[r^2+(h-z)^2]^{5/2}} - \frac{2(1-\nu)(h+z)}{[r^2+(h+z)^2]^{3/2}} + \frac{3/2\, r^2(h+z)}{[r^2+(h+z)^2]^{5/2}}\right.$$

$$\left. - \frac{\{4\nu(1-\nu)(h+z)-2z\}}{[r^2+(h+z)^2]^{3/2}} - \frac{\{3z(4h+z)(h+z)-6(1-\nu)(h+z)^3\}}{[r^2+(h+z)^2]^{5/2}} + \frac{15zh(h+z)^3}{[r^2+(h+z)^2]^{7/2}}\right\}$$

$$u = \frac{M}{8\pi G(1-\nu)}\left\{\frac{r}{[r^2+(h-z)^2]^{3/2}} - \frac{3r(h-z)^2}{[r^2+(h-z)^2]^{5/2}} + \frac{r}{[r^2+(h+z)^2]^{3/2}} - \frac{3r(h+z)^2}{[r^2+(h+z)^2]^{5/2}}\right.$$

$$\left. - \frac{(1-2\nu)^2 r}{[r^2+(h+z)^2]^{3/2}} - \frac{3r\{(1-2\nu)(h^2-z^2)+hz\}}{[r^2+(h+z)^2]^{5/2}} + \frac{15rzh(h+z)^2}{[r^2+(h+z)^2]^{7/2}}\right\}$$

$$\tau = \frac{M}{8\pi(1-\nu)}\left\{\frac{3(1+2\nu)r(h-z)}{[r^2+(h-z)^2]^{5/2}} - \frac{15r(h-z)^3}{[r^2+(h-z)^2]^{7/2}} - \frac{3(1+2\nu)r(h+z)}{[r^2+(h+z)^2]^{5/2}} + \frac{15r(h+z)^3}{[r^2+(h+z)^2]^{7/2}}\right.$$

$$\left. + \frac{6(1-2\nu)rz}{[r^2+(h+z)^2]^{5/2}} + \frac{30\{3rzh(h+z)-(1-2\nu)rz(h+z)^2\}}{[r^2+(h+z)^2]^{7/2}} - \frac{210rzh(h+z)^3}{[r^2+(h+z)^2]^{9/2}}\right\}$$

w = VERTICAL SUBSIDENCE AT DEPTH Z, RADIAL DISTANCE r FROM VERTICAL AXIS.

w_0 = VERTICAL SUBSIDENCE AT SURFACE.

u = HORIZONTAL MOTION TOWARD VERTICAL AXIS

u_0 = HORIZONTAL MOTION AT SURFACE

τ = SHEAR STRESS IN HORIZONTAL PLANE.

$G = \frac{E}{2(1+\nu)}$; G = SHEAR MODULUS; E = YOUNG'S MODULUS; ν = POISSON'S RATIO

M = PΔh P = STRENGTH OF VERTICAL FORCES

Δh = EFFECTIVE SEPARATION OF FORCES

AT SURFACE Z=0, THESE EQUATIONS REDUCE TO THE FOLLOWING.

$$w_0 = \frac{5M}{8\pi G}\frac{h}{(r^2+h^2)^{3/2}}\left\{\frac{6h^2}{5(r^2+h^2)} - \frac{4\nu}{5}\right\}$$

$$u_0 = \frac{5M}{8\pi G}\frac{r}{(r^2+h^2)^{3/2}}\left\{\frac{1}{5(1-\nu}\left[\{2-(1-2\nu)^2\} - \frac{3h^2(3-2\nu)}{r^2+h^2}\right]\right\}$$

$\tau = 0$

FIG. 4 SUMMARY OF ANALYTICAL FORMULAS DERIVED IN APPENDIX II FOR A SINGLE VERTICAL PINCERS BENEATH SURFACE OF A SEMI-INFINITE UNIFORM ISOTROPIC ELASTIC MEDIUM.

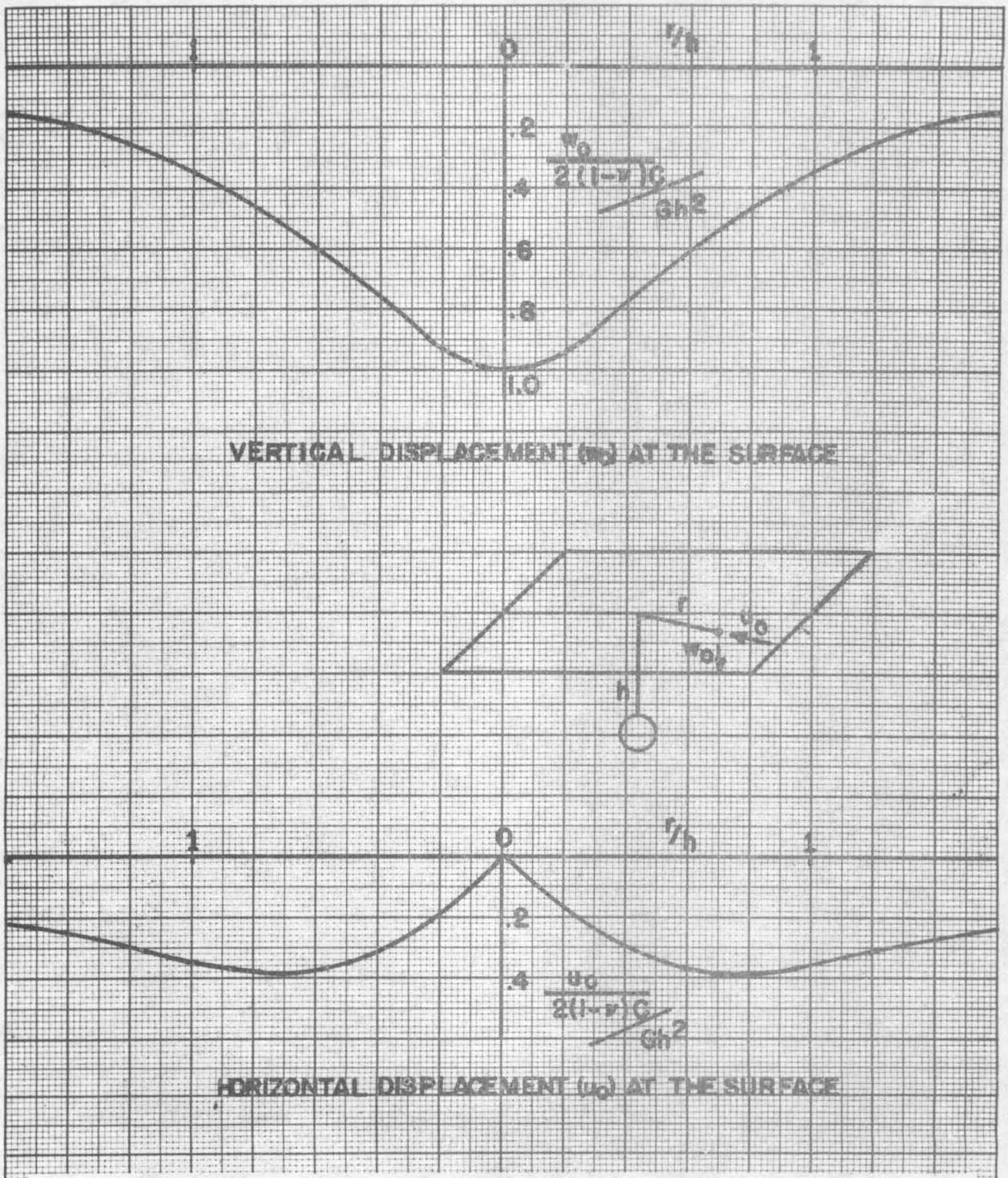

FIG. 5 GRAPHICAL PLOT OF EXACT SOLUTIONS FOR SURFACE MOTION DUE TO A SINGLE TENSION CENTER.

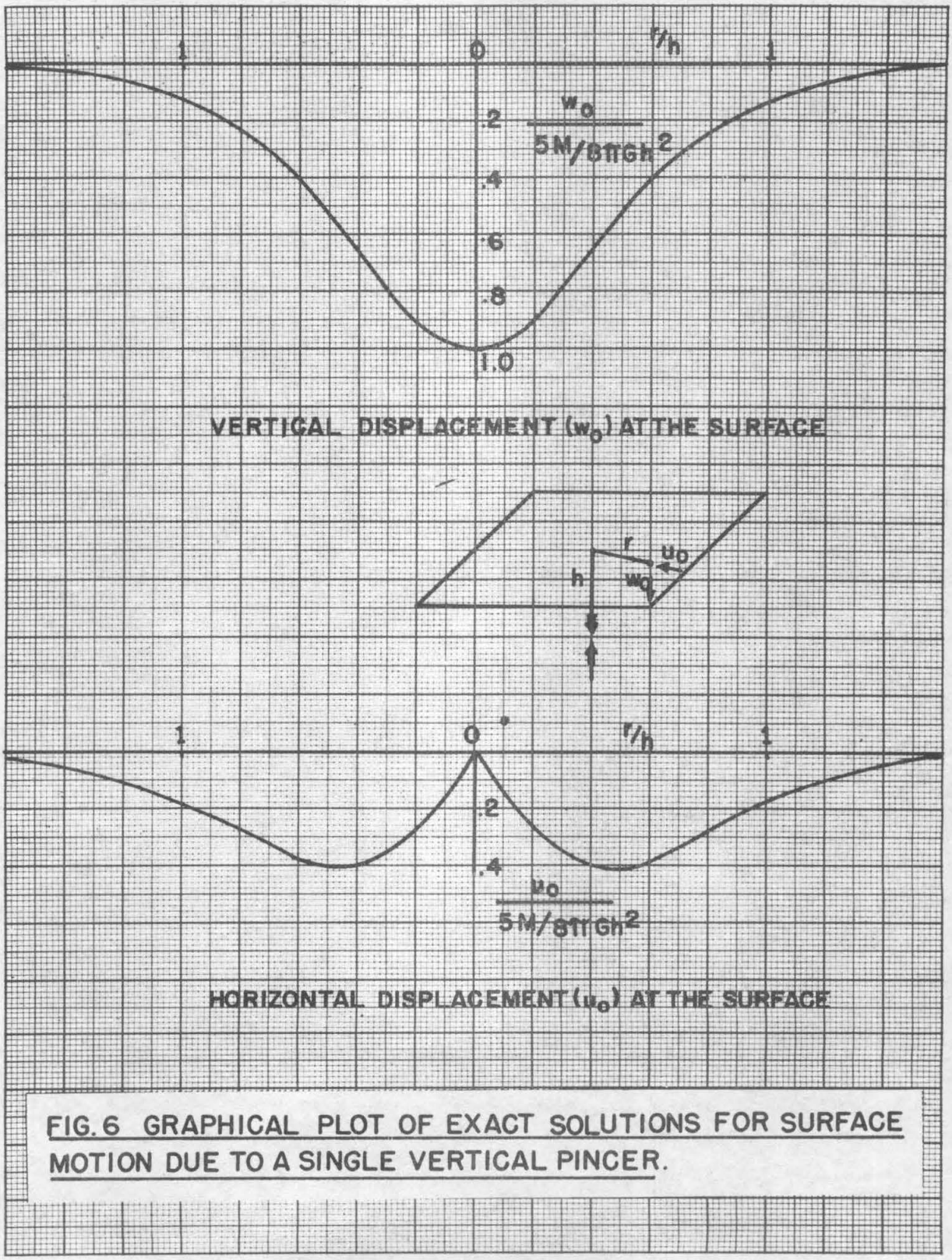

FIG. 6 GRAPHICAL PLOT OF EXACT SOLUTIONS FOR SURFACE MOTION DUE TO A SINGLE VERTICAL PINCER.

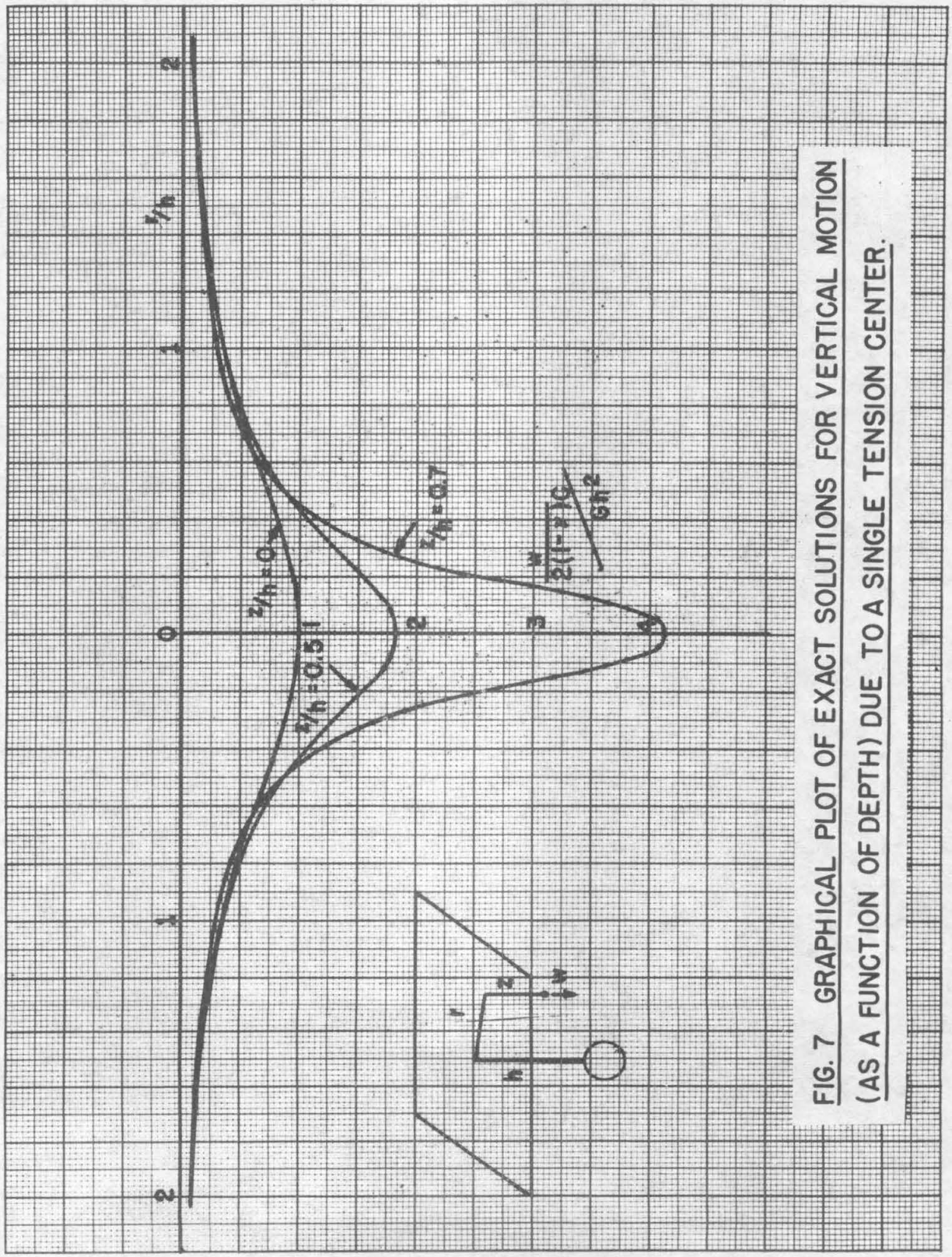

FIG. 7 GRAPHICAL PLOT OF EXACT SOLUTIONS FOR VERTICAL MOTION (AS A FUNCTION OF DEPTH) DUE TO A SINGLE TENSION CENTER.

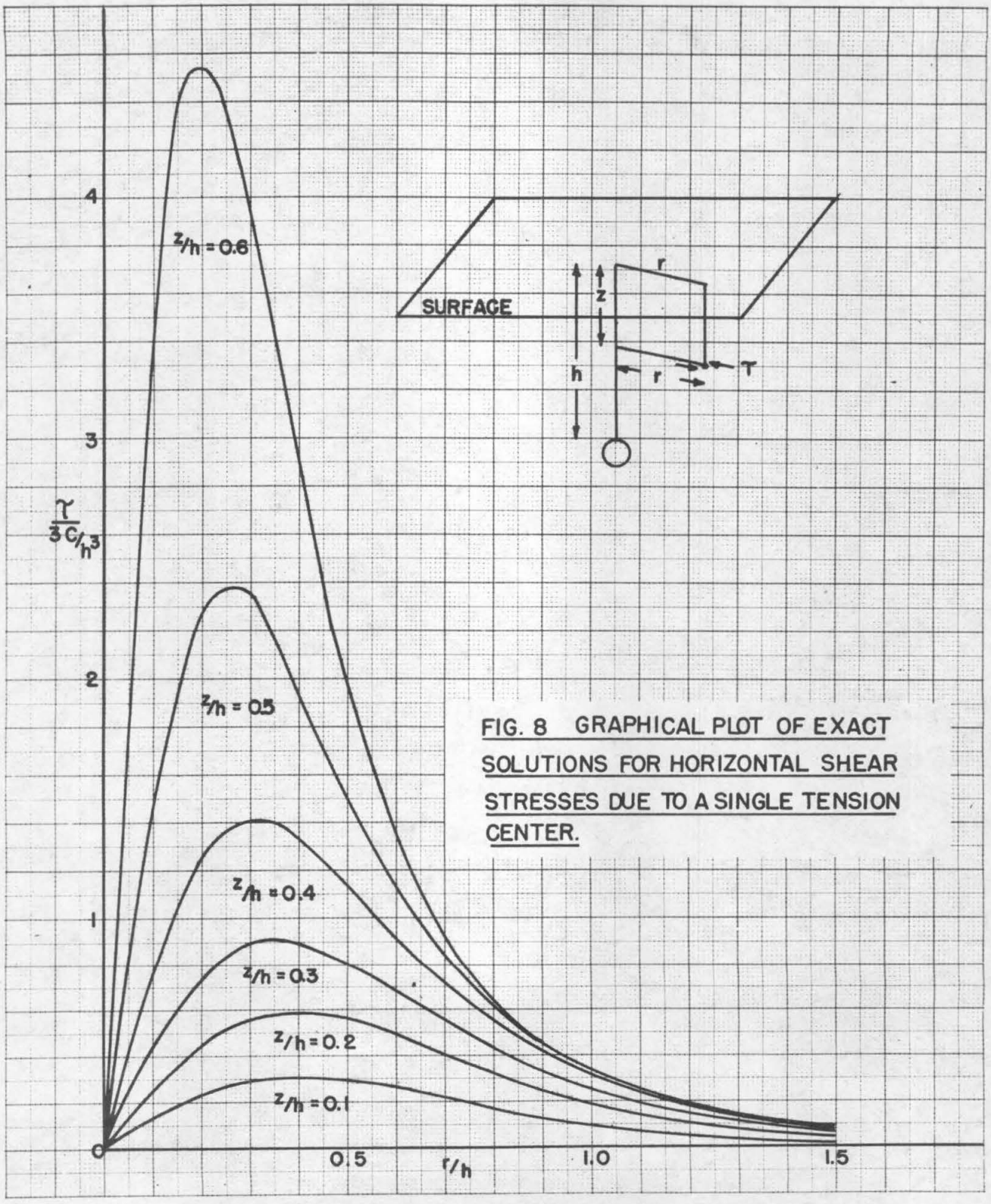

FIG. 8 GRAPHICAL PLOT OF EXACT SOLUTIONS FOR HORIZONTAL SHEAR STRESSES DUE TO A SINGLE TENSION CENTER.

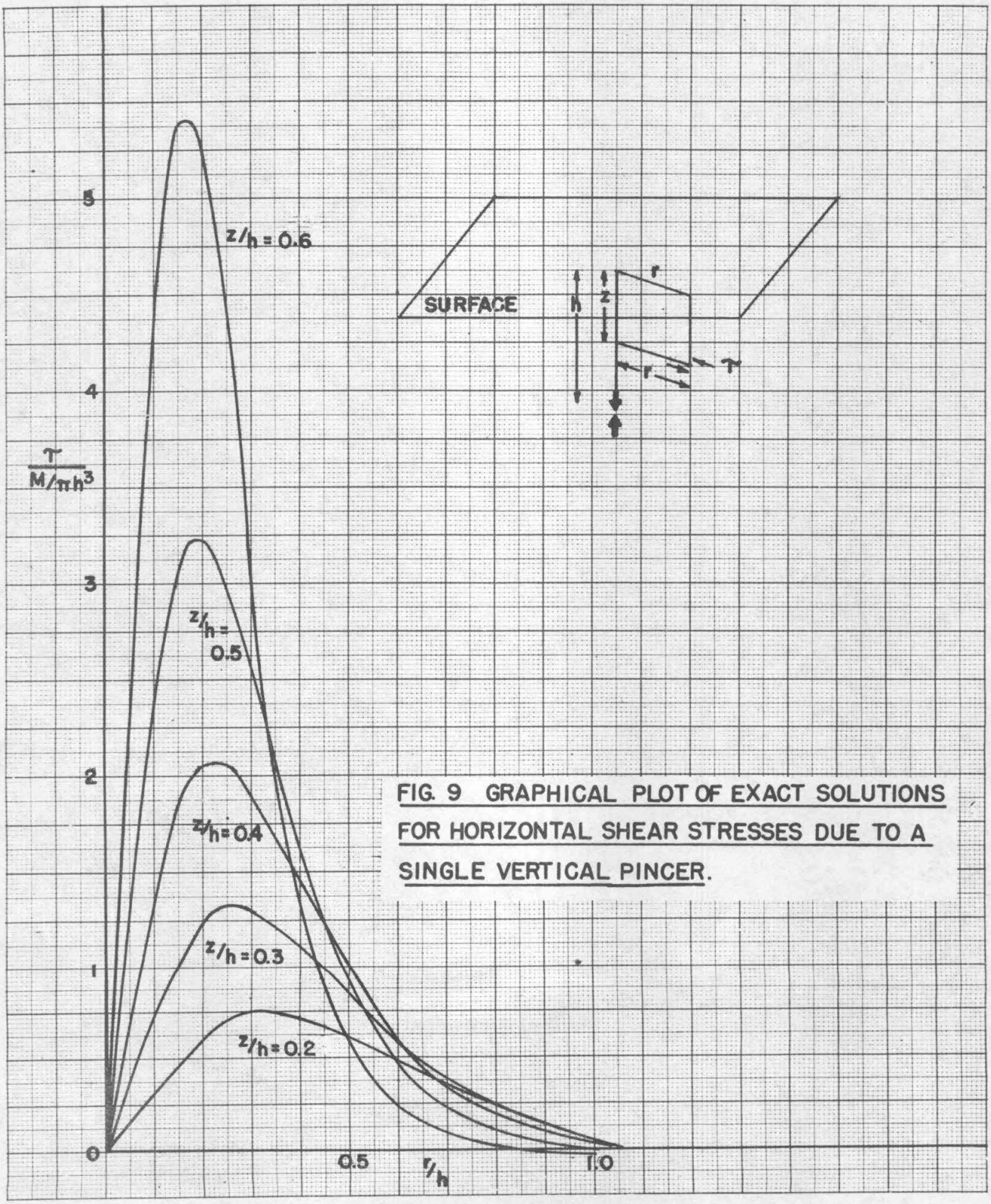

FIG. 9 GRAPHICAL PLOT OF EXACT SOLUTIONS FOR HORIZONTAL SHEAR STRESSES DUE TO A SINGLE VERTICAL PINCER.

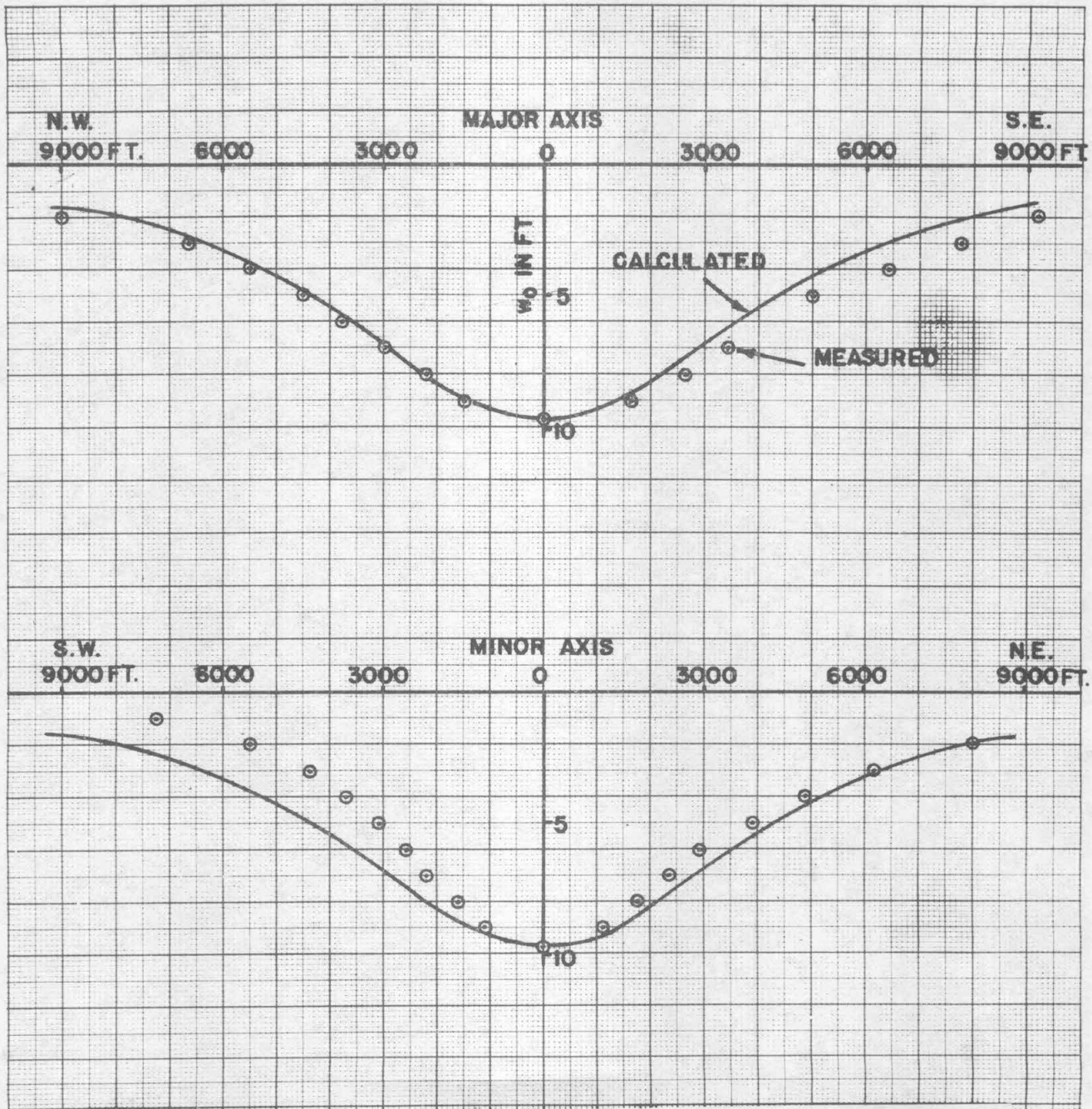

FIG. 10 RESULTS OF ATTEMPT TO FIT ACTUAL SURFACE SUBSIDENCE OF 1949 (w_o) WITH ONE TENSION CENTER AT A DEPTH (h) OF 6000 FT.

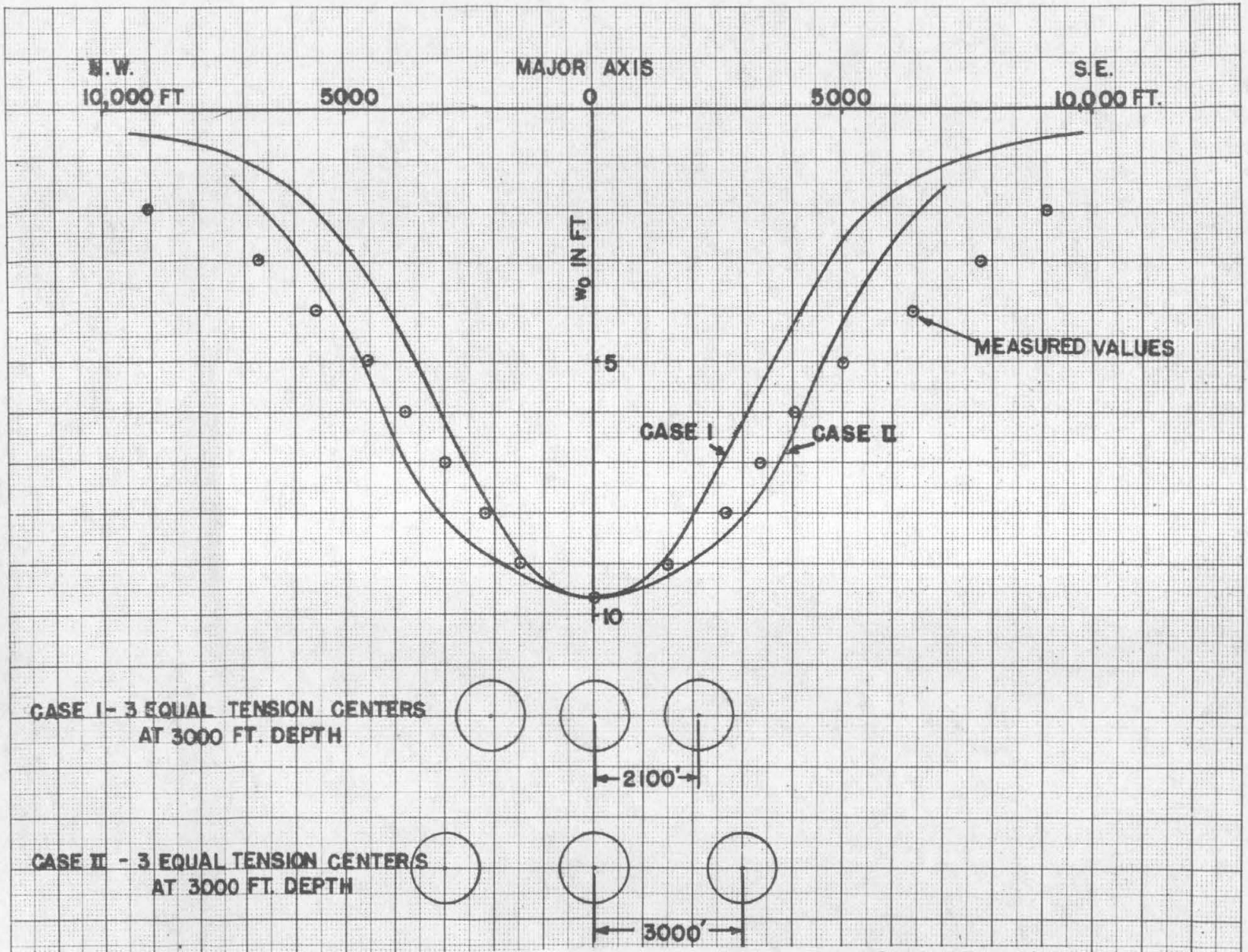

FIG.11 RESULTS OF ATTEMPTS TO FIT ACTUAL SURFACE SUBSIDENCE ALONG MAJOR AXIS WITH THREE TENSION CENTERS IN A ROW ON MAJOR AXIS.

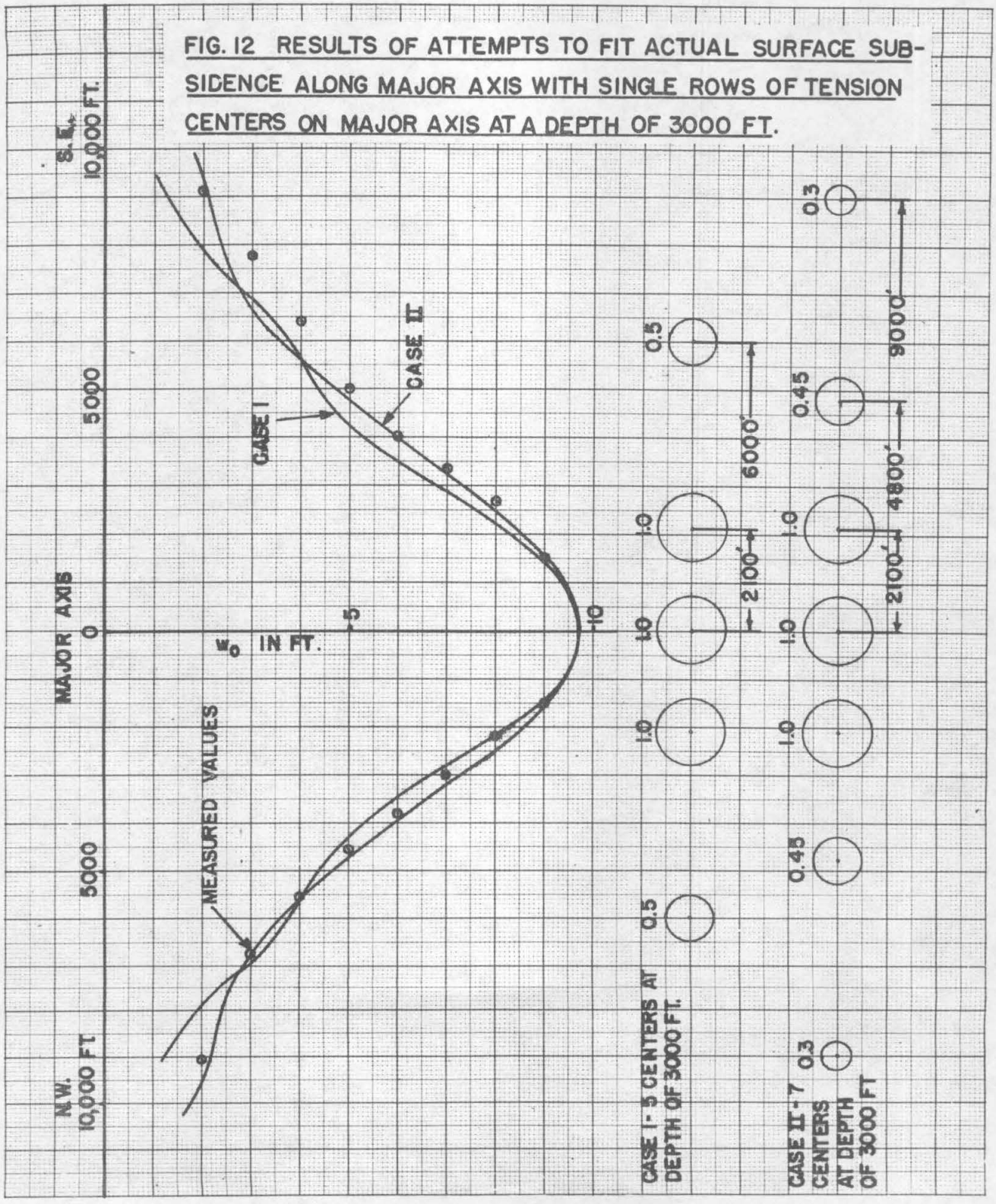

FIG. 12 RESULTS OF ATTEMPTS TO FIT ACTUAL SURFACE SUBSIDENCE ALONG MAJOR AXIS WITH SINGLE ROWS OF TENSION CENTERS ON MAJOR AXIS AT A DEPTH OF 3000 FT.

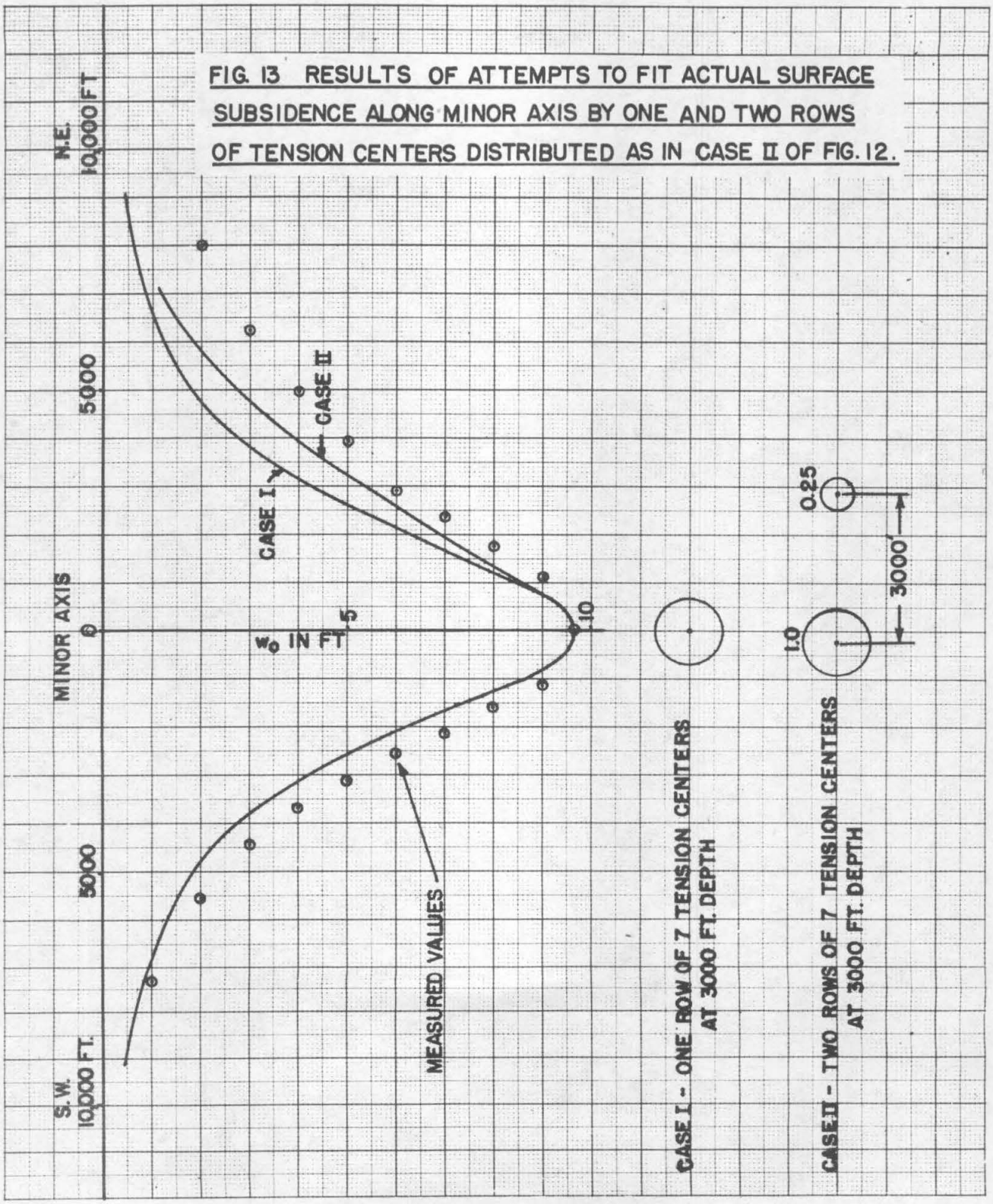

FIG. 13 RESULTS OF ATTEMPTS TO FIT ACTUAL SURFACE SUBSIDENCE ALONG MINOR AXIS BY ONE AND TWO ROWS OF TENSION CENTERS DISTRIBUTED AS IN CASE II OF FIG. 12.

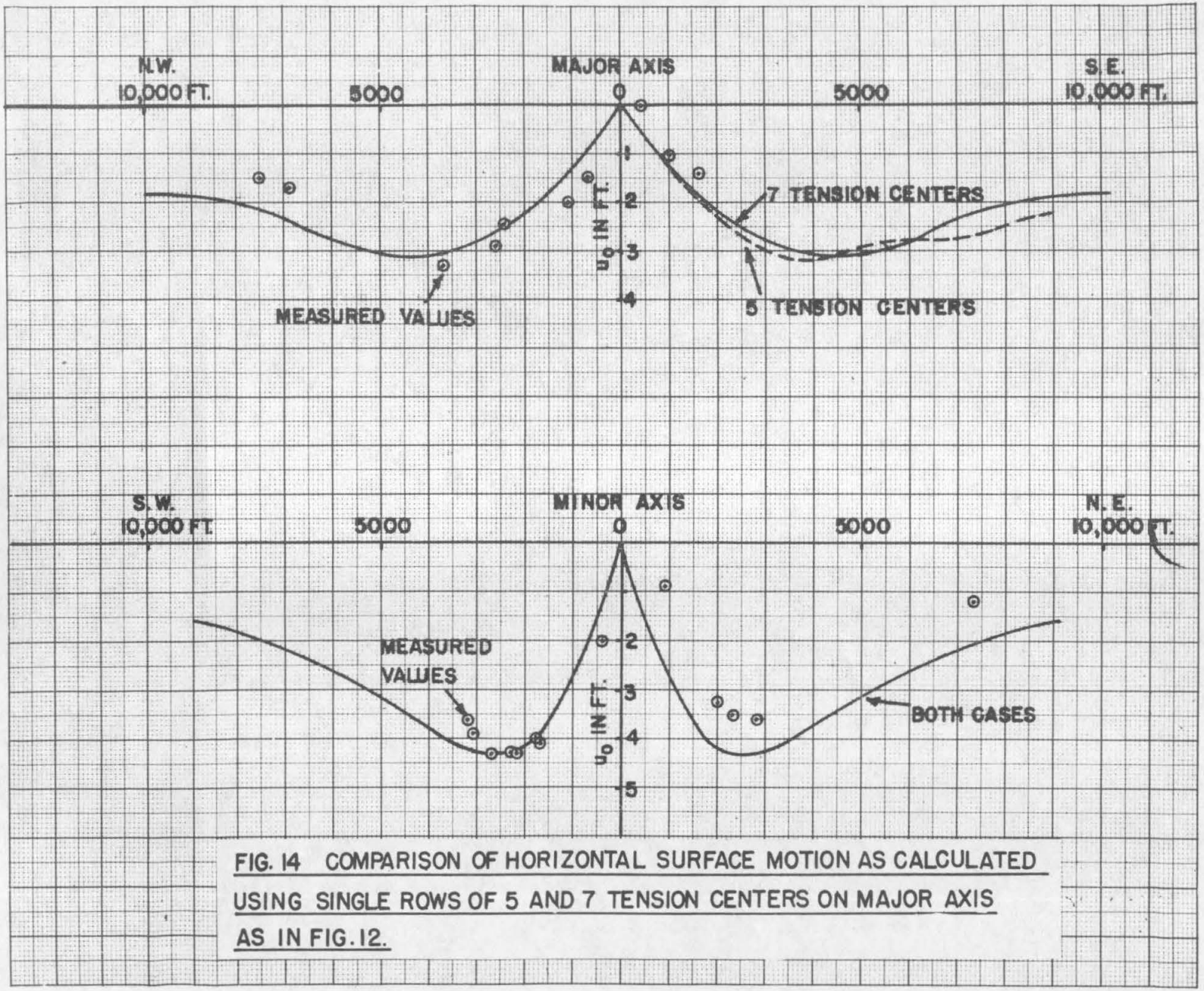

FIG. 14 COMPARISON OF HORIZONTAL SURFACE MOTION AS CALCULATED USING SINGLE ROWS OF 5 AND 7 TENSION CENTERS ON MAJOR AXIS AS IN FIG. 12.

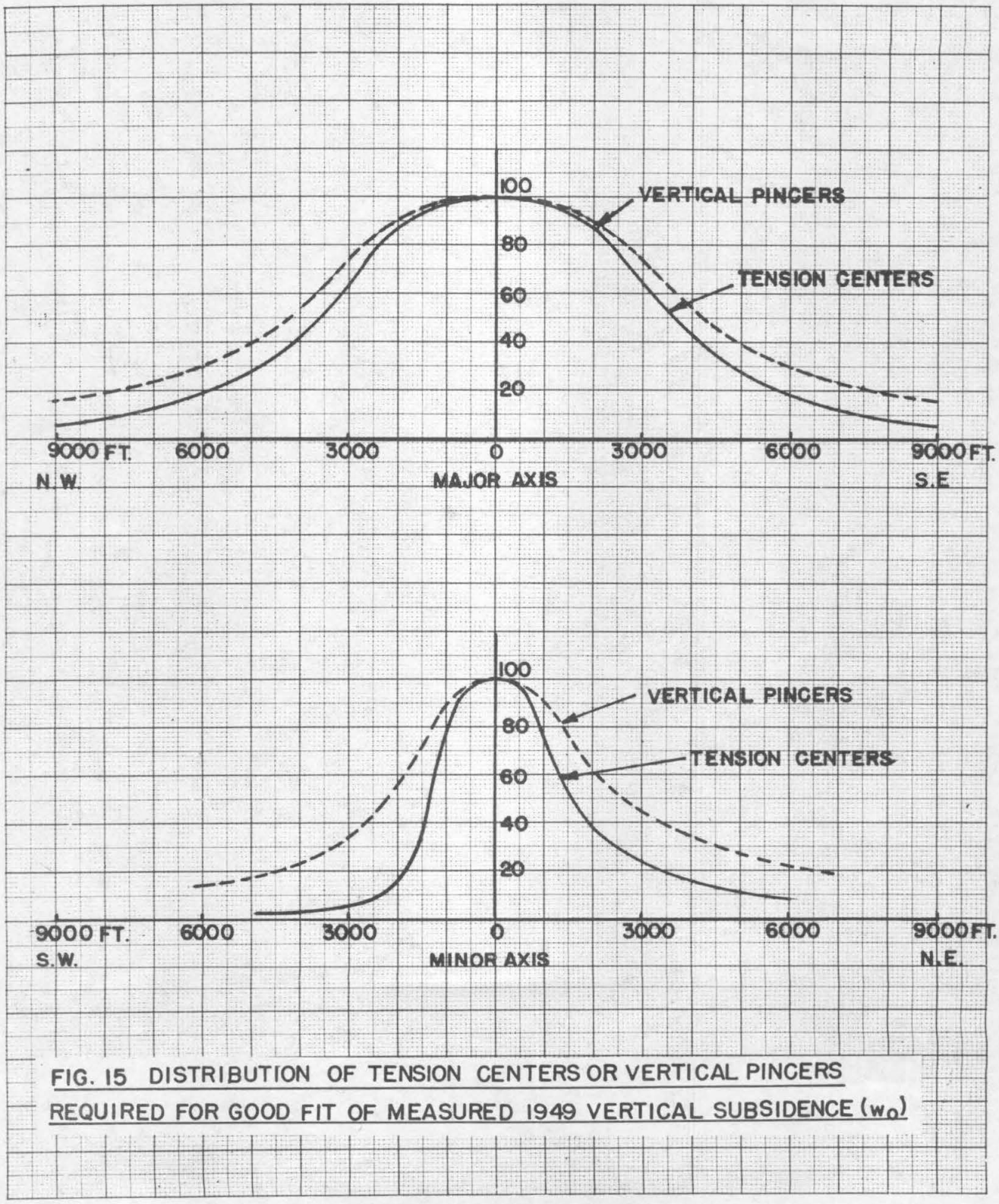

FIG. 15 DISTRIBUTION OF TENSION CENTERS OR VERTICAL PINCERS REQUIRED FOR GOOD FIT OF MEASURED 1949 VERTICAL SUBSIDENCE (w_o)

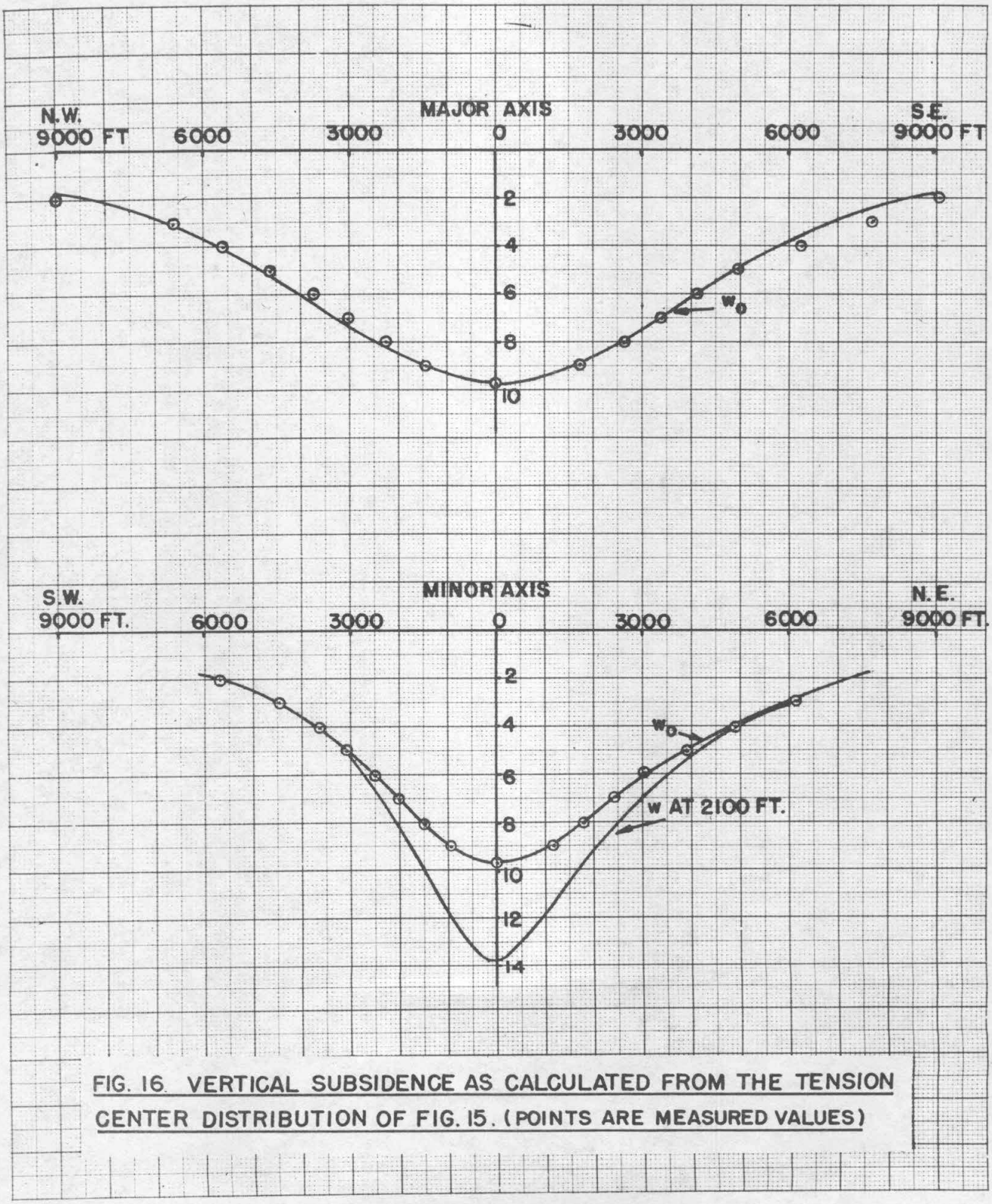

FIG. 16. VERTICAL SUBSIDENCE AS CALCULATED FROM THE TENSION CENTER DISTRIBUTION OF FIG. 15. (POINTS ARE MEASURED VALUES)

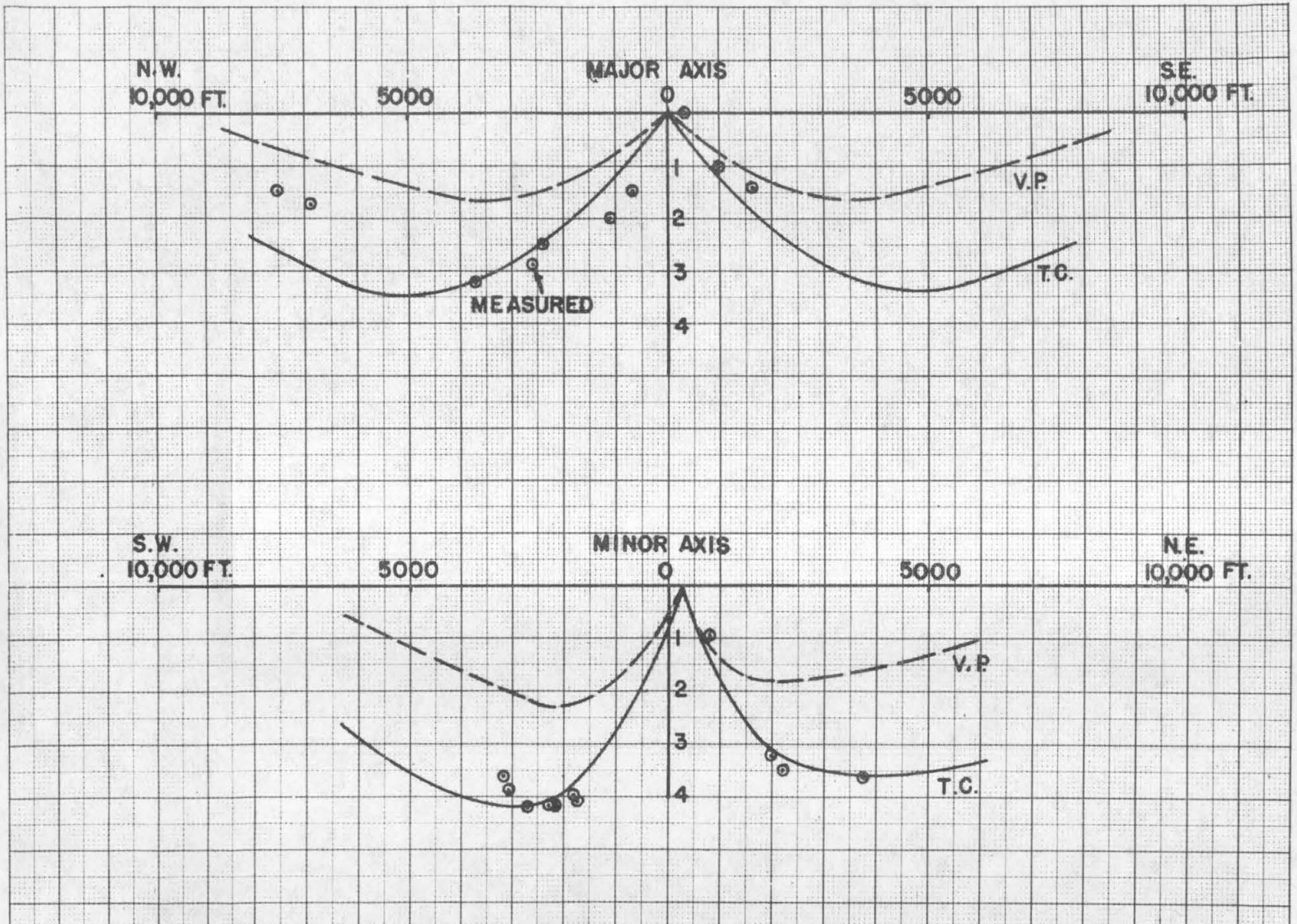

FIG. 17 HORIZONTAL SURFACE MOTION (u_0) AS CALCULATED FROM TENSION CENTER AND VERTICAL PINCERS DISTRIBUTIONS OF FIG. 15 AND COMPARED WITH MEASURED VALUES OF 1949.

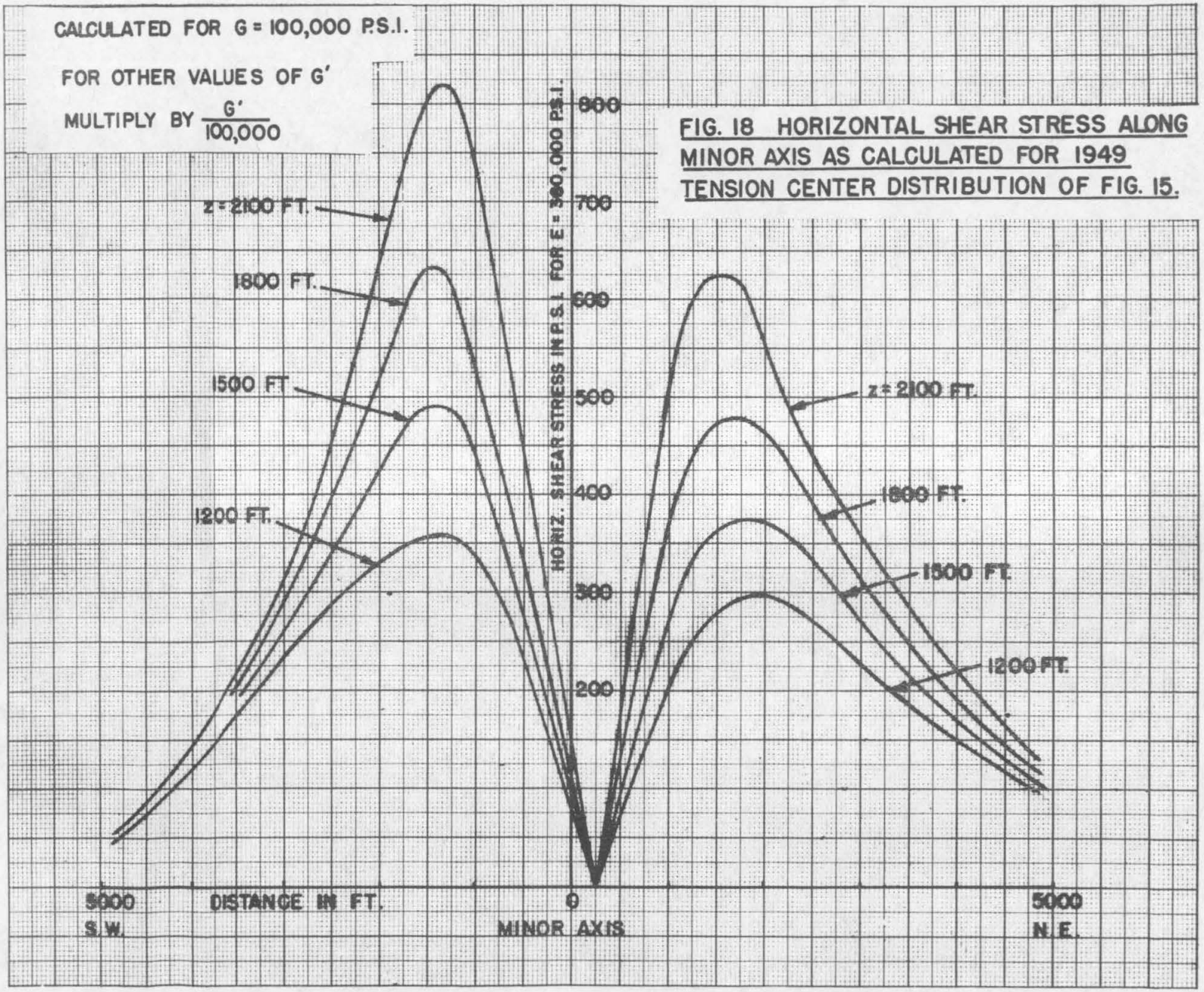
CALCULATED FOR G = 100,000 P.S.I.
FOR OTHER VALUES OF G'
MULTIPLY BY G'/100,000
FIG. 18 HORIZONTAL SHEAR STRESS ALONG MINOR AXIS AS CALCULATED FOR 1949 TENSION CENTER DISTRIBUTION OF FIG. 15.
HORIZ. SHEAR STRESS IN P.S.I. FOR E = 30,000 P.S.I.
800
700
600
500
400
300
200
z = 2100 FT.
1800 FT.
1500 FT.
1200 FT.
z = 2100 FT.
1800 FT.
1500 FT.
1200 FT.
5000
S.W.
DISTANCE IN FT.
0
MINOR AXIS
5000
N.E.

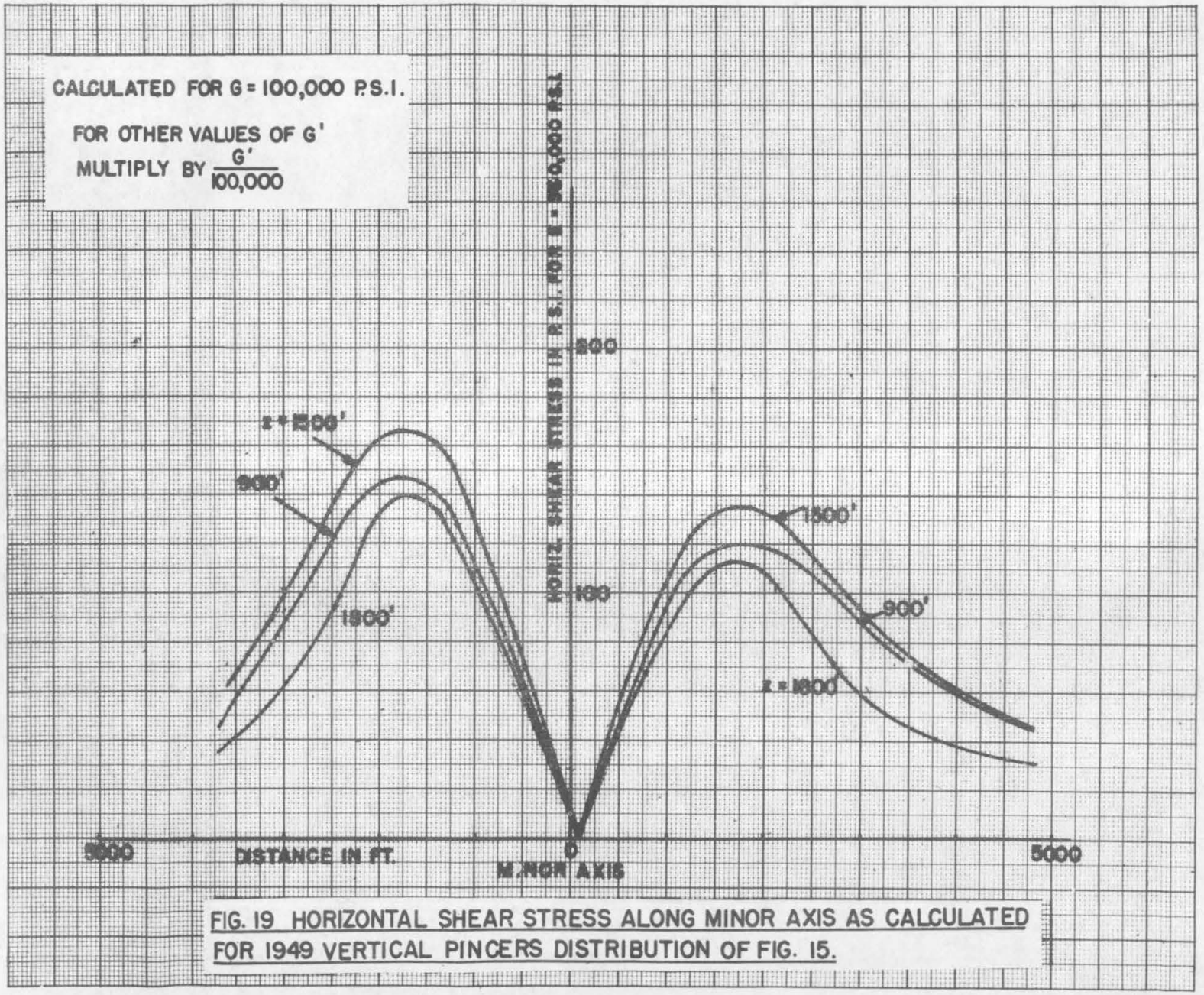

FIG. 19 HORIZONTAL SHEAR STRESS ALONG MINOR AXIS AS CALCULATED FOR 1949 VERTICAL PINCERS DISTRIBUTION OF FIG. 15.

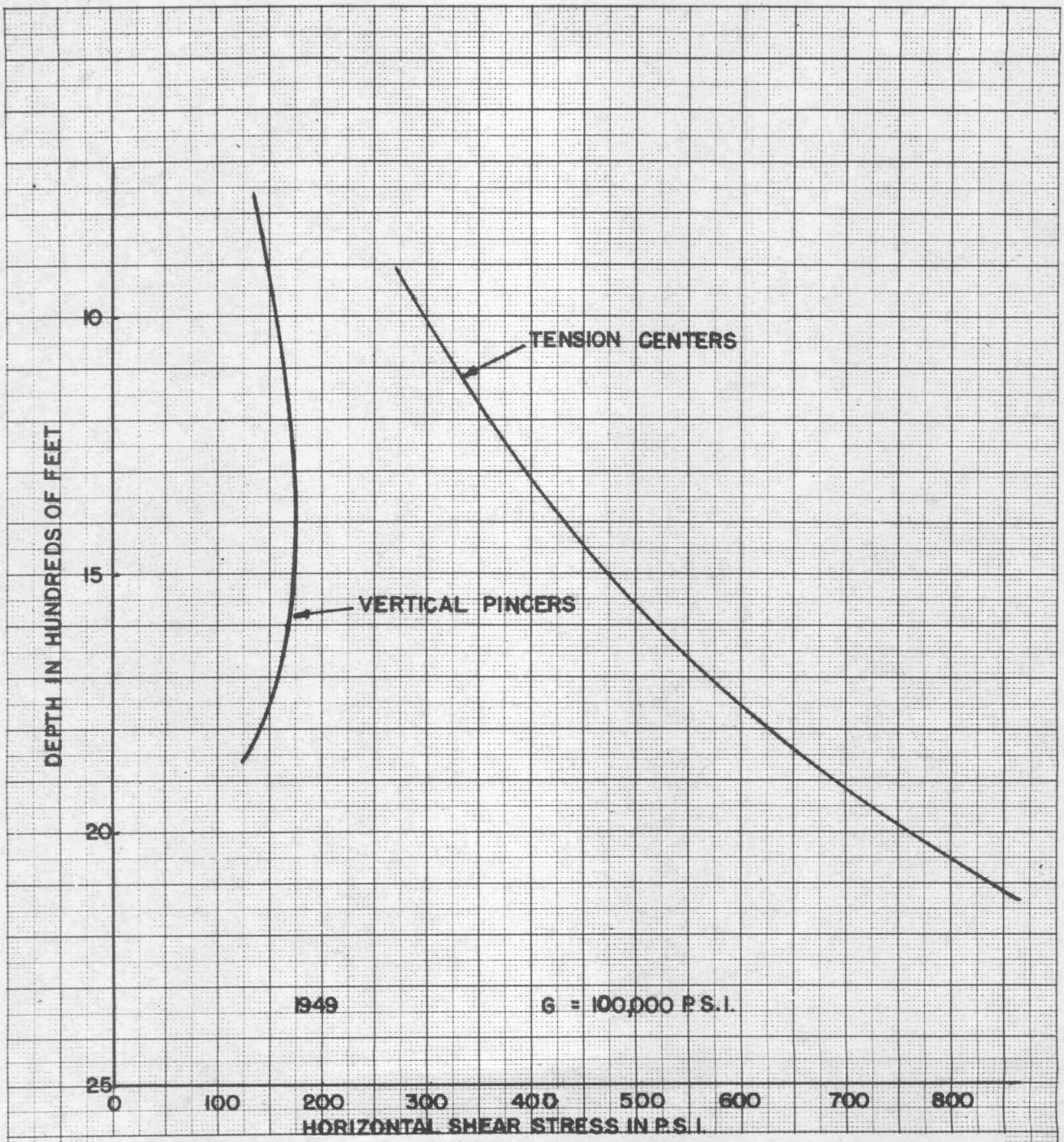

FIG. 20 VARIATION OF HORIZONTAL SHEAR STRESS WITH DEPTH AS COMPUTED FROM TENSION CENTER AND VERTICAL PINCER DISTRIBUTIONS OF FIG. 15 (VALUES TAKEN AT POINT OF MAXIMUM STRESS ON S.W. SIDE OF MINOR AXIS)

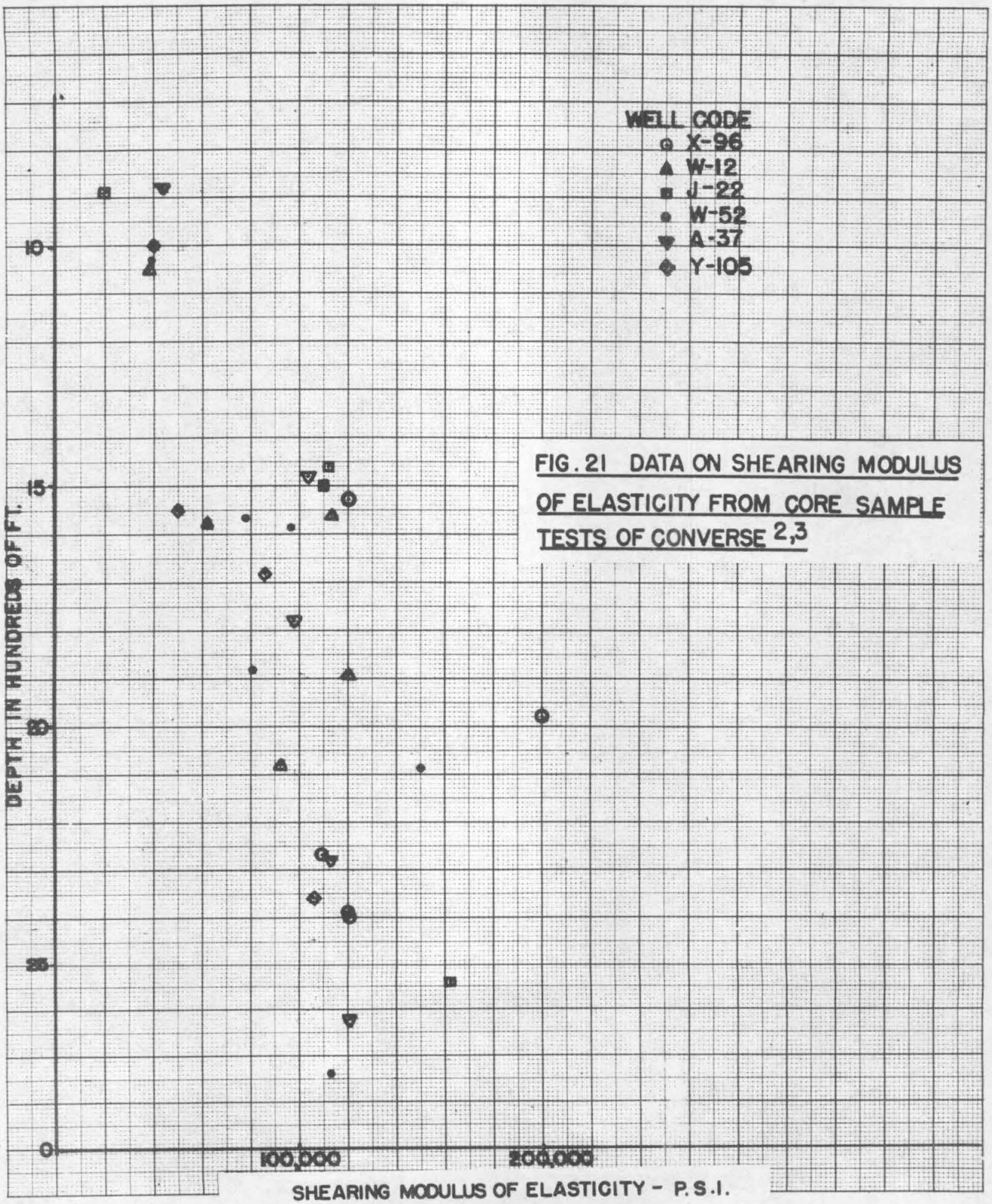

FIG. 21 DATA ON SHEARING MODULUS OF ELASTICITY FROM CORE SAMPLE TESTS OF CONVERSE [2,3]

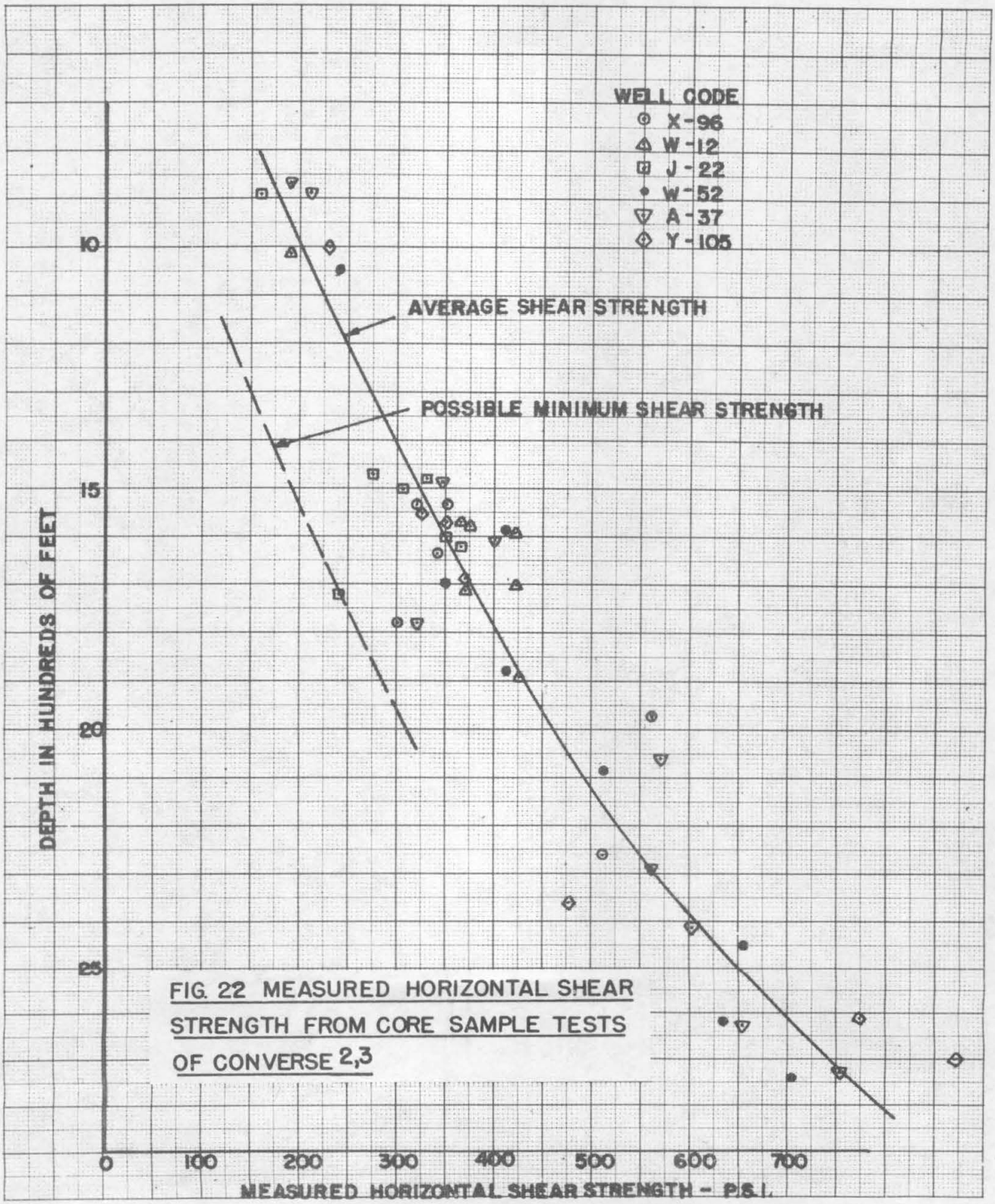

FIG. 22 MEASURED HORIZONTAL SHEAR STRENGTH FROM CORE SAMPLE TESTS OF CONVERSE [2,3]

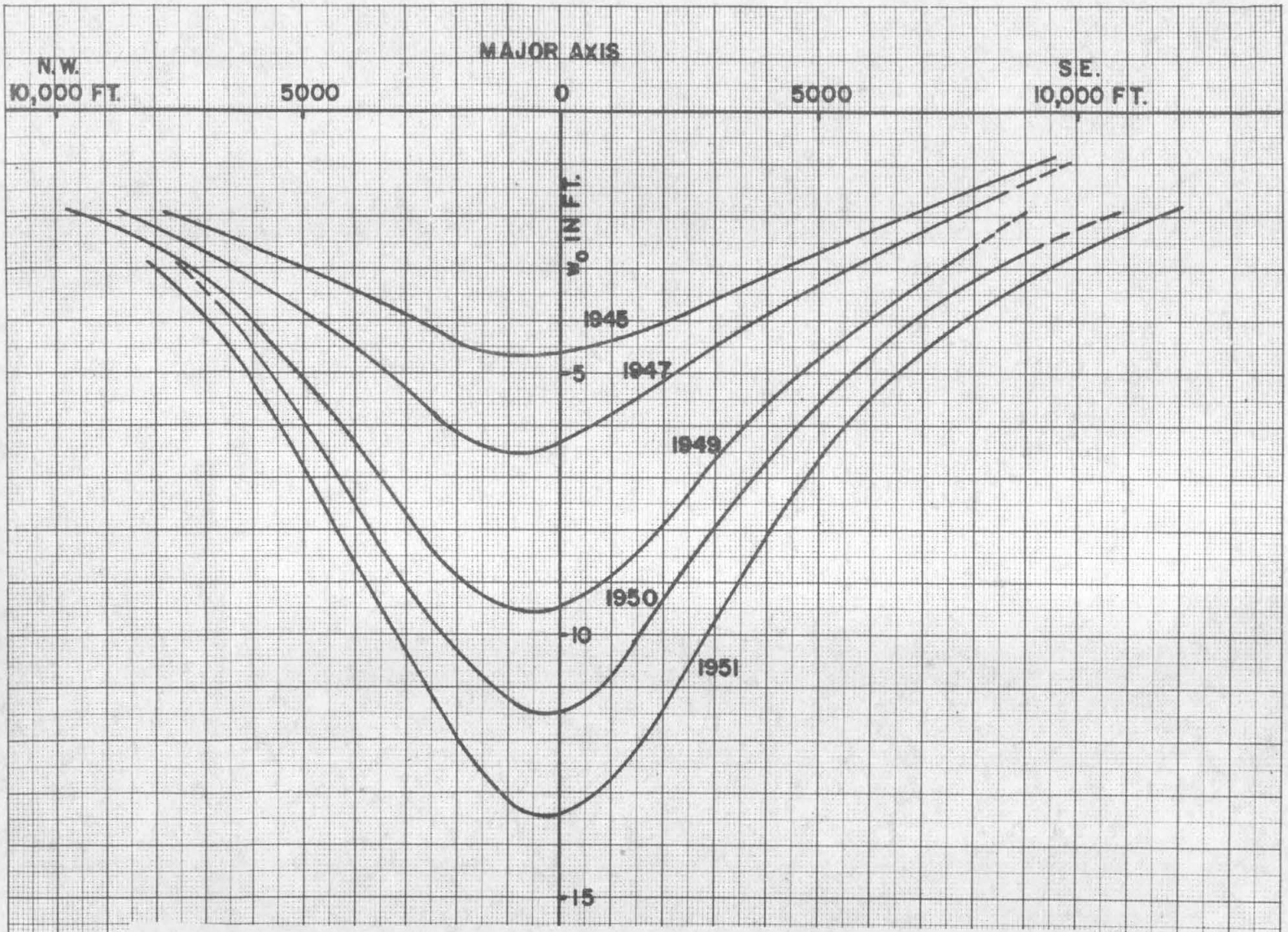

FIG.23 PROFILES OF ACTUAL MEASURED VERTICAL SUBSIDENCES (w_o) AT THE SURFACE AND ALONG THE MAJOR AXIS.

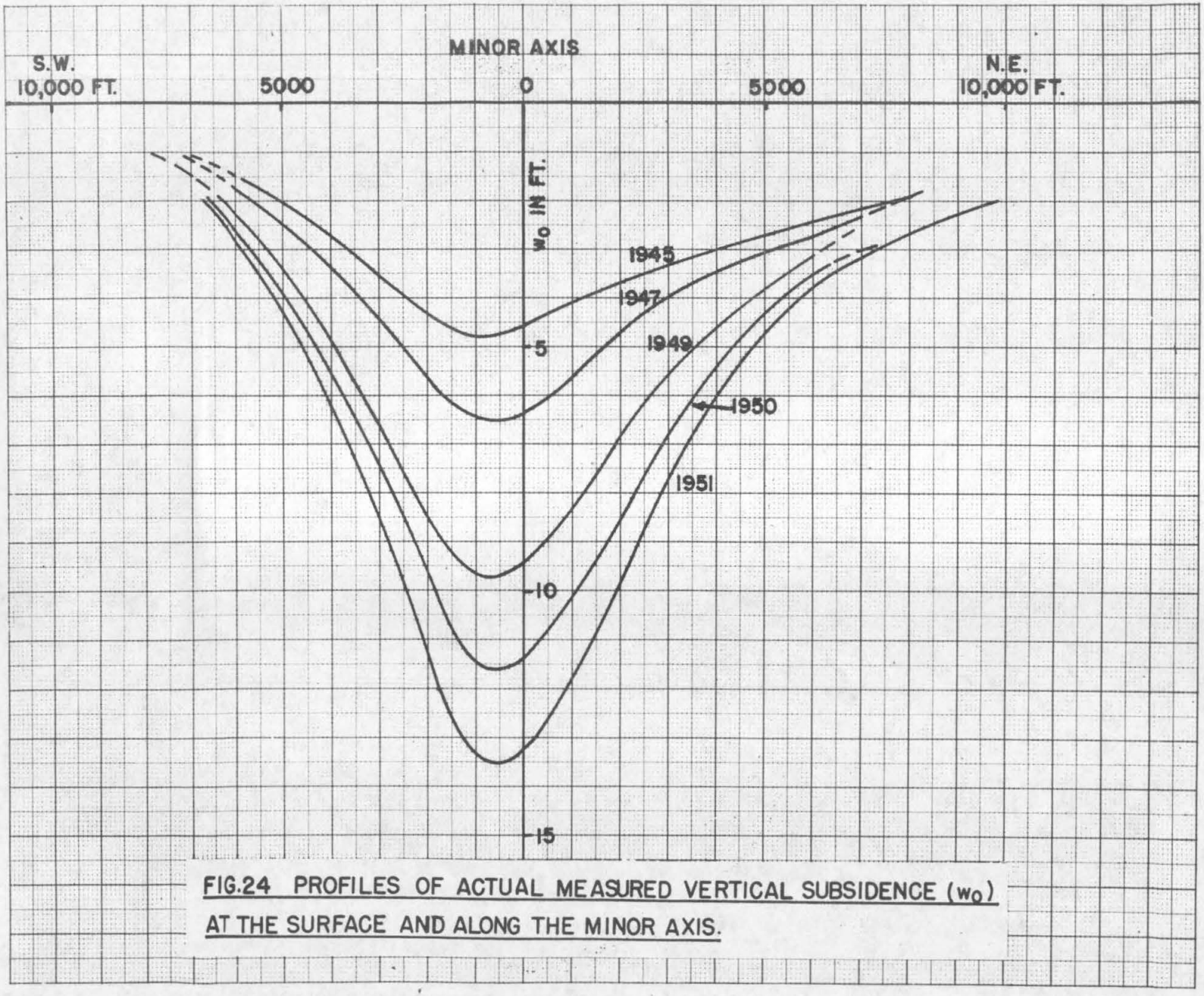

FIG.24 PROFILES OF ACTUAL MEASURED VERTICAL SUBSIDENCE (w_o) AT THE SURFACE AND ALONG THE MINOR AXIS.

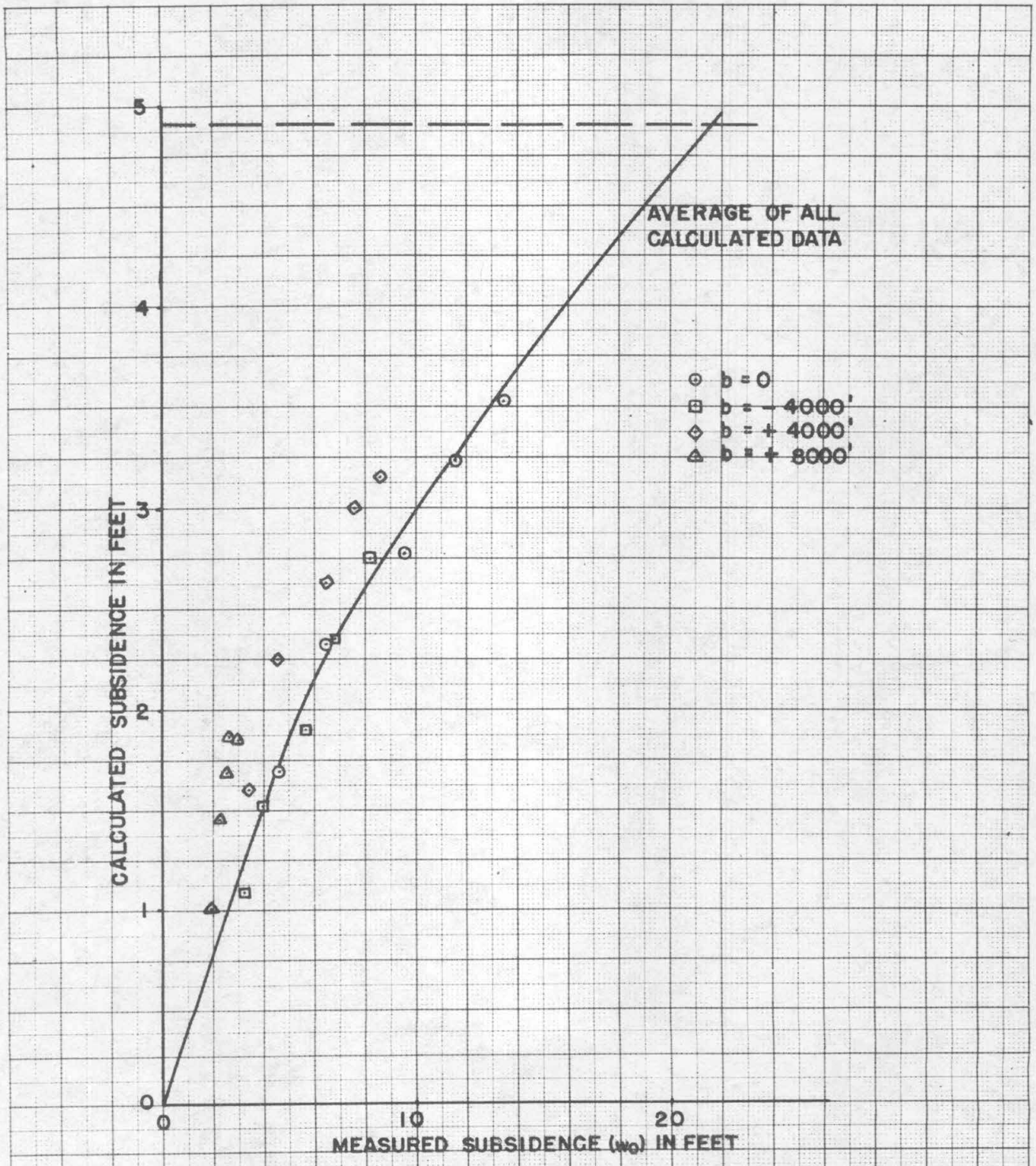

FIG. 25 COMPARISON OF MEASURED AND CALCULATED SUBSIDENCES AT VARIOUS LOCATIONS ALONG THE MAJOR AXIS. ORIGINAL ΔPxT. DATA.

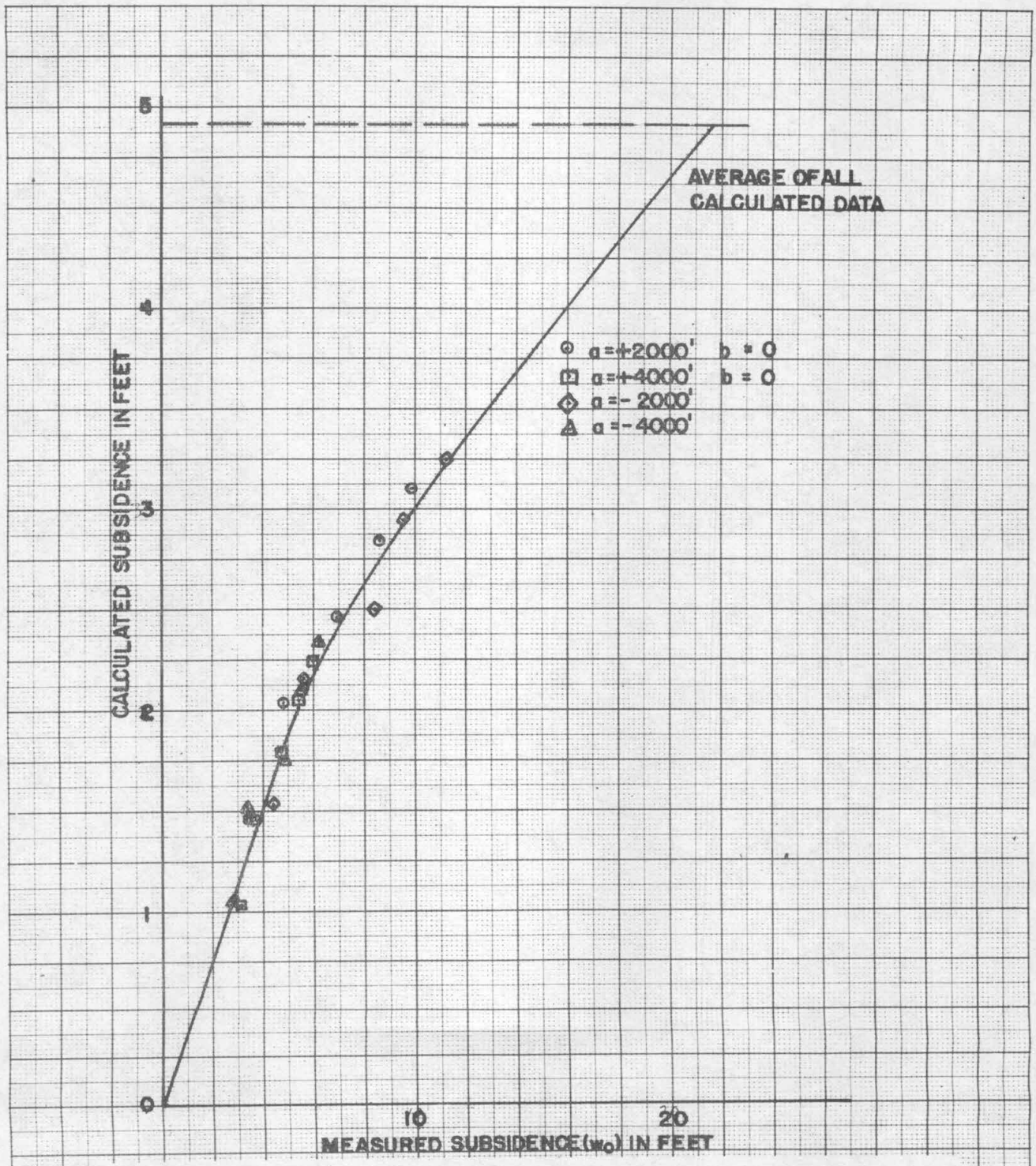

FIG. 26 COMPARISON OF MEASURED AND CALCULATED SUBSIDENCES AT VARIOUS LOCATIONS ALONG THE MINOR AXIS. ORIGINAL ΔPxT DATA.

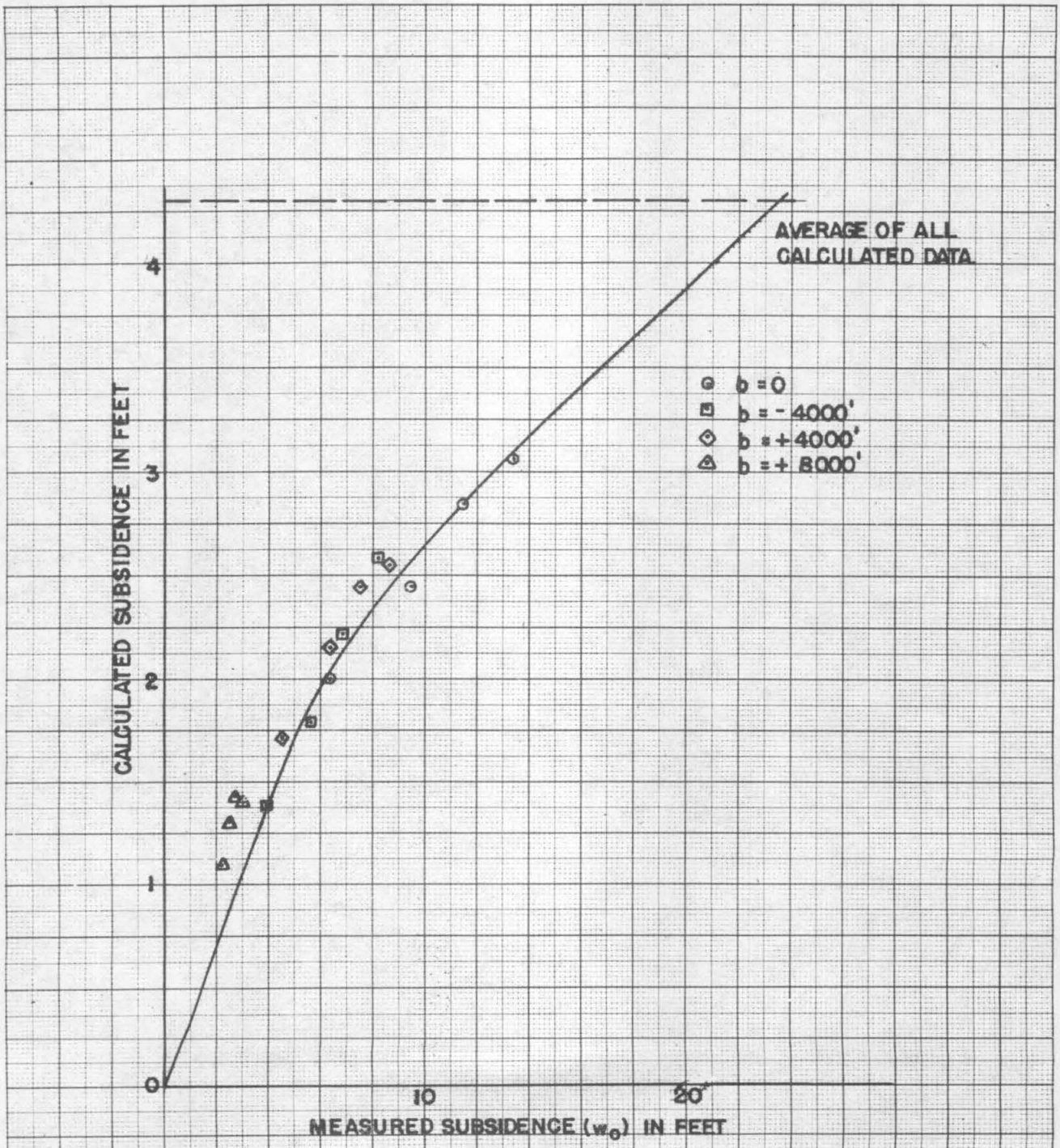

FIG. 27 COMPARISON OF MEASURED AND CALCULATED SUBSIDENCES AT VARIOUS LOCATIONS ALONG THE MAJOR AXIS. REVISED ΔPxT DATA

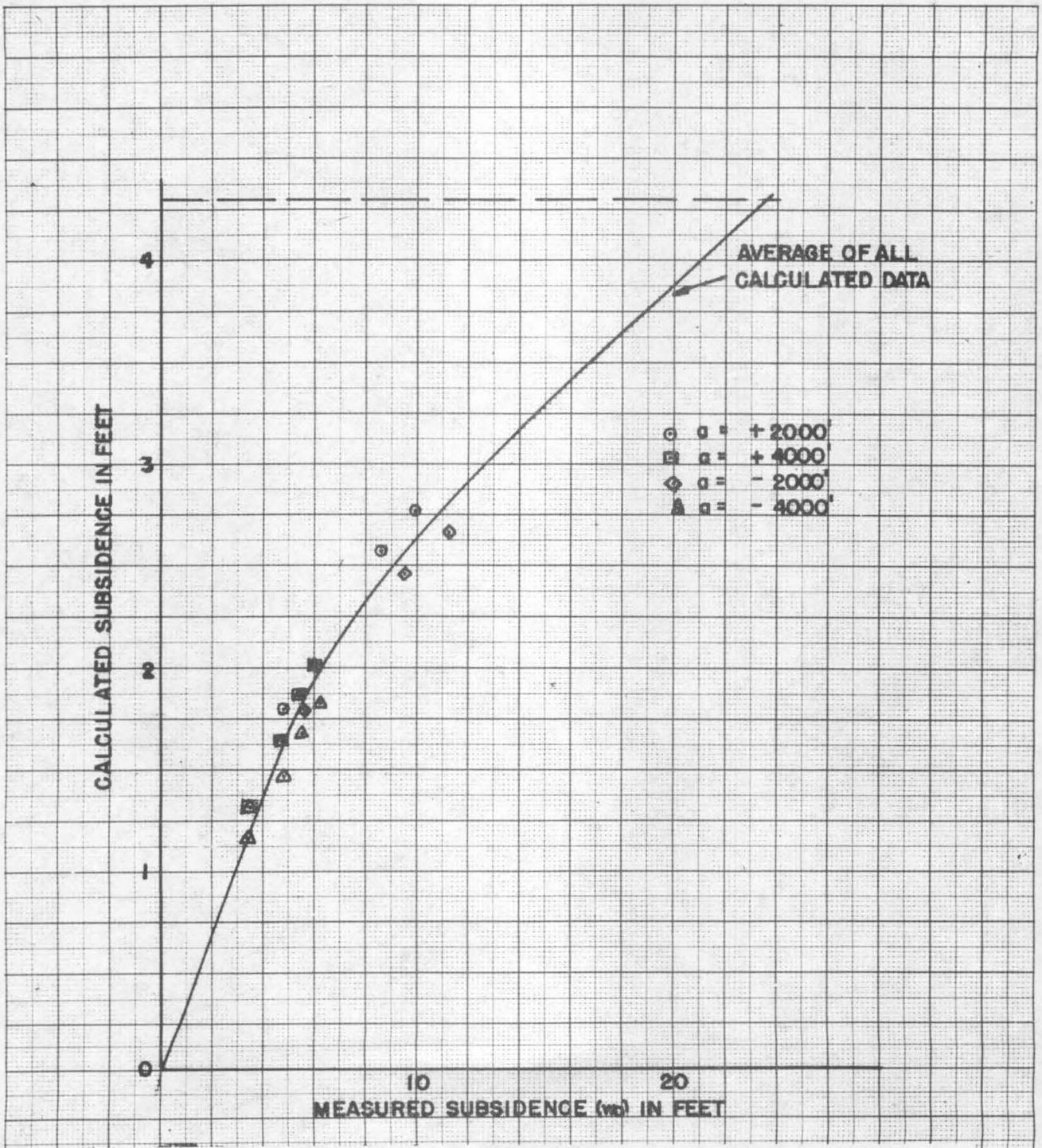

FIG. 28 COMPARISON OF MEASURED AND CALCULATED SUBSIDENCES AT VARIOUS LOCATIONS ALONG THE MINOR AXIS. REVISED ΔPxT DATA

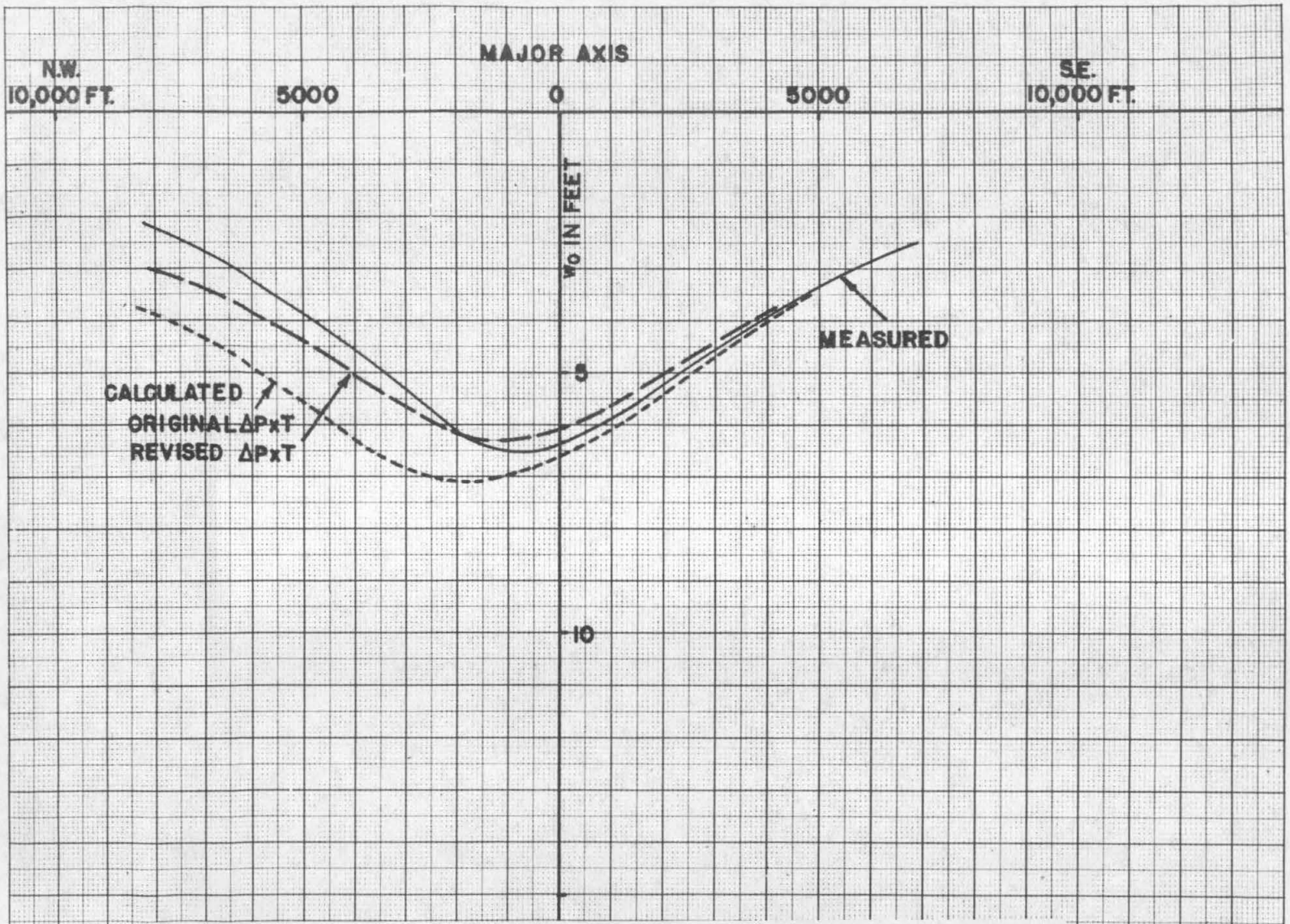

FIG.29 COMPARISON OF VERTICAL SUBSIDENCES OF 1947 ALONG MAJOR AXIS AS MEASURED AND AS CALCULATED FROM (ΔPxT) DATA.

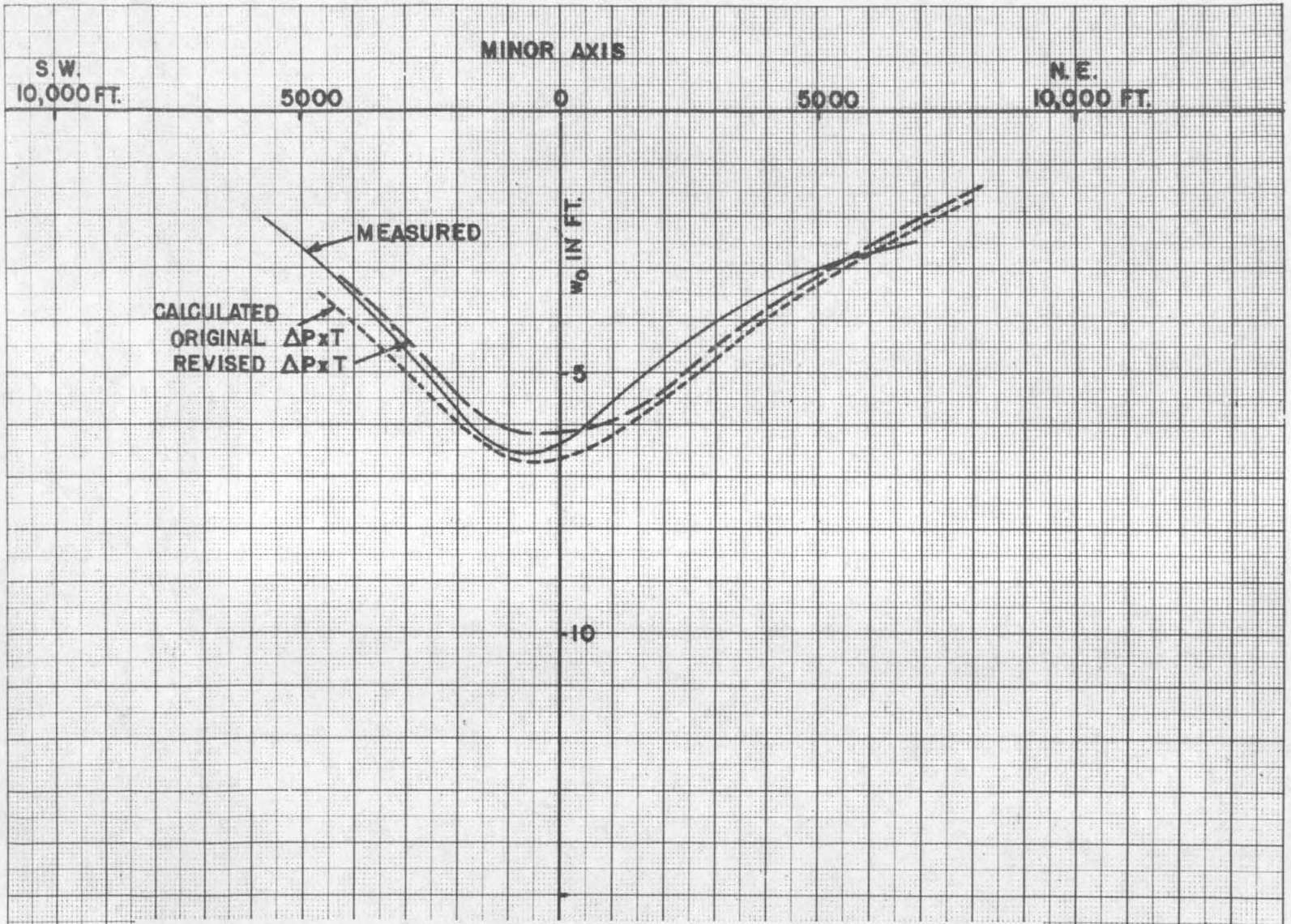

FIG.30 COMPARISON OF VERTICAL SUBSIDENCE OF 1947 ALONG MINOR AXIS AS MEASURED AND AS CALCULATED FROM (ΔPxT) DATA

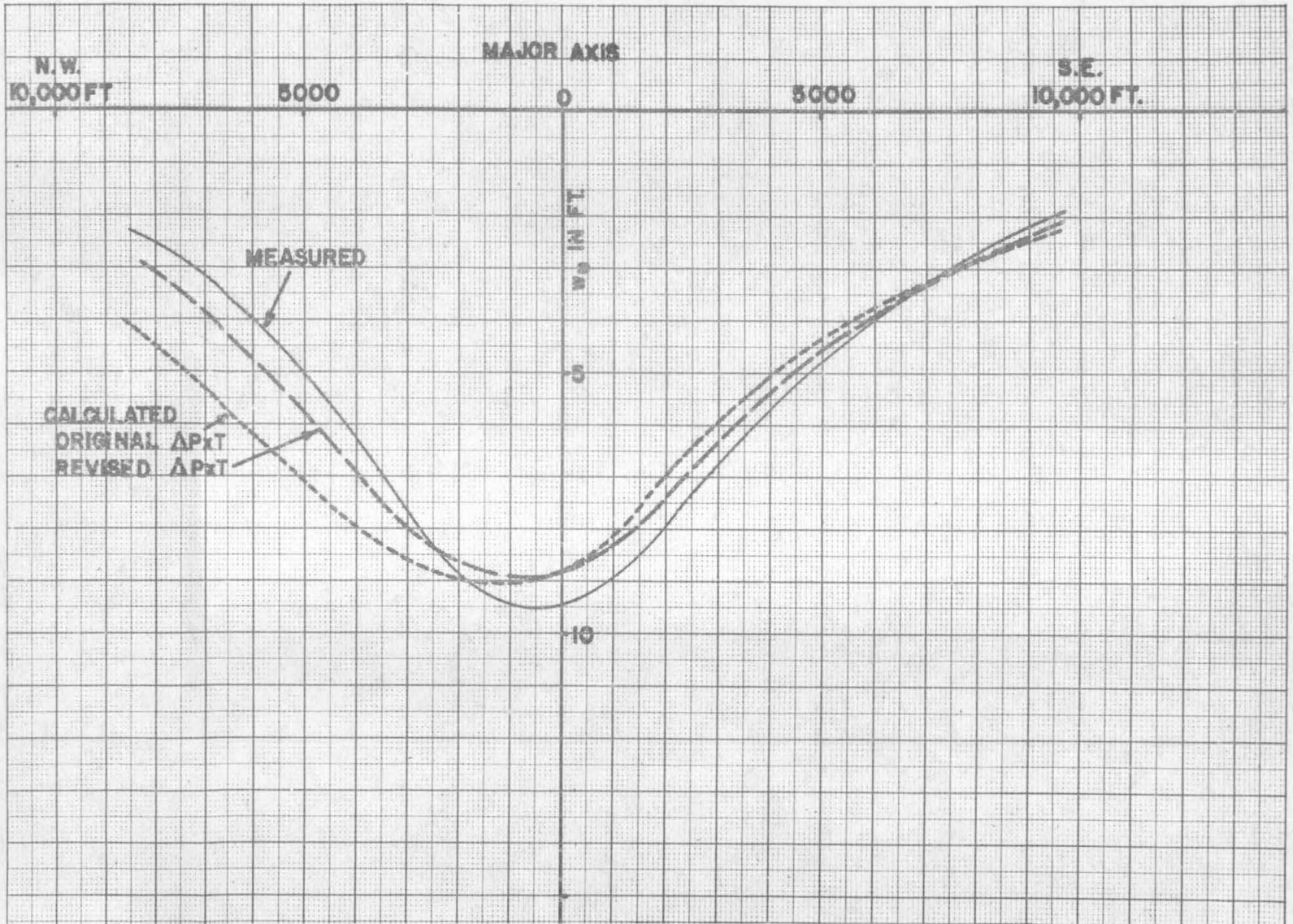

FIG.31 COMPARISON OF VERTICAL SUBSIDENCE OF 1949 ALONG MAJOR AXIS AS MEASURED AND AS CALCULATED FROM (ΔPxT) DATA.

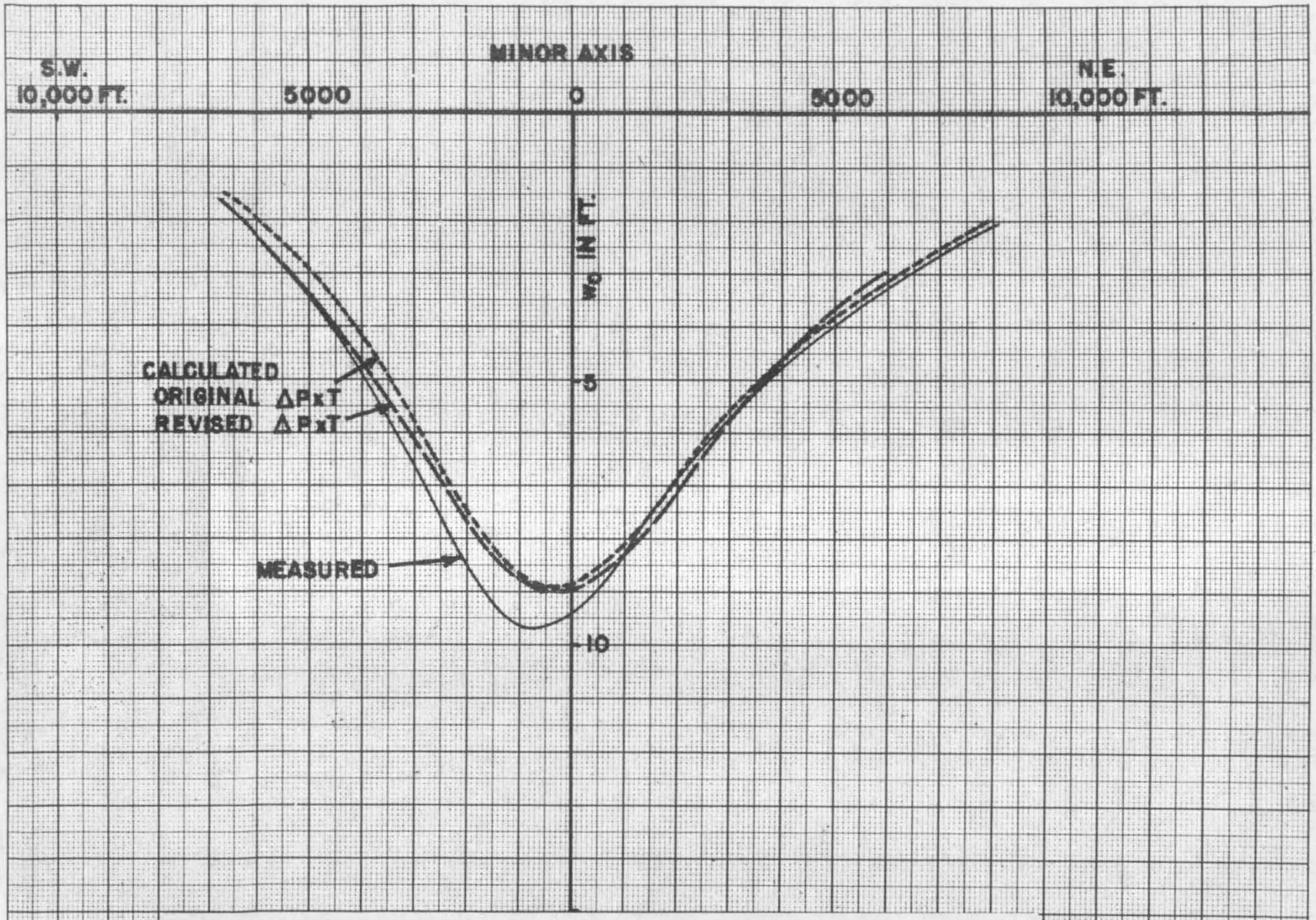

FIG.32 COMPARISON OF VERTICAL SUBSIDENCE OF 1949 ALONG MINOR AXIS AS MEASURED AND AS CALCULATED FROM (ΔPxT) DATA.

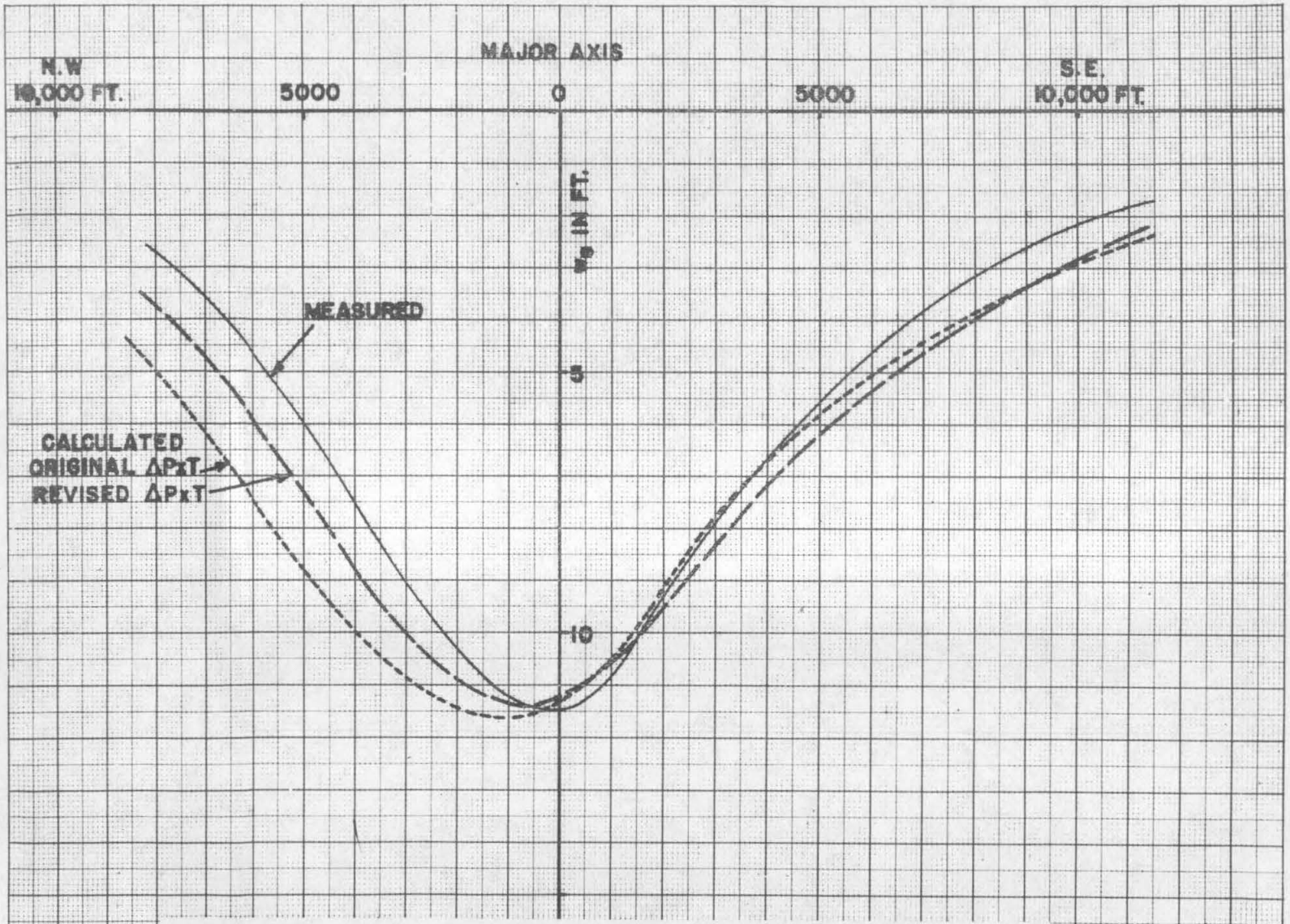

FIG.33 COMPARISON OF VERTICAL SUBSIDENCE OF 1950 ALONG MAJOR AXIS AS MEASURED AND AS CALCULATED FROM (ΔPxT) DATA.

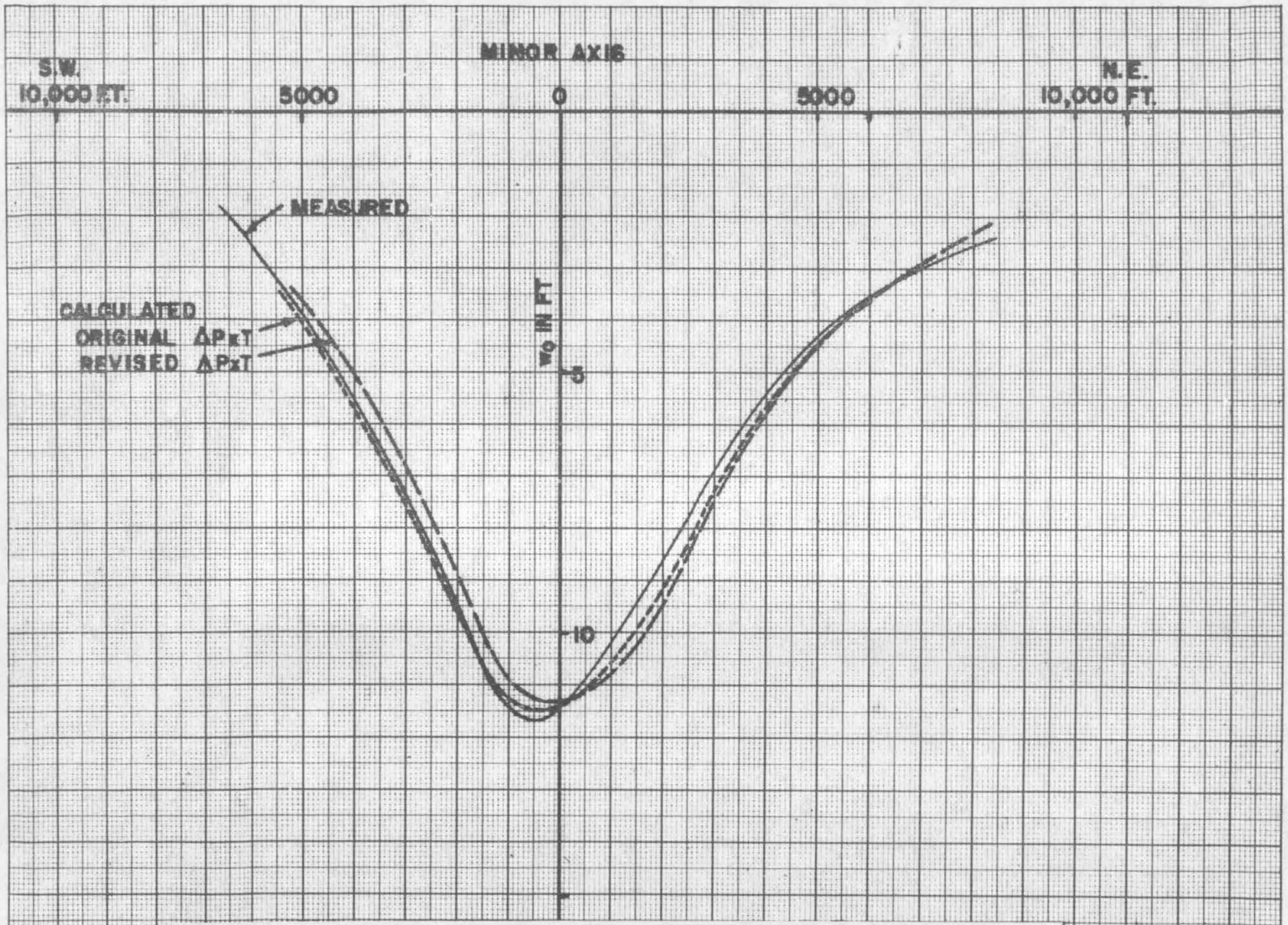

FIG. 34 COMPARISON OF VERTICAL SUBSIDENCE OF 1950 ALONG MINOR AXIS AS MEASURED AND AS CALCULATED FROM (ΔPxT) DATA.

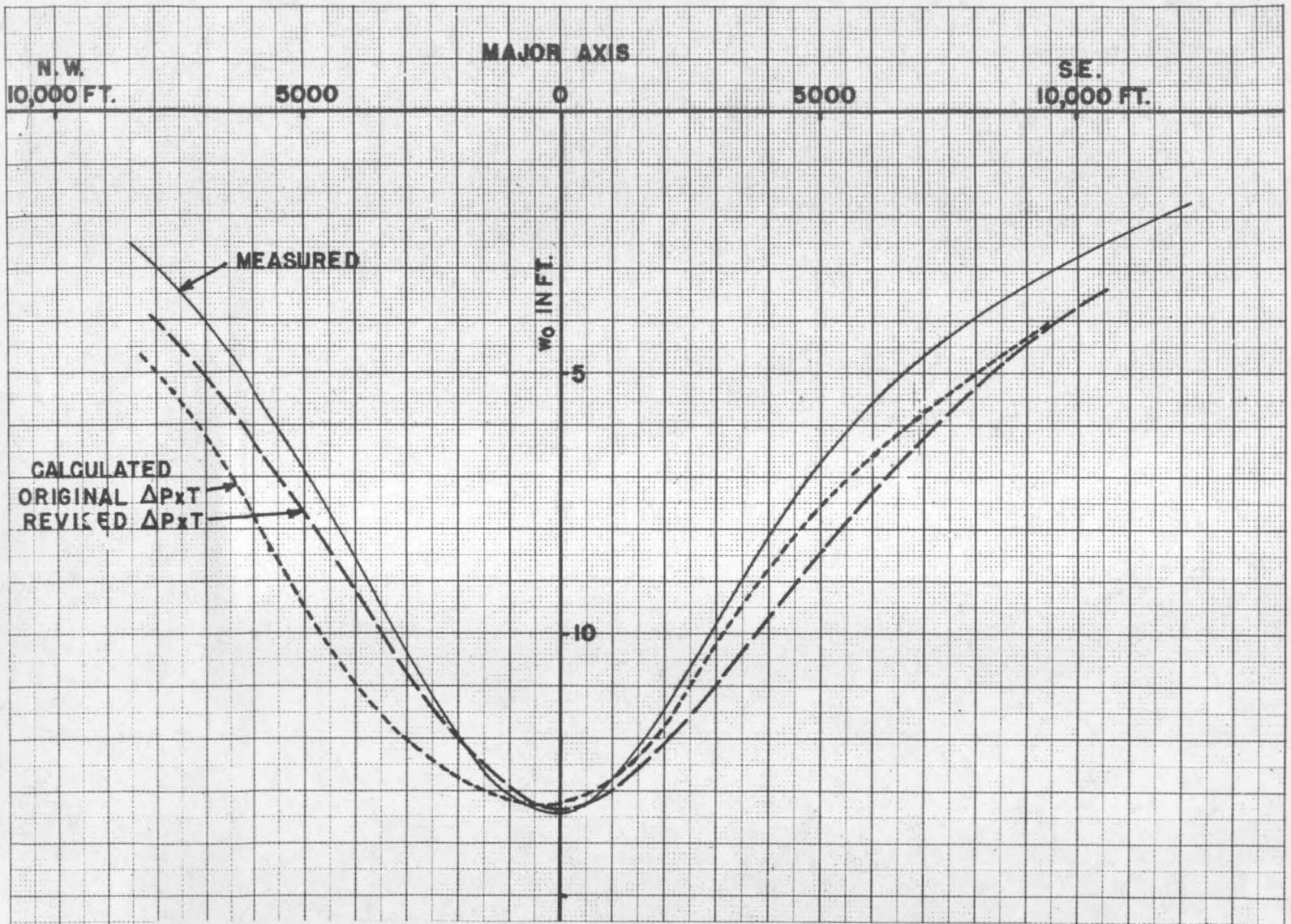

FIG. 35 COMPARISON OF VERTICAL SUBSIDENCE OF 1951 ALONG MAJOR AXIS AS MEASURED AND AS CALCULATED FROM (ΔPxT) DATA.

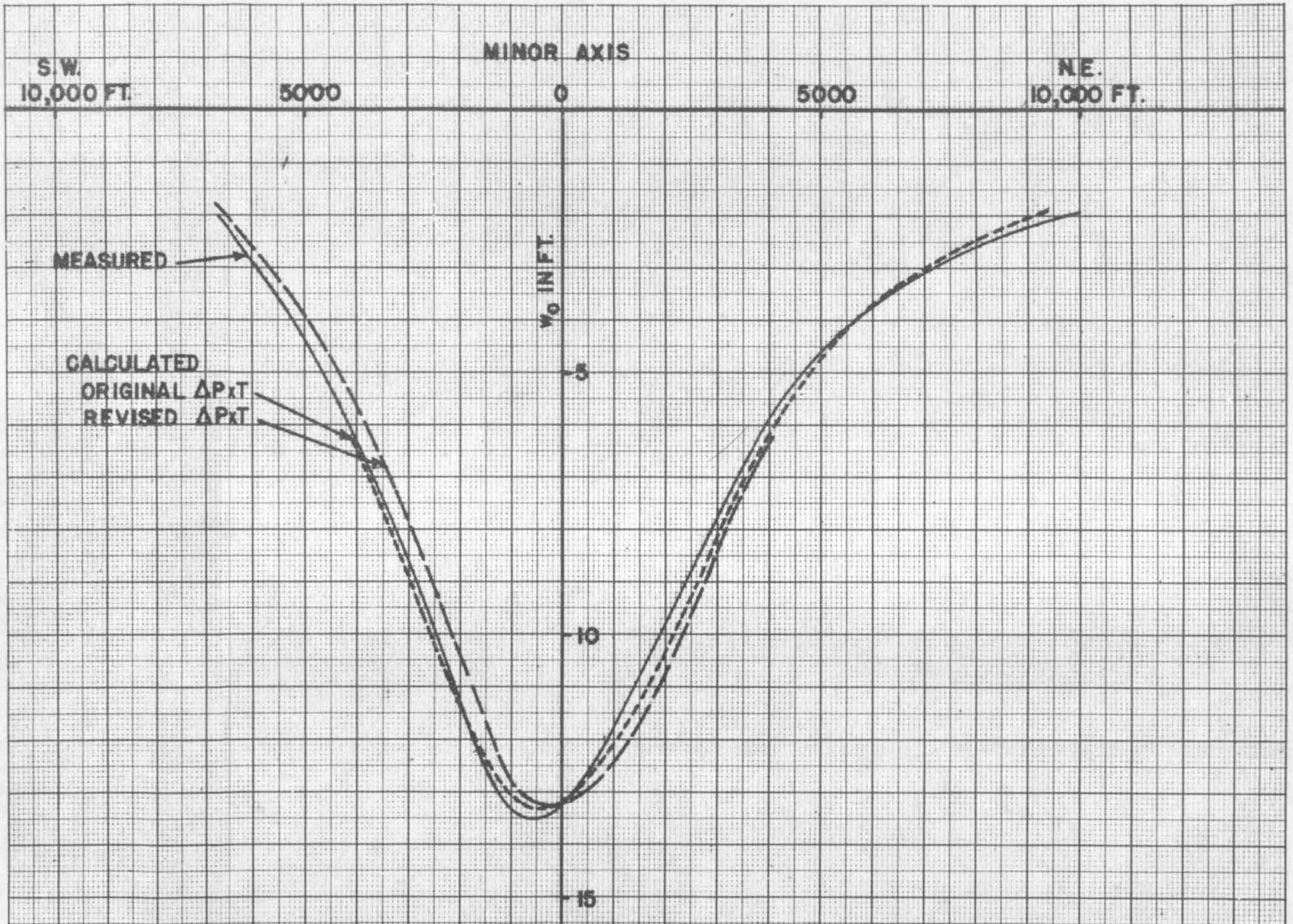

FIG. 36 COMPARISON OF VERTICAL SUBSIDENCE OF 1951 ALONG MINOR AXIS AS MEASURED AND AS CALCULATED FROM (ΔPxT) DATA.

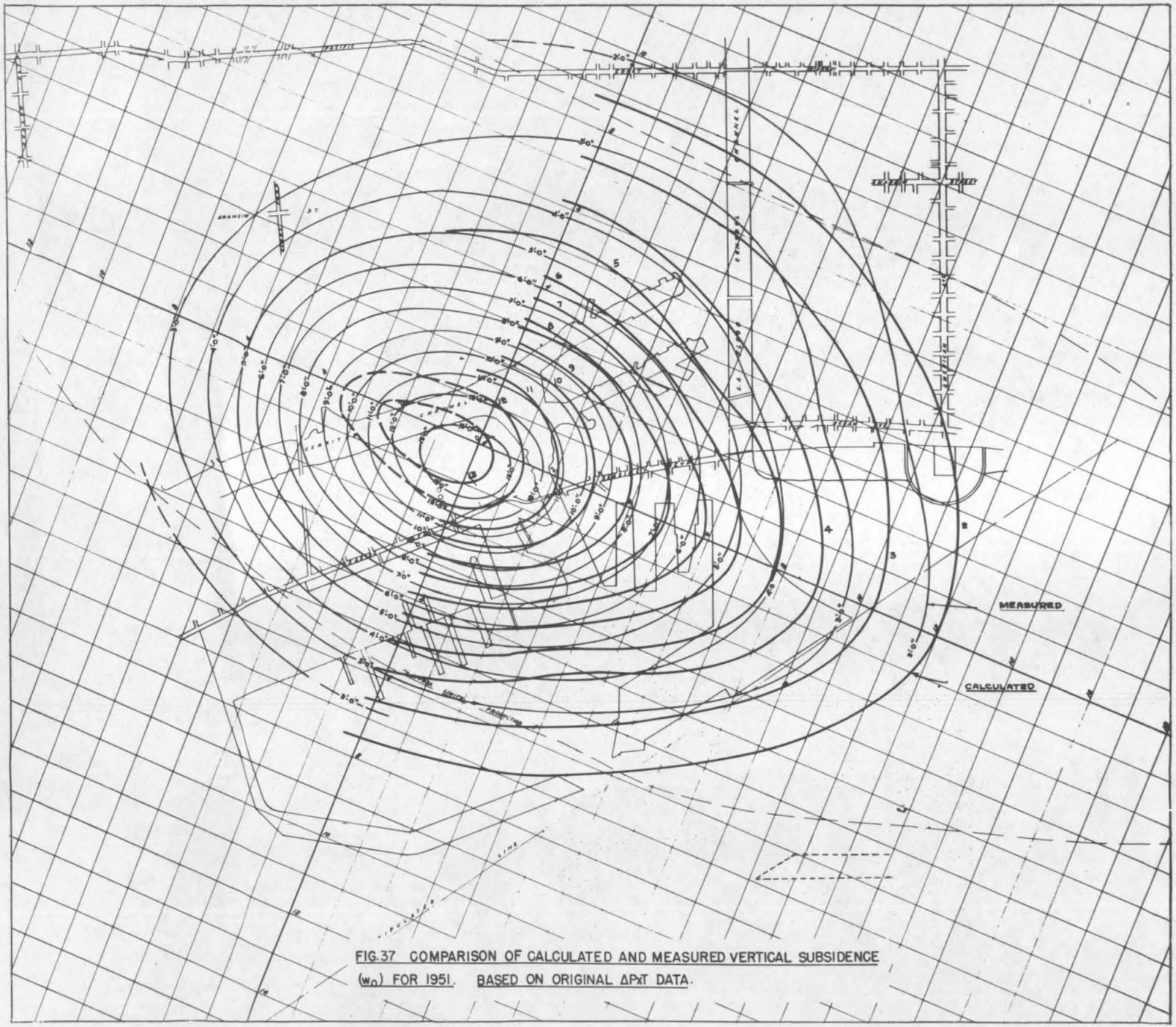

FIG.37 COMPARISON OF CALCULATED AND MEASURED VERTICAL SUBSIDENCE (w_o) FOR 1951. BASED ON ORIGINAL $\Delta P_x T$ DATA.

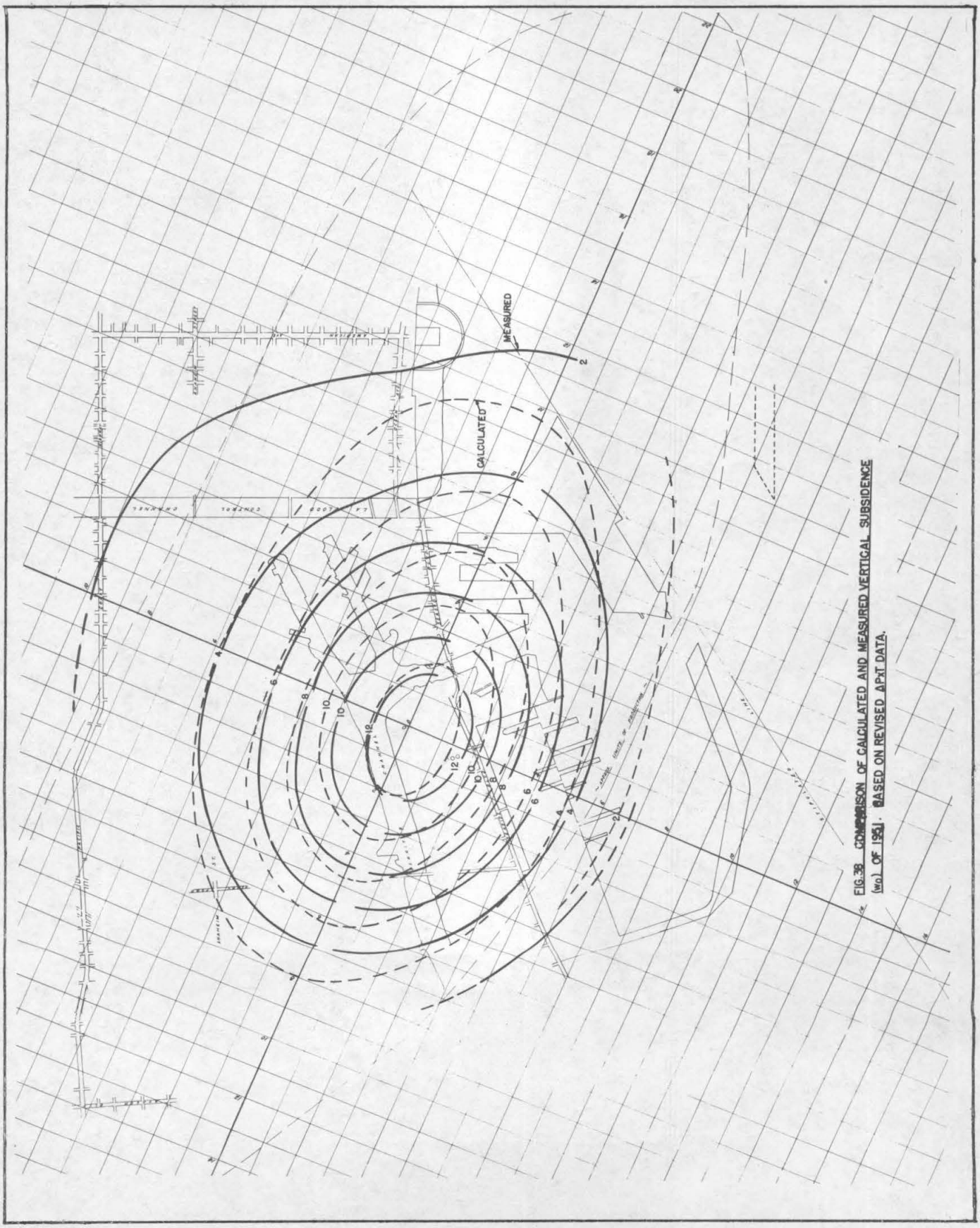

FIG.38 COMPARISON OF CALCULATED AND MEASURED VERTICAL SUBSIDENCE (m.) OF 1951. BASED ON REVISED A-P-T DATA.

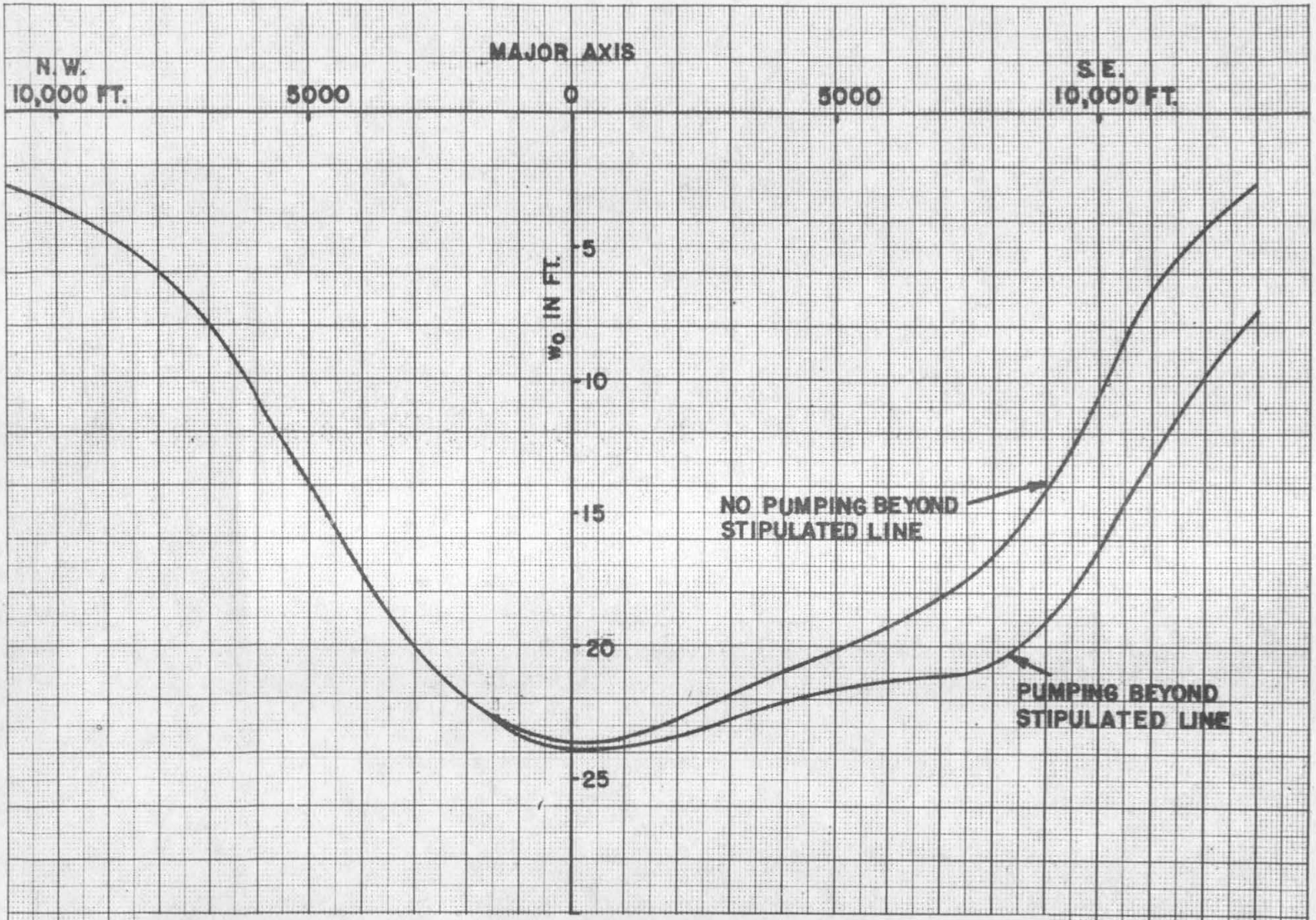

FIG. 39 VERTICAL SUBSIDENCE ALONG MAJOR AXIS AS CALCULATED FOR TWO PROPOSED ULTIMATE PUMPING SCHEDULES.

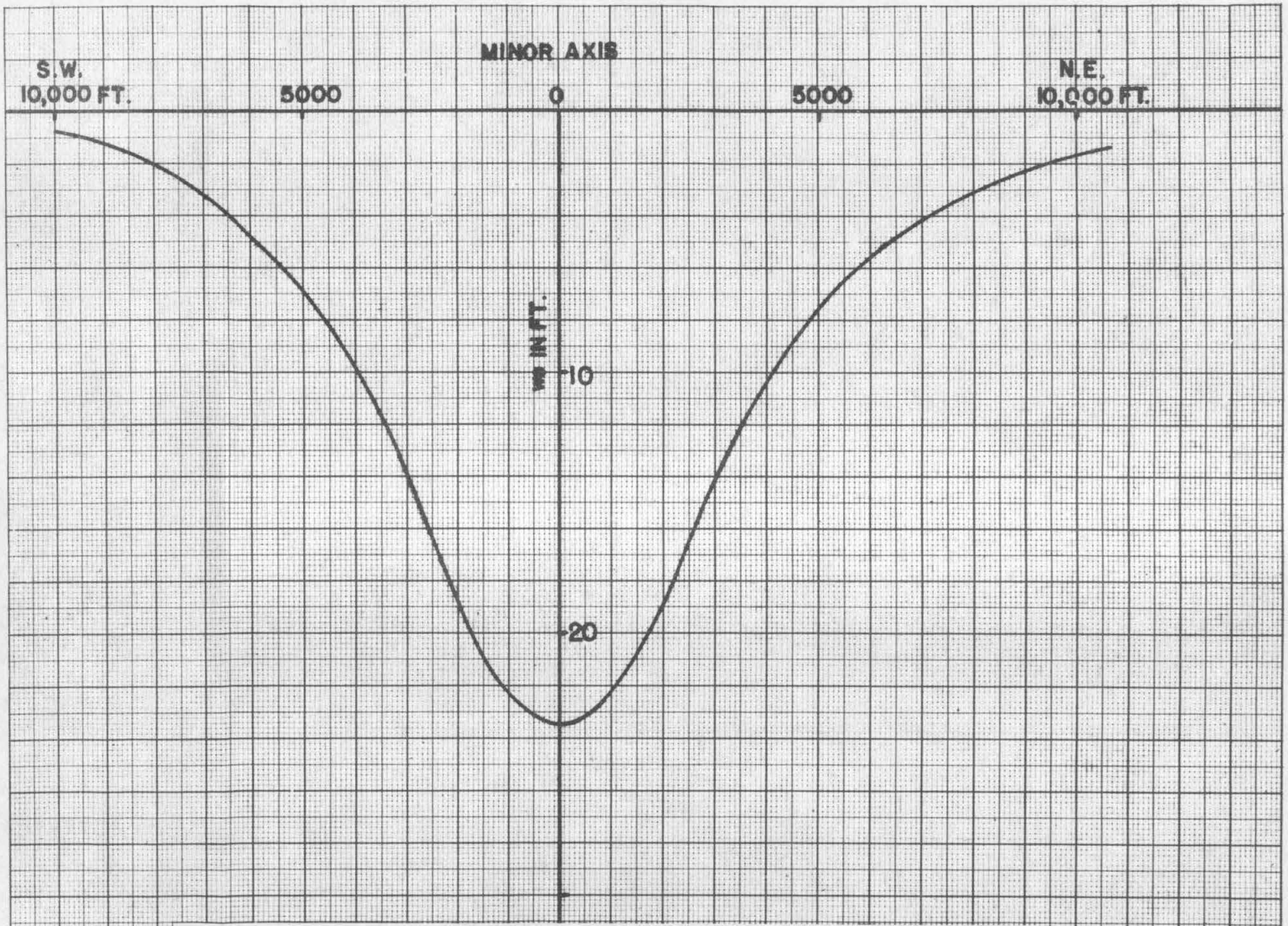

FIG. 40 VERTICAL SUBSIDENCE ALONG MINOR AXIS AS CALCULATED FOR BOTH PROPOSED ULTIMATE PUMPING SCHEDULES.

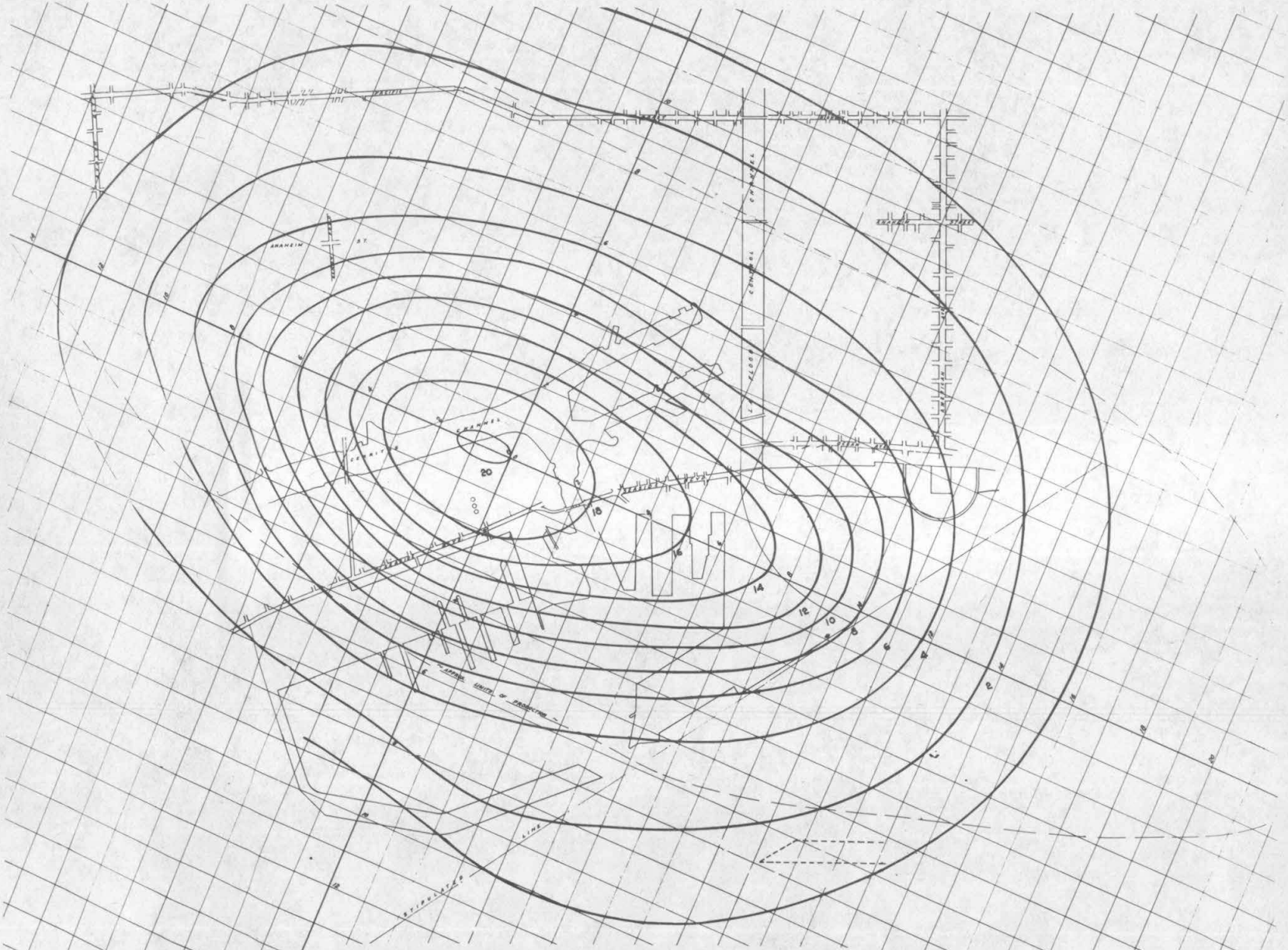

FIG. 41 CALCULATED VERTICAL SUBSIDENCE (w_o) IN FEET FOR PROPOSED ULTIMATE SCHEDULE OF PUMPING JUST TO THE STIPULATED LINE. ORIGINAL $\Delta P \times T$ DATA.

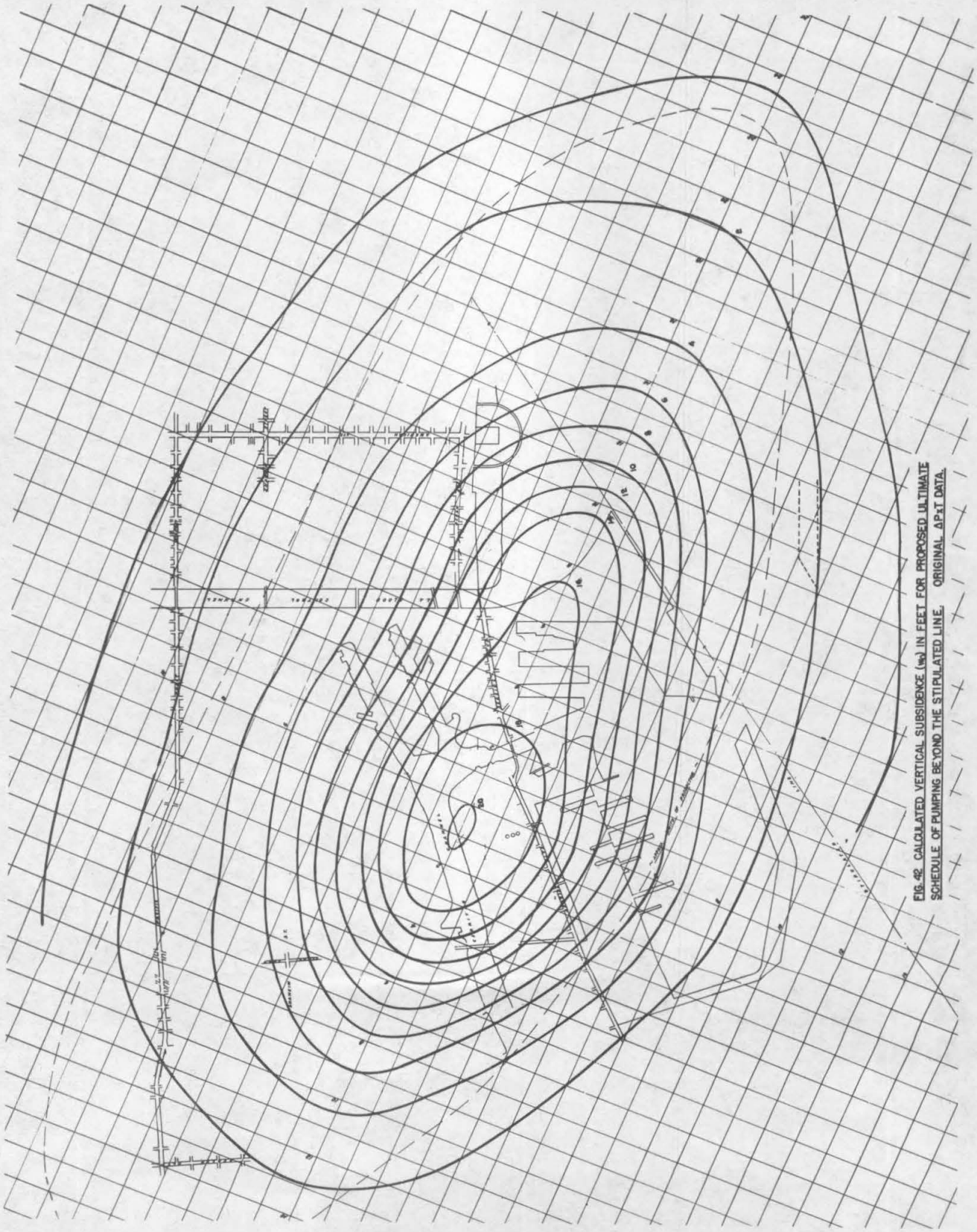

FIG. 42 CALCULATED VERTICAL SUBSIDENCE (w) IN FEET FOR PROPOSED ULTIMATE SCHEDULE OF PUMPING BEYOND THE STIPULATED LINE. ORIGINAL $\Delta P_2 T$ DATA.

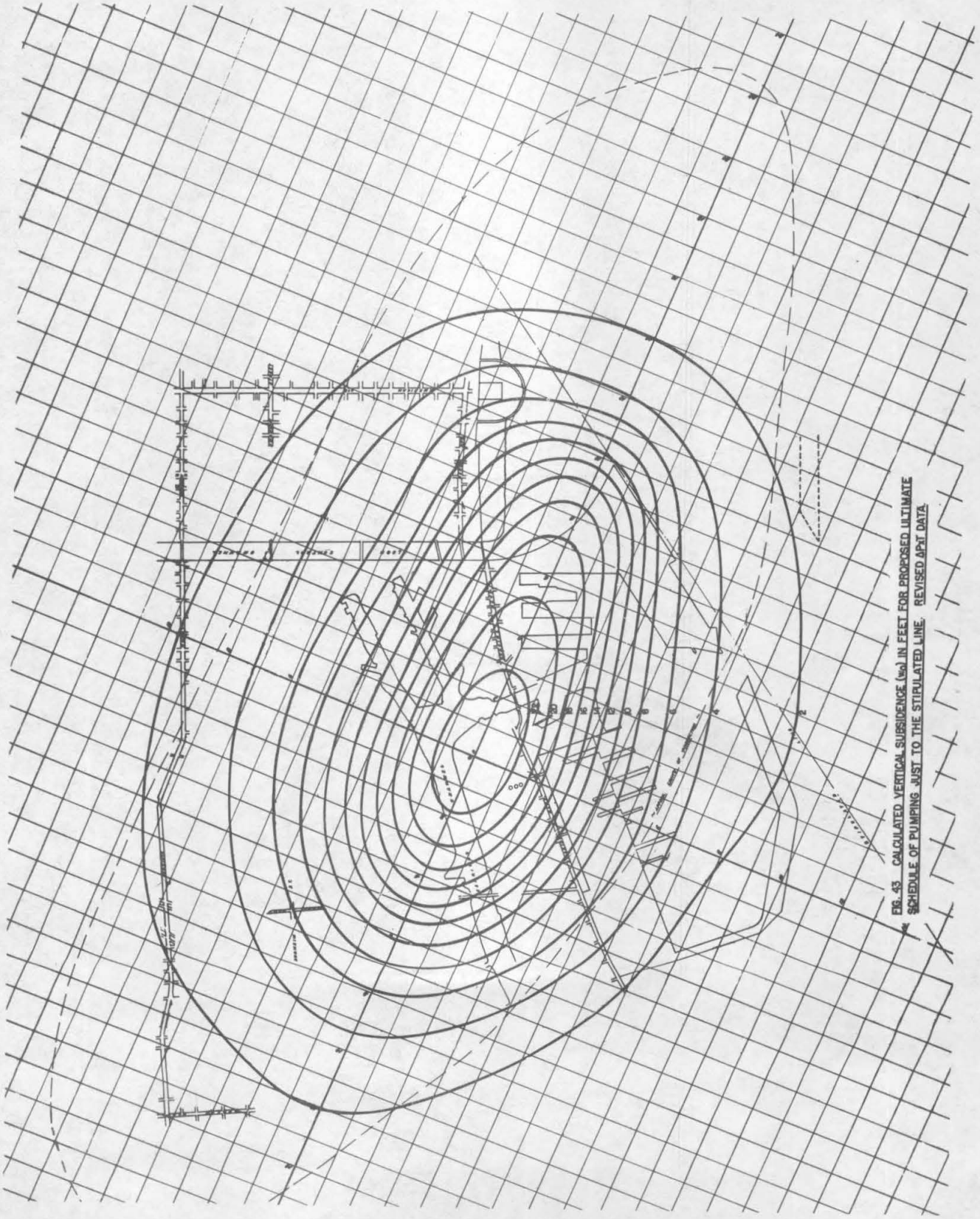

FIG. 43 CALCULATED VERTICAL SUBSIDENCE (ω) IN FEET FOR PROPOSED ULTIMATE SCHEDULE OF PUMPING JUST TO THE STIPULATED LINE. REVISED APT DATA

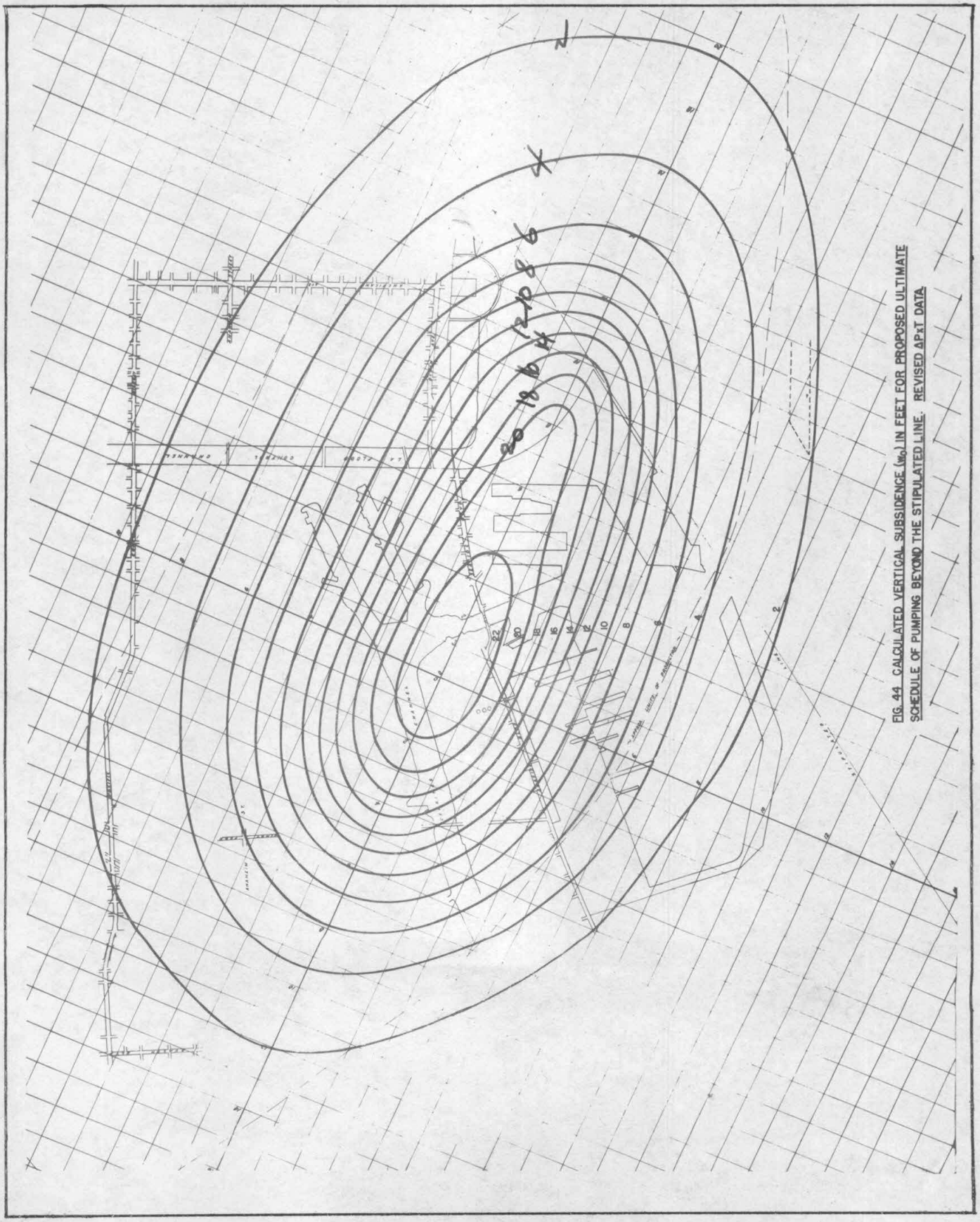

FIG. 44 CALCULATED VERTICAL SUBSIDENCE (w_0) IN FEET FOR PROPOSED ULTIMATE SCHEDULE OF PUMPING BEYOND THE STIPULATED LINE. REVISED ΔPxT DATA

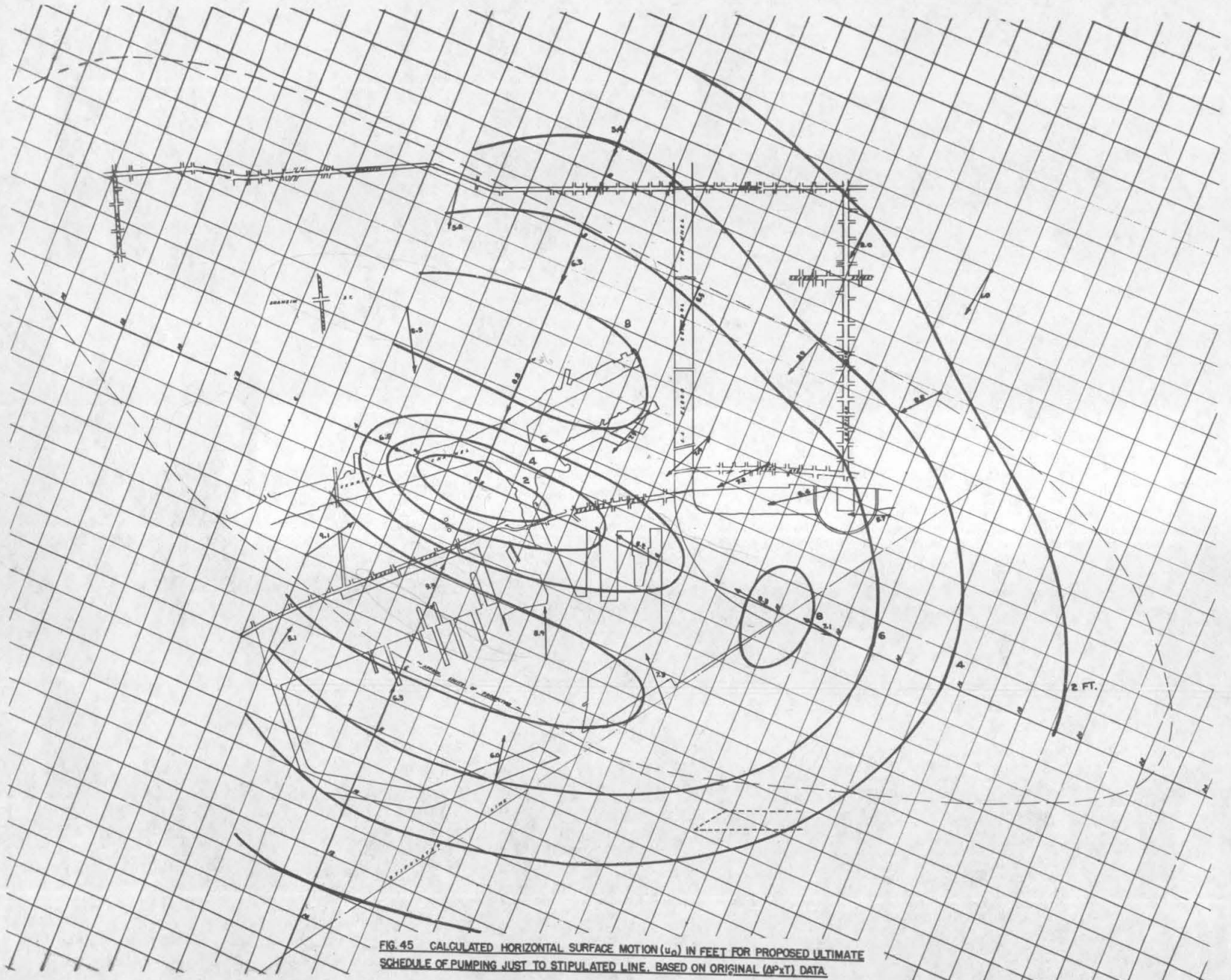

FIG. 45 CALCULATED HORIZONTAL SURFACE MOTION (u_o) IN FEET FOR PROPOSED ULTIMATE SCHEDULE OF PUMPING JUST TO STIPULATED LINE, BASED ON ORIGINAL ($\Delta P \times T$) DATA.

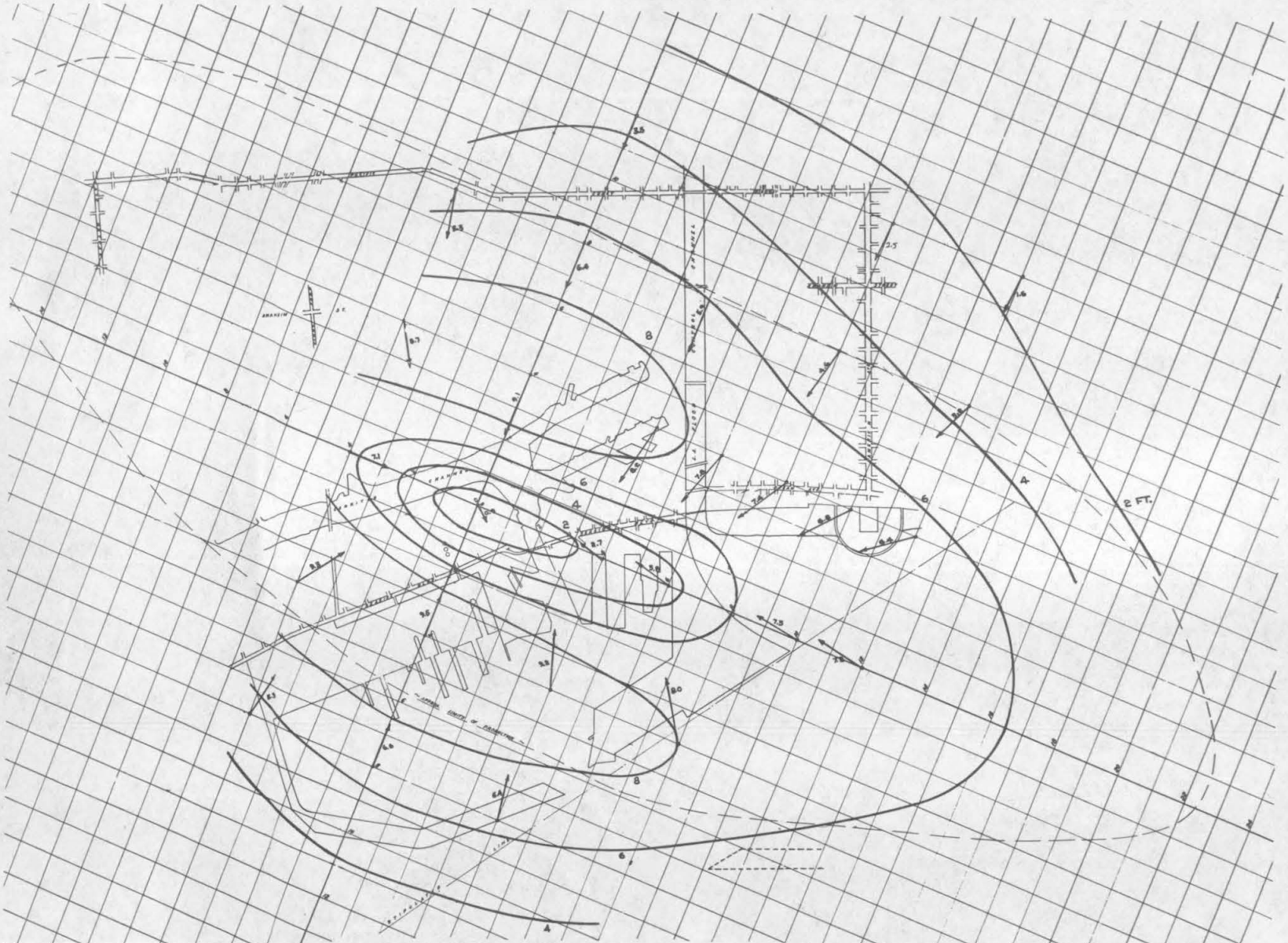

FIG. 46 CALCULATED HORIZONTAL SURFACE MOTION (u_o) IN FEET FOR PROPOSED ULTIMATE SCHEDULE OF PUMPING BEYOND STIPULATED LINE. BASED ON ORIGINAL $\Delta P_x T$ DATA.

FIG. 47 CALCULATED HORIZONTAL SHEAR STRESSES (IN P.S.I.) FROM 1950 DATA AND AT A DEPTH OF 1200 FEET. G = 120,000 P.S.I.

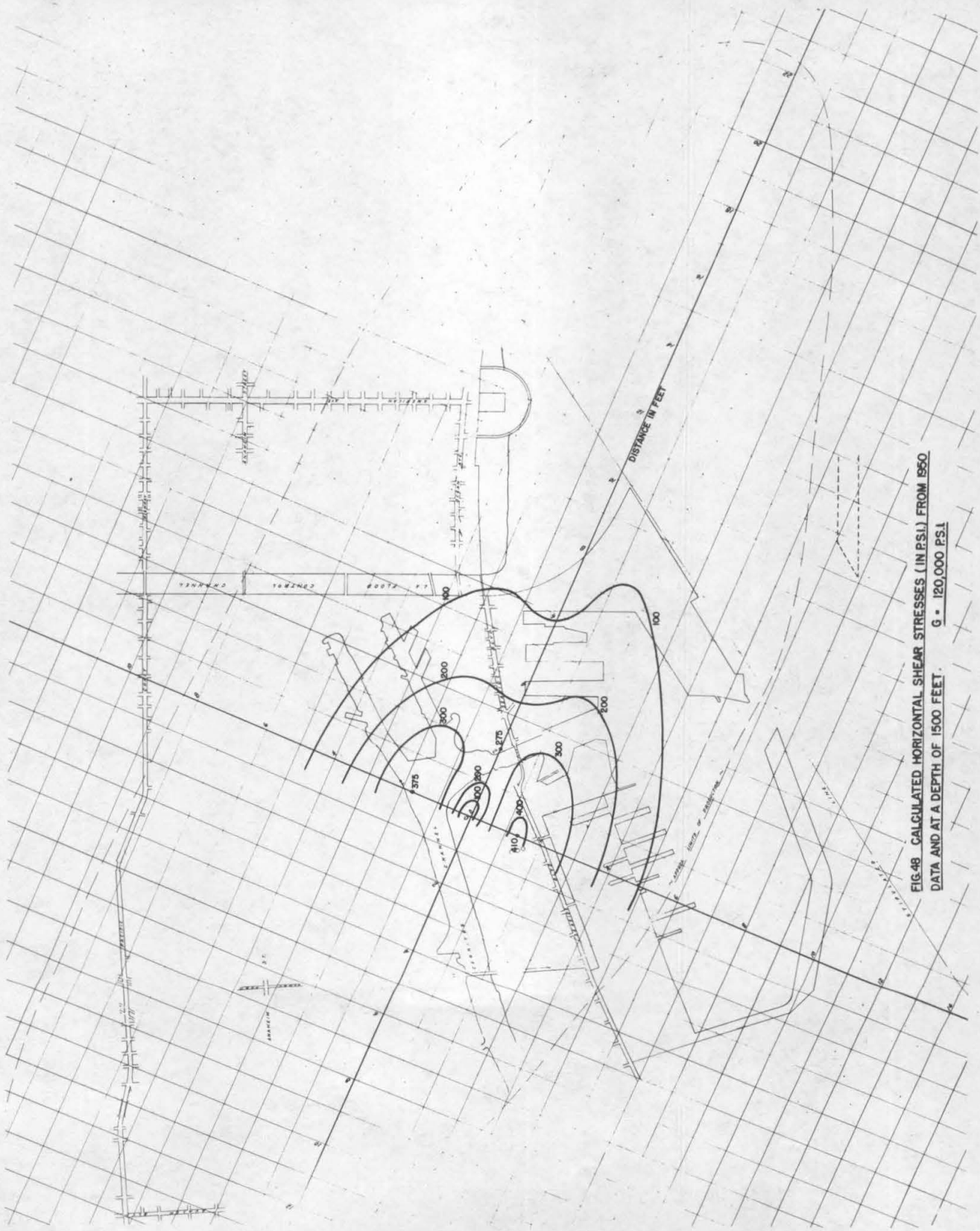

FIG.48 CALCULATED HORIZONTAL SHEAR STRESSES (IN P.S.I.) FROM 1950 DATA AND AT A DEPTH OF 1500 FEET. G = 120,000 P.S.I.

FIG. 49 CALCULATED HORIZONTAL SHEAR STRESSES (IN P.S.I.) FROM 1950 AND AT A DEPTH OF 1800 FEET. G = 120,000 P.S.I.

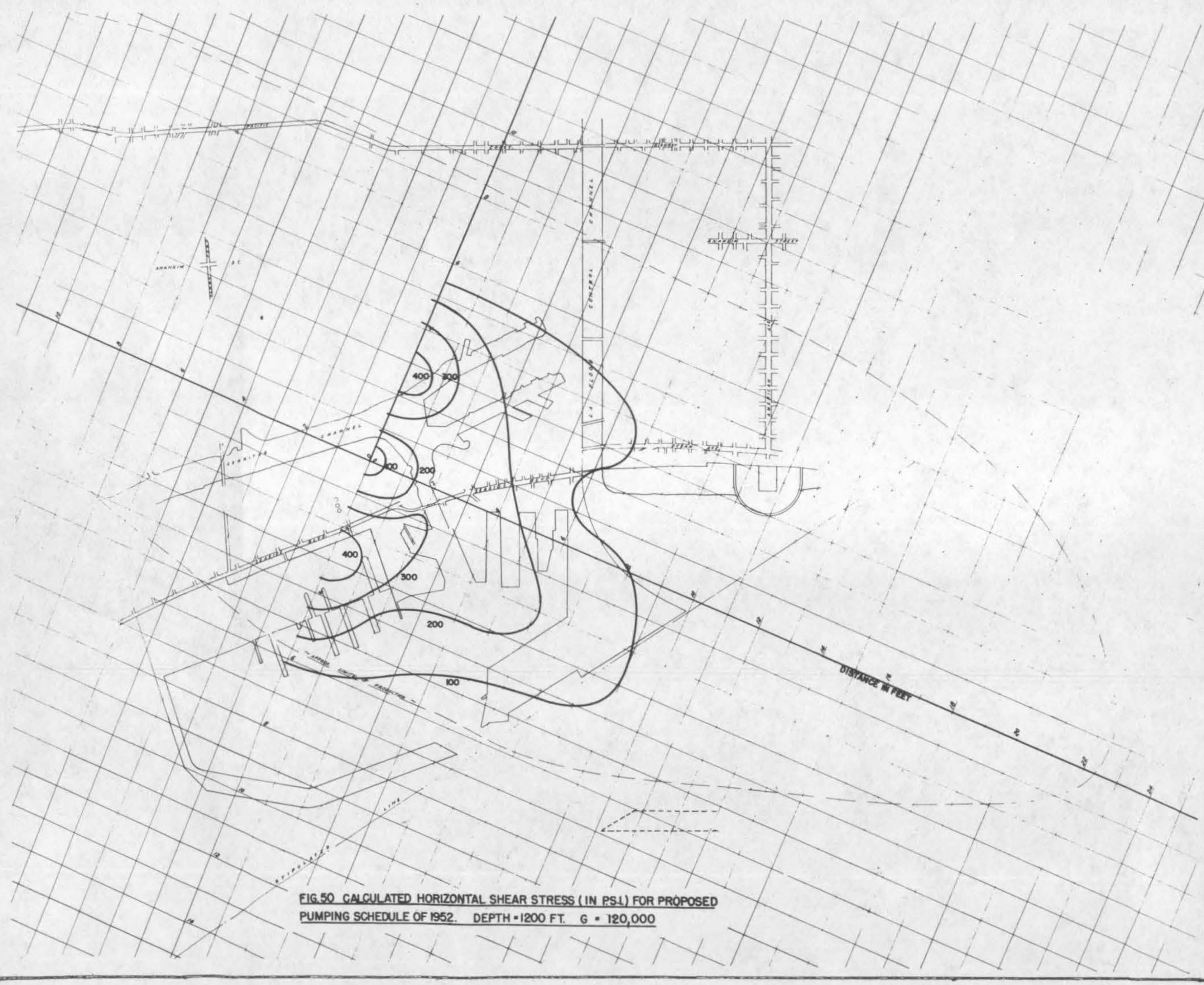

FIG. 50 CALCULATED HORIZONTAL SHEAR STRESS (IN P.S.I.) FOR PROPOSED PUMPING SCHEDULE OF 1952. DEPTH = 1200 FT. G = 120,000

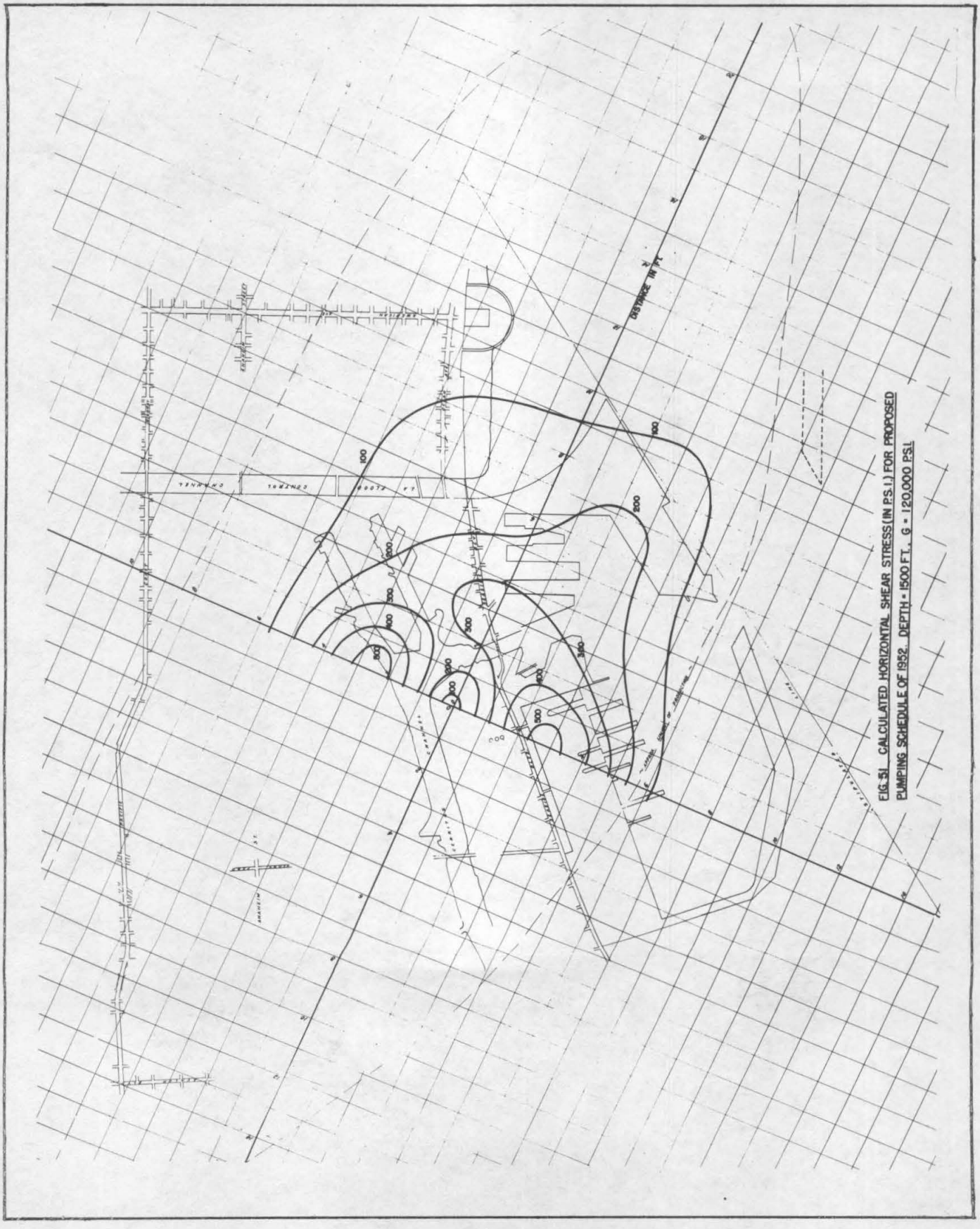

FIG. 51 CALCULATED HORIZONTAL SHEAR STRESS (IN P.S.I.) FOR PROPOSED PUMPING SCHEDULE OF 1952. DEPTH = 1500 FT., G = 120,000 PSI.

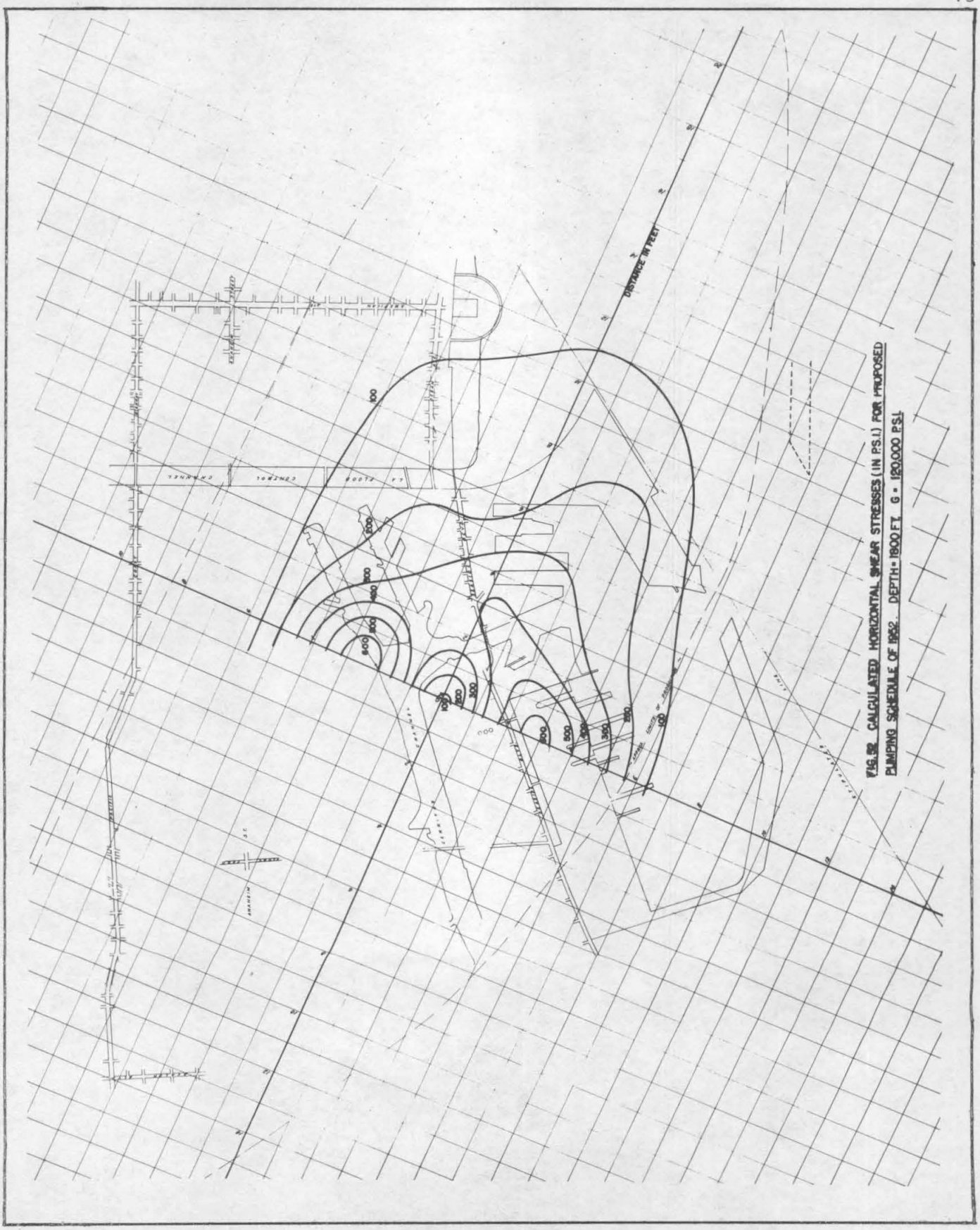

FIG. 52. CALCULATED HORIZONTAL SHEAR STRESSES (IN P.S.I.) FOR PROPOSED PUMPING SCHEDULE OF 1952. DEPTH = 1800 FT. G = 120,000 P.S.I.

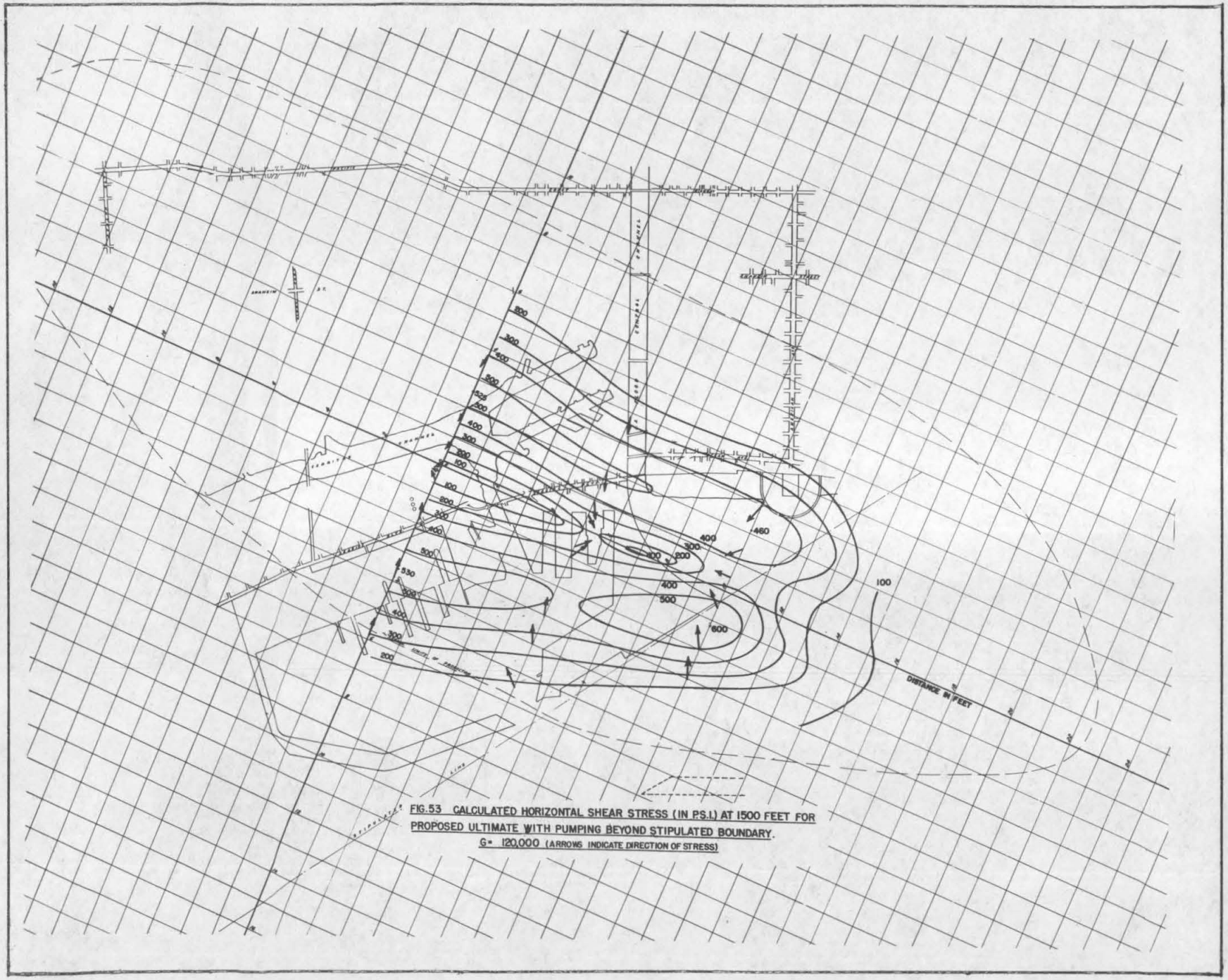

FIG. 53 CALCULATED HORIZONTAL SHEAR STRESS (IN P.S.I.) AT 1500 FEET FOR PROPOSED ULTIMATE WITH PUMPING BEYOND STIPULATED BOUNDARY.
G= 120,000 (ARROWS INDICATE DIRECTION OF STRESS)

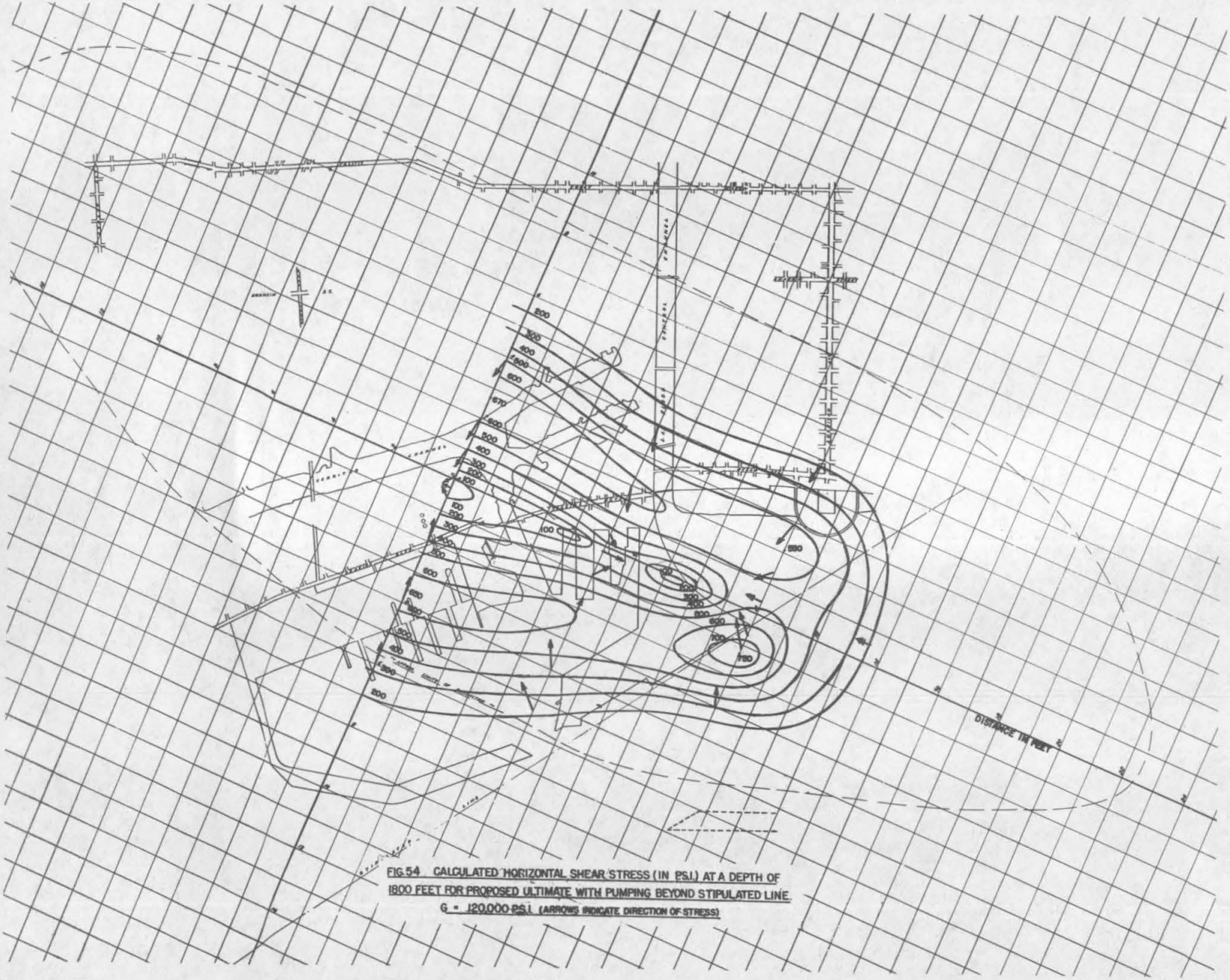

FIG. 54 CALCULATED HORIZONTAL SHEAR STRESS (IN P.S.I.) AT A DEPTH OF 1800 FEET FOR PROPOSED ULTIMATE WITH PUMPING BEYOND STIPULATED LINE. G = 120,000 P.S.I. (ARROWS INDICATE DIRECTION OF STRESS)

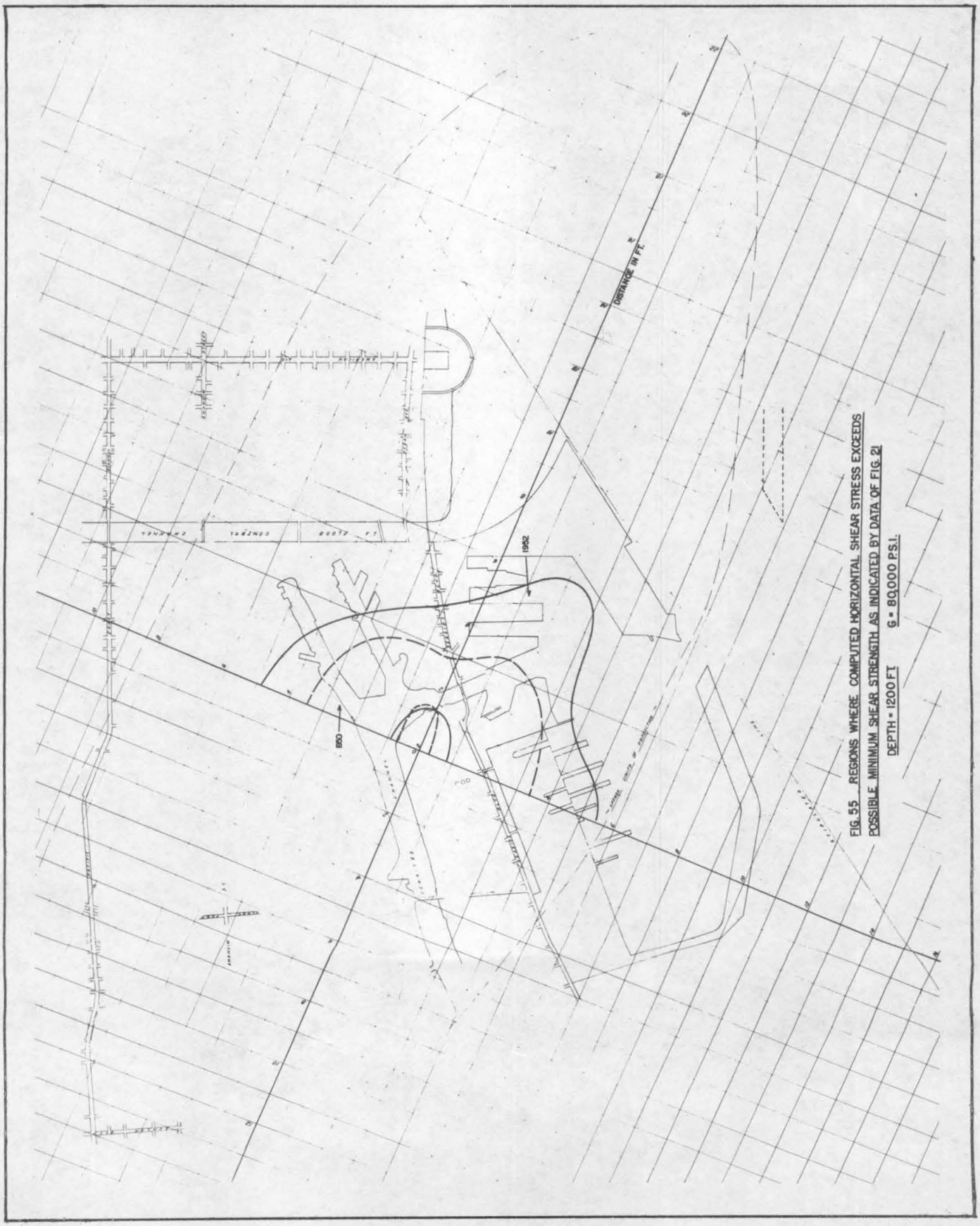

FIG. 55 REGIONS WHERE COMPUTED HORIZONTAL SHEAR STRESS EXCEEDS POSSIBLE MINIMUM SHEAR STRENGTH AS INDICATED BY DATA OF FIG. 21

DEPTH = 1200 FT G = 80,000 P.S.I.

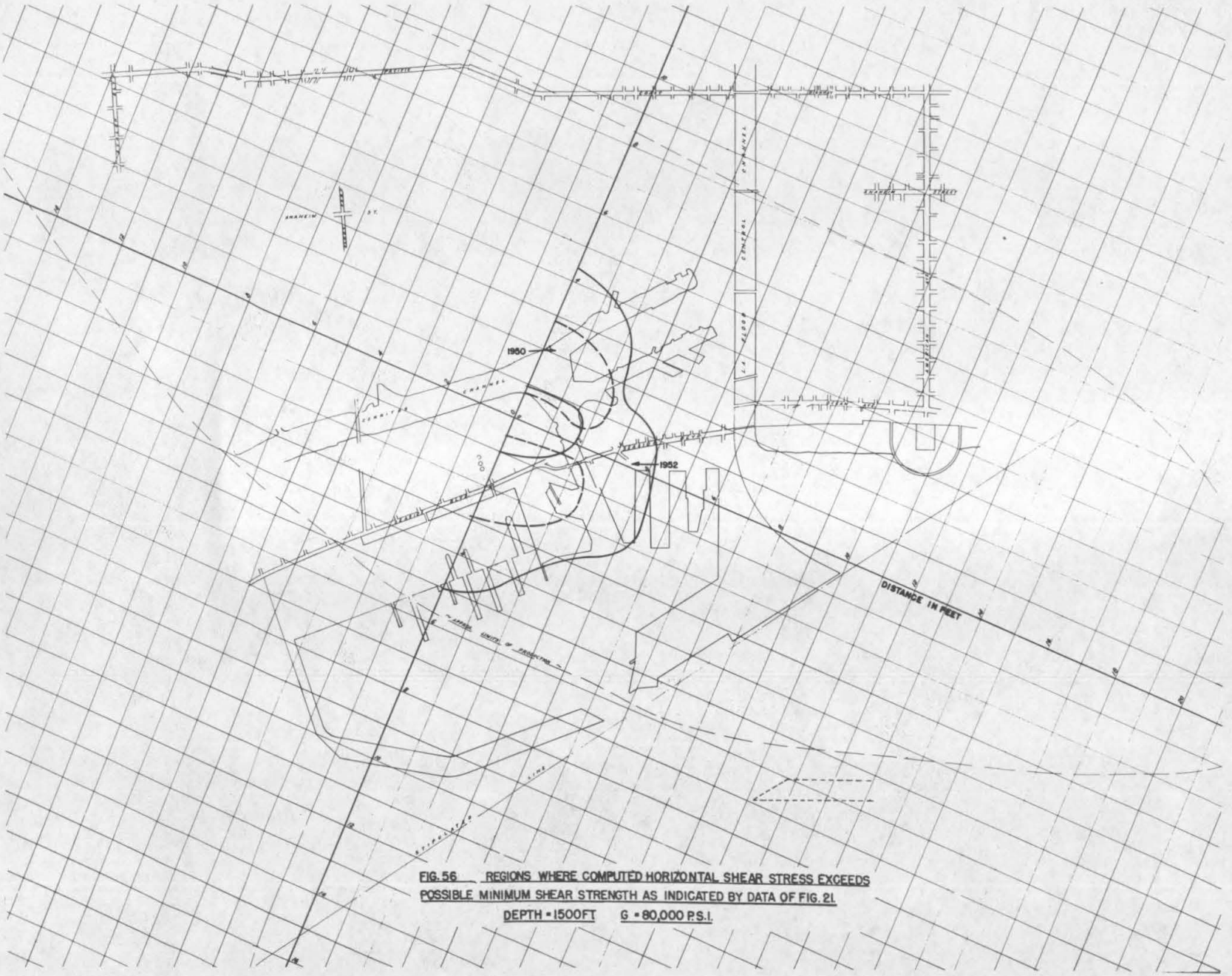

FIG. 56 REGIONS WHERE COMPUTED HORIZONTAL SHEAR STRESS EXCEEDS POSSIBLE MINIMUM SHEAR STRENGTH AS INDICATED BY DATA OF FIG. 21

DEPTH = 1500FT G = 80,000 P.S.I.

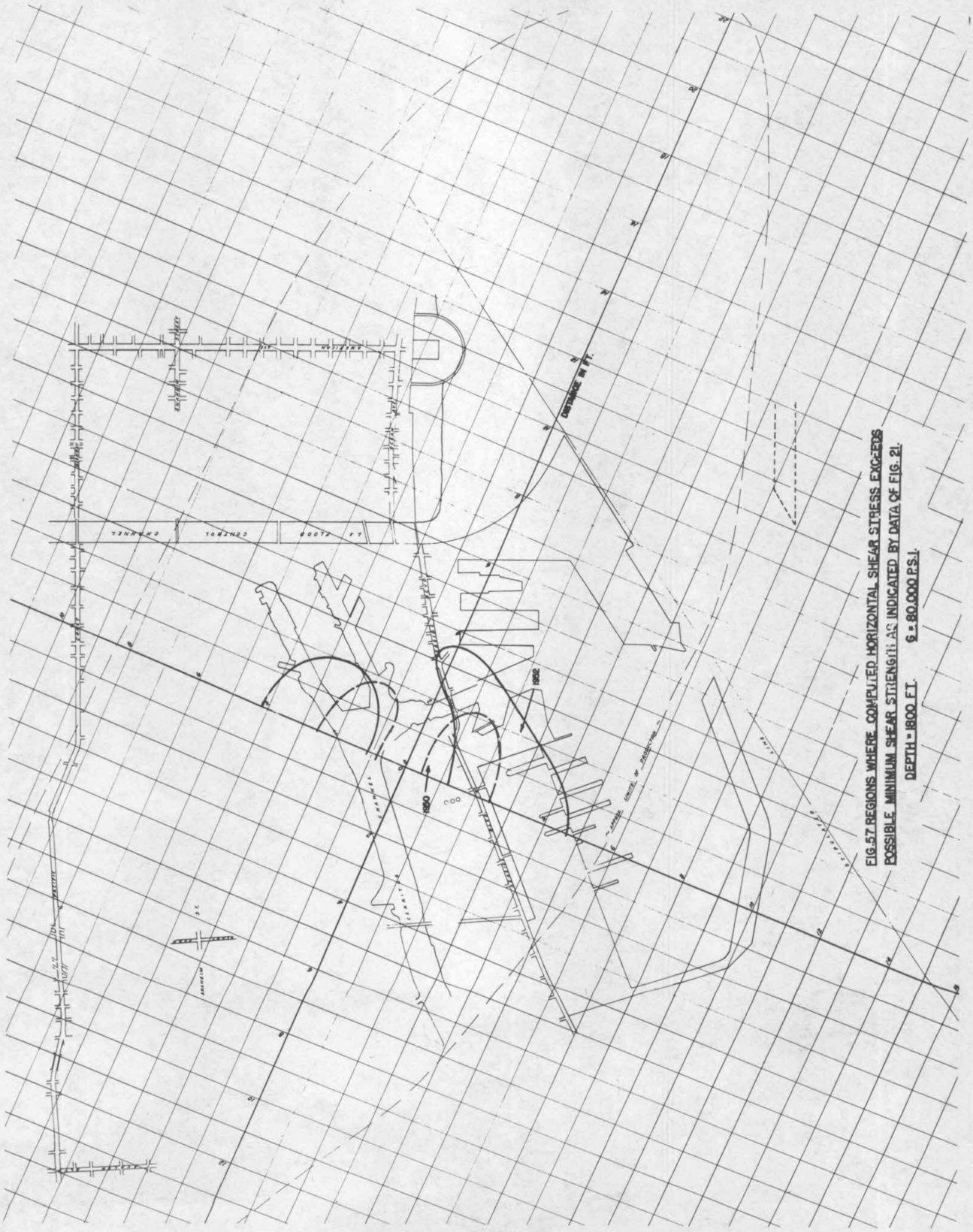

FIG.57 REGIONS WHERE COMPUTED HORIZONTAL SHEAR STRESS EXCEEDS POSSIBLE MINIMUM SHEAR STRENGTH AS INDICATED BY DATA OF FIG. 21.

DEPTH = 1800 F.T. $S = 80,000$ P.S.I.

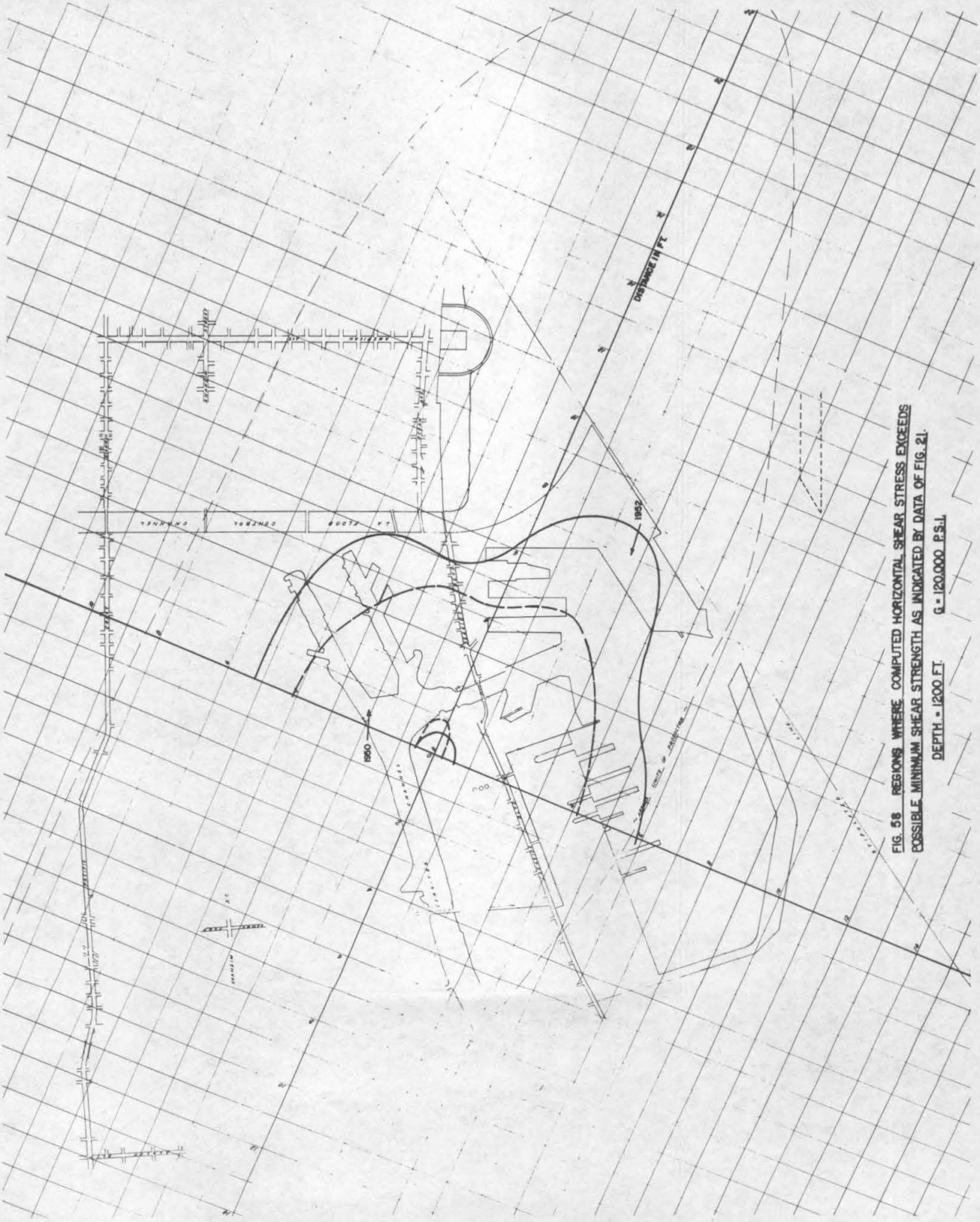

FIG. 58 REGIONS WHERE COMPUTED HORIZONTAL SHEAR STRESS EXCEEDS POSSIBLE MINIMUM SHEAR STRENGTH AS INDICATED BY DATA OF FIG. 21.

DEPTH = 1200 FT. G = 120,000 P.S.I.

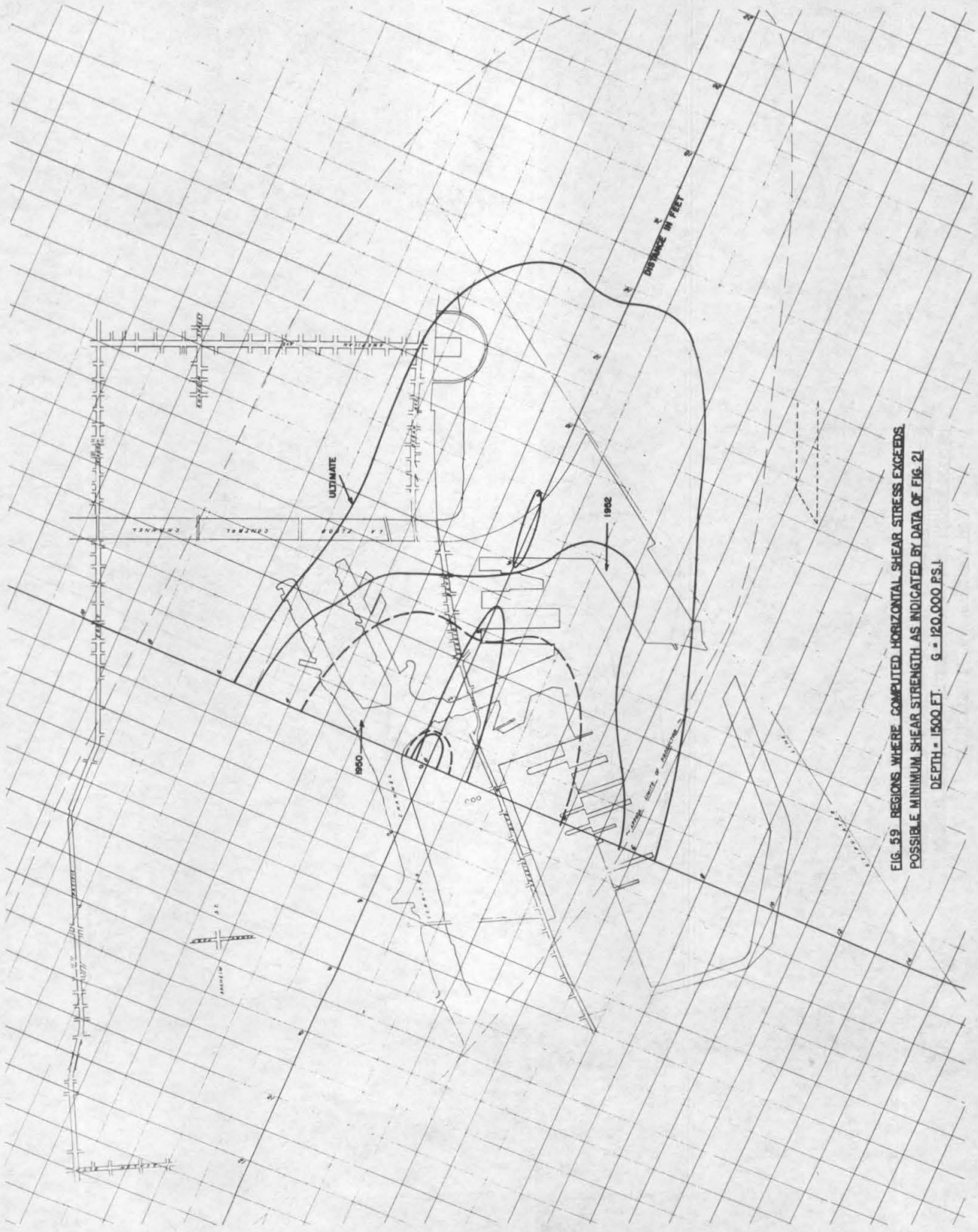

FIG. 59 REGIONS WHERE COMPUTED HORIZONTAL SHEAR STRESS EXCEEDS POSSIBLE MINIMUM SHEAR STRENGTH AS INDICATED BY DATA OF FIG. 21
DEPTH = 1500 FT. G = 120,000 P.S.I.

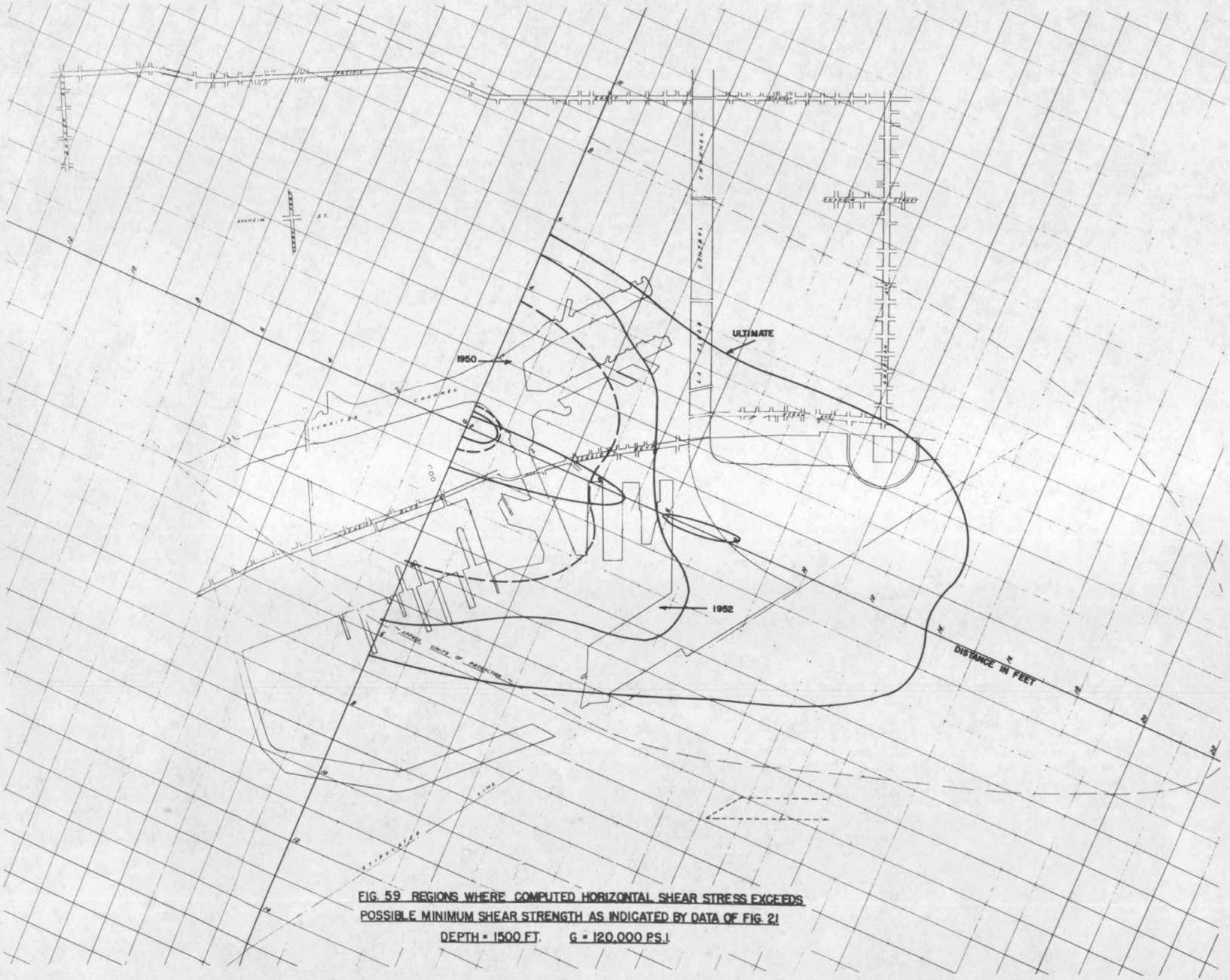

FIG. 59 REGIONS WHERE COMPUTED HORIZONTAL SHEAR STRESS EXCEEDS POSSIBLE MINIMUM SHEAR STRENGTH AS INDICATED BY DATA OF FIG. 21

DEPTH = 1500 FT. G = 120,000 P.S.I.

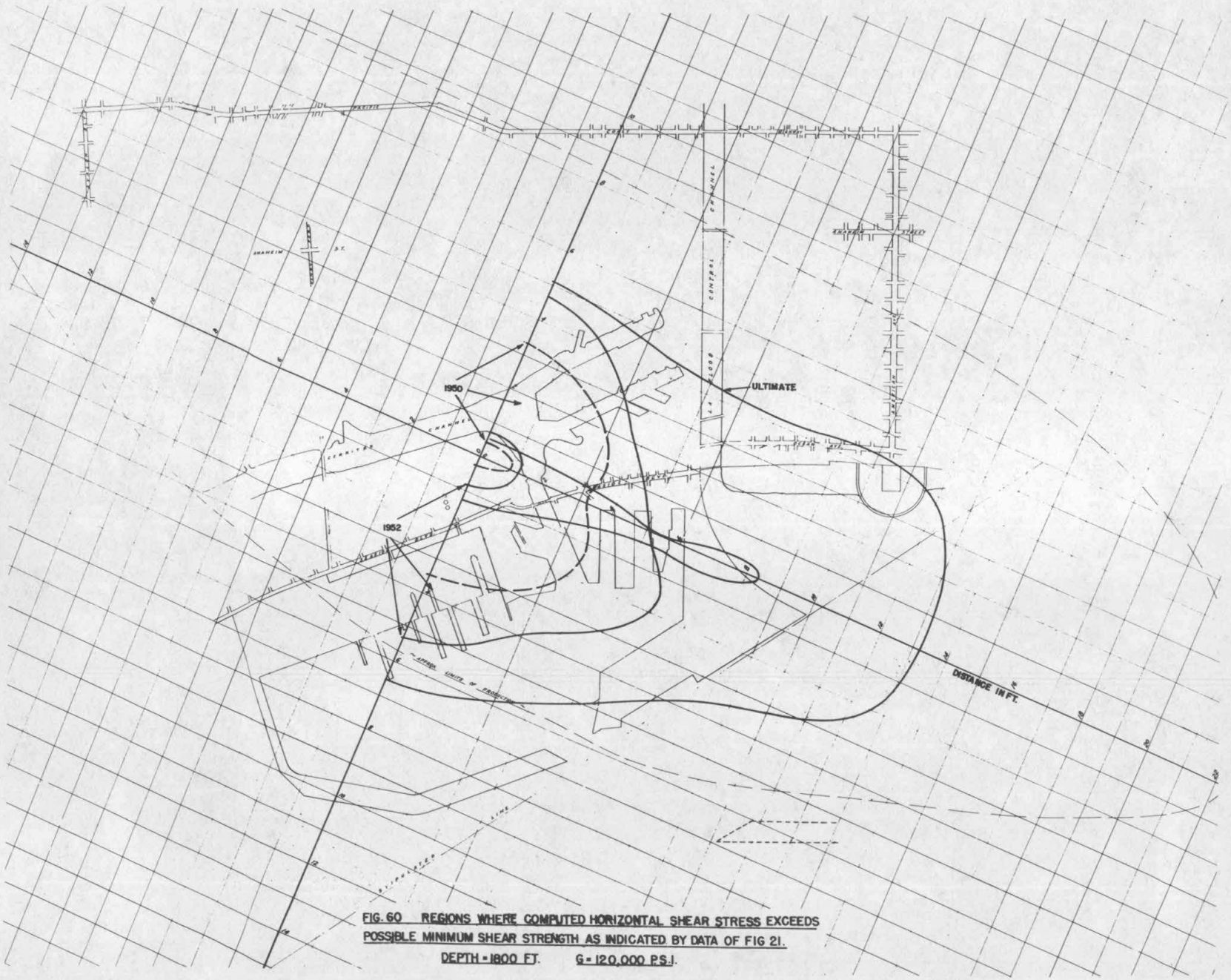

FIG. 60 REGIONS WHERE COMPUTED HORIZONTAL SHEAR STRESS EXCEEDS POSSIBLE MINIMUM SHEAR STRENGTH AS INDICATED BY DATA OF FIG 21.
DEPTH = 1800 FT. G = 120,000 P.S.I.

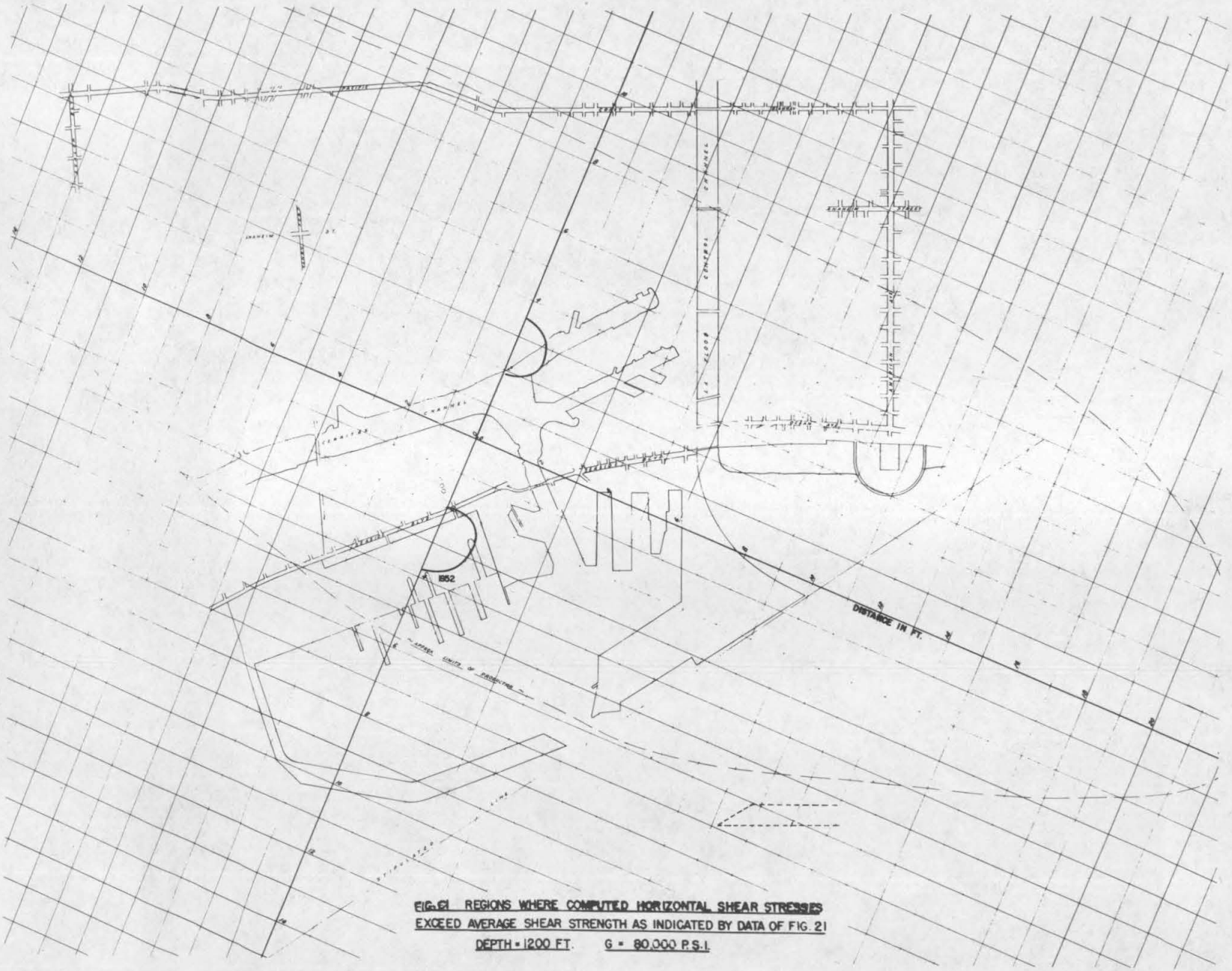

FIG. 21 REGIONS WHERE COMPUTED HORIZONTAL SHEAR STRESSES EXCEED AVERAGE SHEAR STRENGTH AS INDICATED BY DATA OF FIG. 21

DEPTH = 1200 FT. G = 80,000 P.S.I.

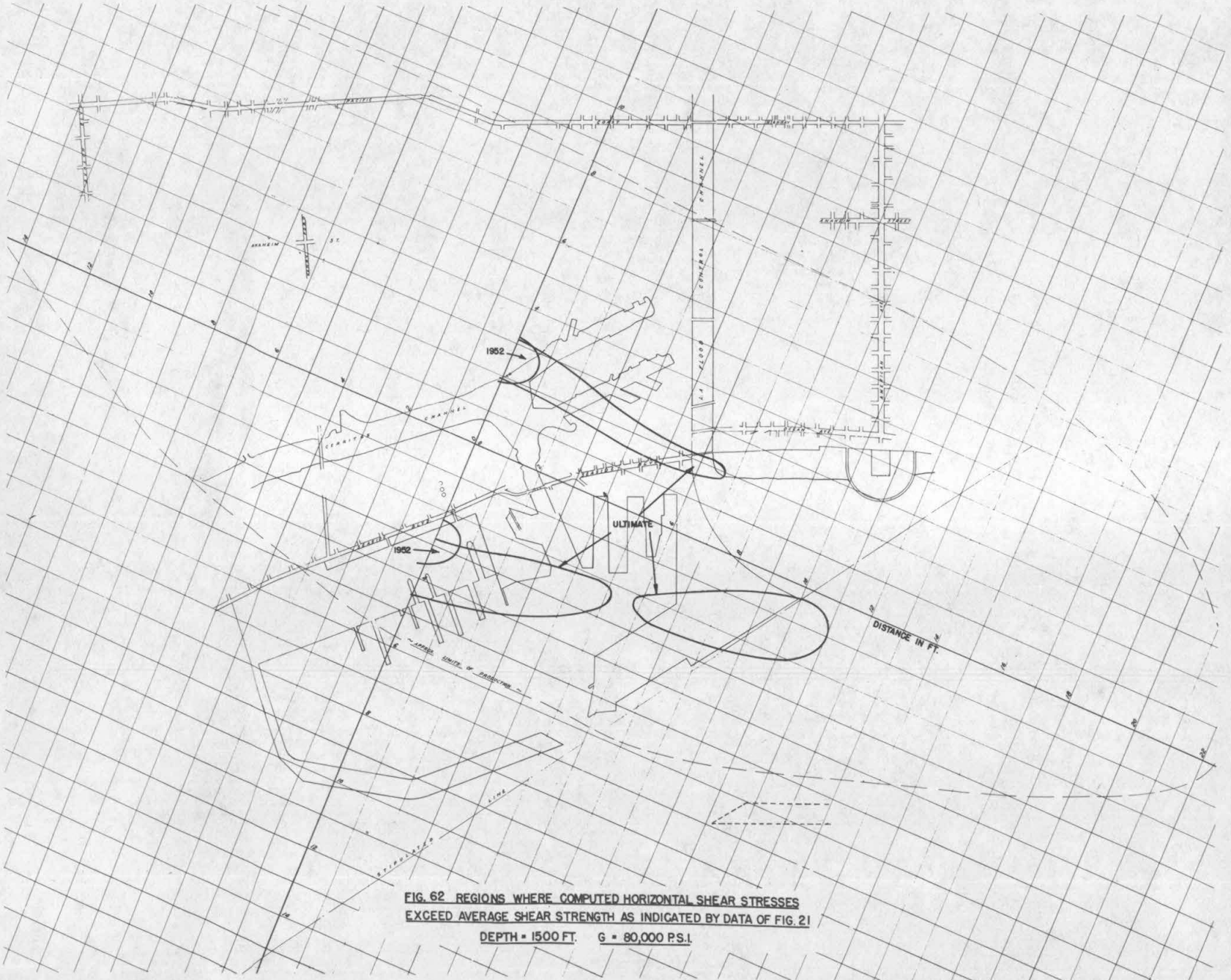

FIG. 62 REGIONS WHERE COMPUTED HORIZONTAL SHEAR STRESSES EXCEED AVERAGE SHEAR STRENGTH AS INDICATED BY DATA OF FIG. 21

DEPTH = 1500 FT. G = 80,000 P.S.I.

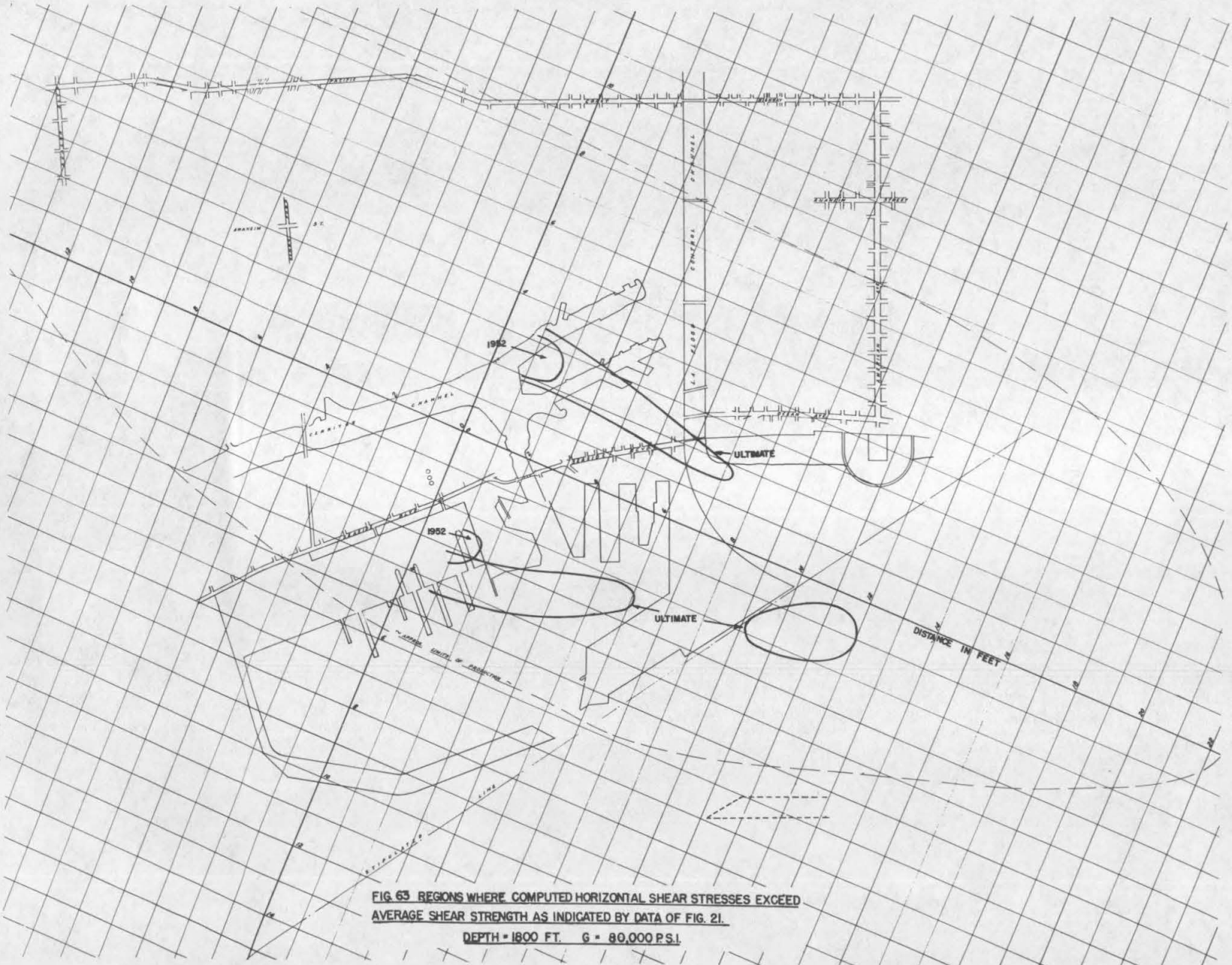

FIG. 63 REGIONS WHERE COMPUTED HORIZONTAL SHEAR STRESSES EXCEED AVERAGE SHEAR STRENGTH AS INDICATED BY DATA OF FIG. 21.
DEPTH = 1800 FT. G = 80,000 P.S.I.

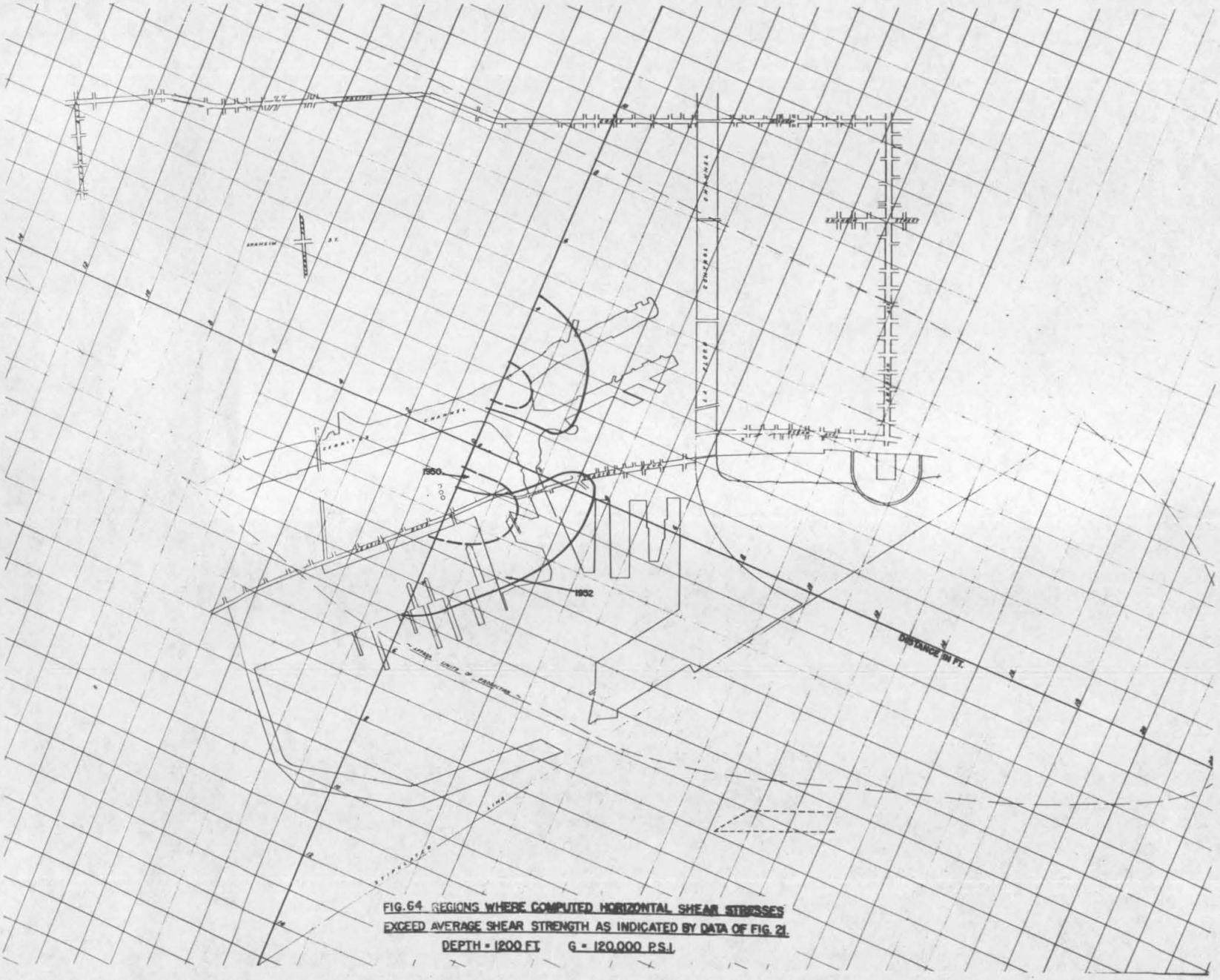

FIG. 64 REGIONS WHERE COMPUTED HORIZONTAL SHEAR STRESSES EXCEED AVERAGE SHEAR STRENGTH AS INDICATED BY DATA OF FIG. 21.
DEPTH = 1200 FT. G = 120,000 P.S.I.

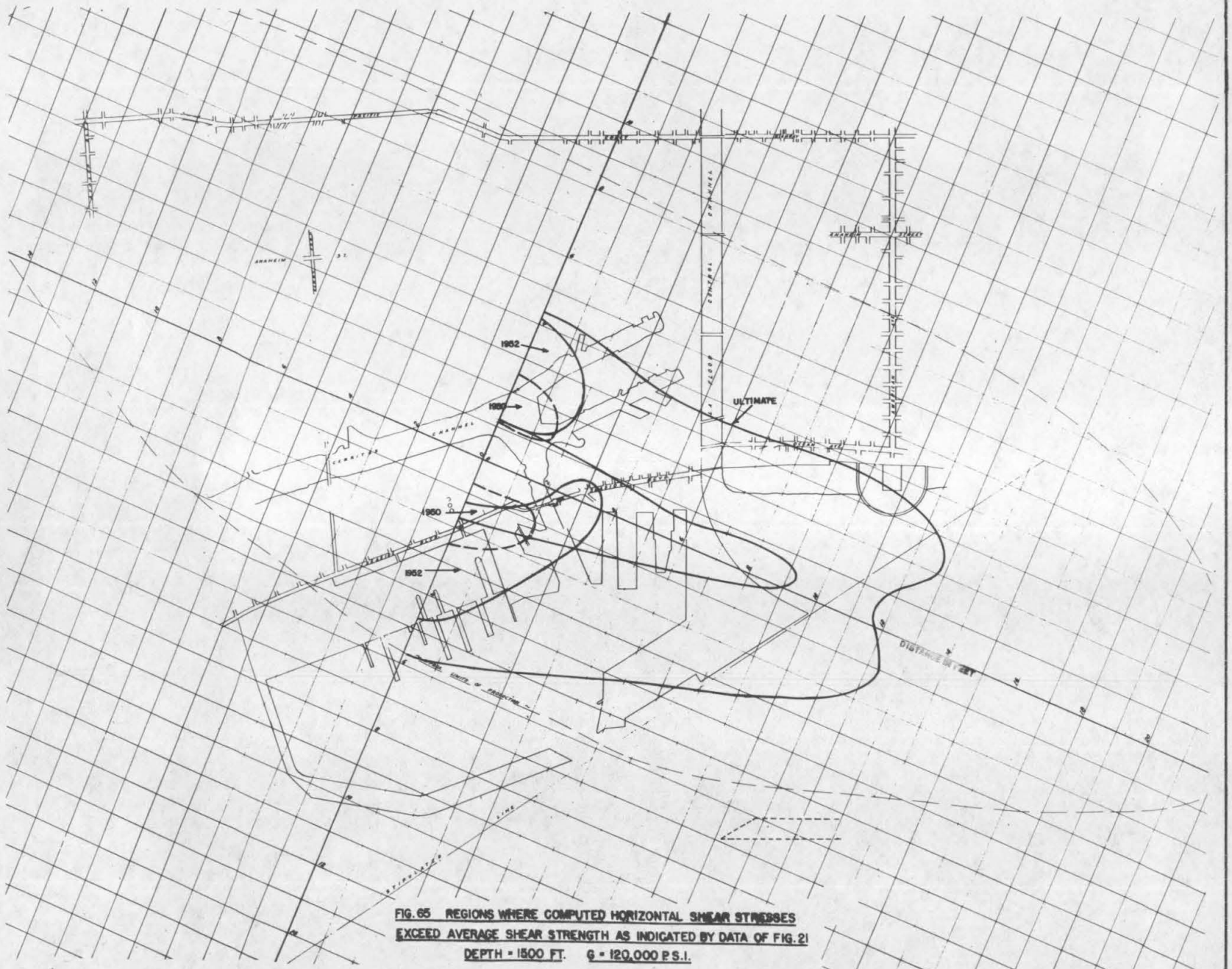

FIG. 65 REGIONS WHERE COMPUTED HORIZONTAL SHEAR STRESSES EXCEED AVERAGE SHEAR STRENGTH AS INDICATED BY DATA OF FIG. 21
DEPTH = 1500 FT. G = 120,000 P.S.I.

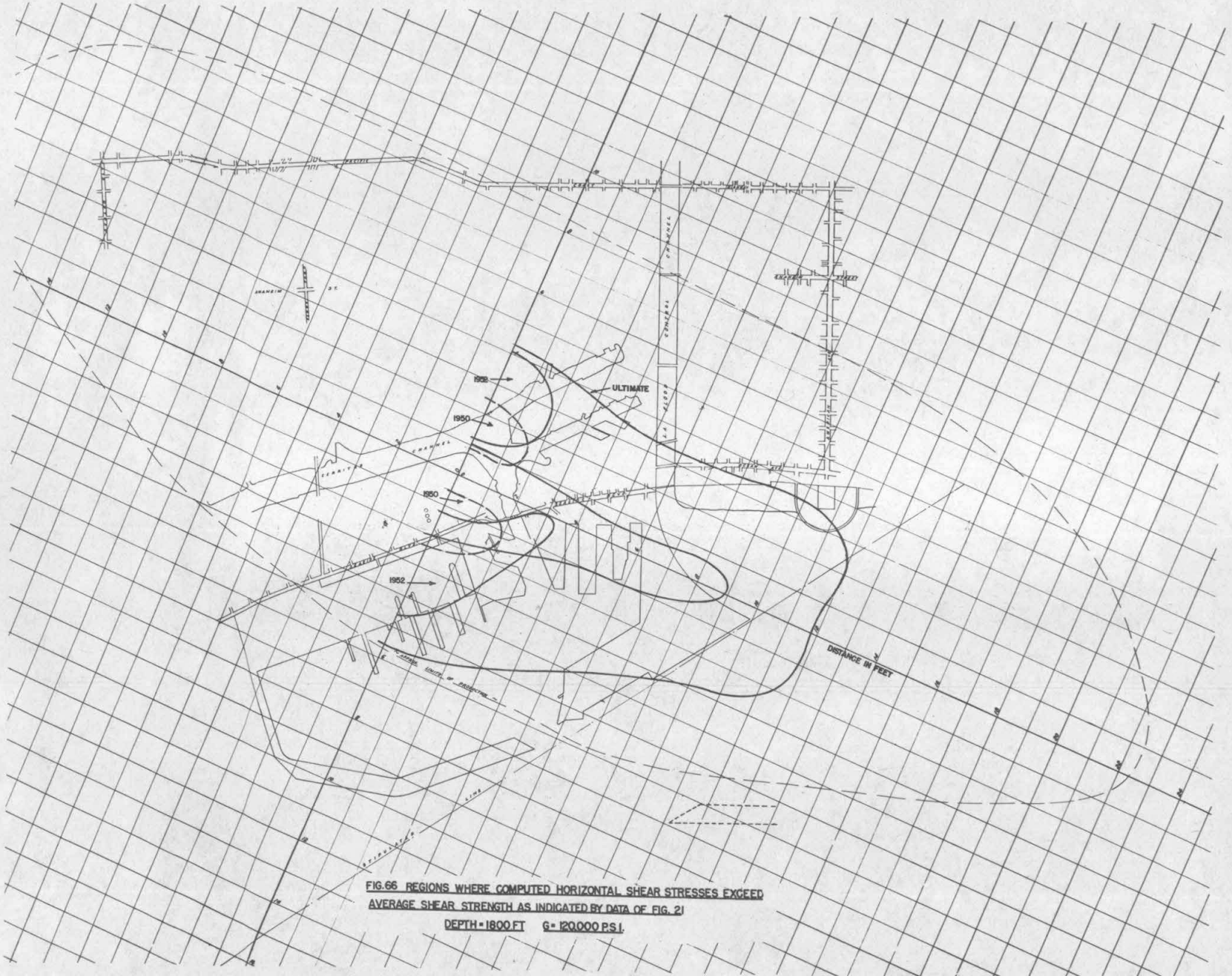

FIG.66 REGIONS WHERE COMPUTED HORIZONTAL SHEAR STRESSES EXCEED AVERAGE SHEAR STRENGTH AS INDICATED BY DATA OF FIG. 21
DEPTH = 1800 FT G = 120,000 P.S.I.

TABLE I

Thickness of the Oil Bearing Sands in the Three Upper Zones

+18	0	0	0	0	0	0	0	0	20	30	40	20	0	0	0	0	0	0	0	0	0	0	0	0
+17	0	0	0	0	0	0	0	0	0	50	70	80	20	0	0	0	0	0	0	0	0	0	0	0
+16	0	0	0	0	0	0	0	30	80	100	100	90	40	20	0	0	0	0	0	0	0	0	0	0
+15	0	0	0	0	0	0	0	60	110	110	110	100	60	30	0	0	0	0	0	0	0	0	0	0
+14	0	0	0	0	0	30	100	120	120	120	120	100	70	40	20	0	0	0	0	0	0	0	0	0
+13	0	0	0	0	0	90	120	120	120	120	110	80	50	50	50	0	0	0	0	0	0	0	0	0
+12	0	0	0	0	30	100	120	120	120	120	110	80	50	50	50	0	0	0	0	0	0	0	0	0
+11	0	0	0	80	110	120	120	120	120	120	110	50	50	50	50	20	20	20	20	20	20	20	20	20
+10	0	0	0	50	100	110	120	120	120	120	50	50	50	50	50	20	20	20	20	20	20	20	20	20
+ 9	0	0	20	100	110	130	160	140	90	80	60	50	50	50	50	20	20	20	20	20	20	20	20	20
+ 8	0	0	50	100	140	290	335	260	110	90	80	60	60	50	30	20	20	20	20	20	20	20	20	20
+ 7	0	0	130	180	375	430	440	485	340	110	90	40	40	30	30	20	20	20	20	20	20	20	20	20
+ 6	0	0	20	210	415	430	420	495	500	450	120	70	50	30	30	20	20	20	20	20	20	20	20	20
+ 5	0	0	50	400	420	485	485	485	485	140	90	80	60	40	30	20	20	20	20	20	20	20	20	20
+ 4	0	0	240	420	495	485	485	585	590	190	110	90	70	50	30	20	20	20	20	20	20	20	20	20
+ 3	0	20	390	505	505	495	610	605	600	540	110	100	80	100	100	0	0	0	0	0	0	0	0	0
+ 2	0	40	480	485	505	610	610	595	570	540	120	100	100	100	100	0	0	0	0	0	0	0	0	0
+ 1	0	60	470	475	605	600	600	595	480	400	160	100	100	100	100	0	0	0	0	0	0	0	0	0
0	0	100	420	560	590	600	550	540	540	405	160	100	100	100	100	0	0	0	0	0	0	0	0	0
- 1	0	80	515	540	590	540	545	540	540	405	160	100	100	100	100	0	0	0	0	0	0	0	0	0
- 2	0	70	515	160	540	570	545	540	520	120	110	125	120	115	100	0	0	0	0	0	0	0	0	0
- 3	0	50	160	260	540	570	535	260	220	140	110	125	120	115	100	0	0	0	0	0	0	0	0	0
- 4	0	160	160	280	530	570	320	320	260	140	110	125	120	115	100	0	0	0	0	0	0	0	0	0
- 5	0	160	160	290	520	380	460	520	430	160	110	125	120	115	100	0	0	0	0	0	0	0	0	0
- 6	0	160	160	290	535	460	600	600	530	250	120	120	120	115	50	0	0	0	0	0	0	0	0	0
- 7	0	160	160	175	255	320	600	600	590	320	130	120	120	115	50	0	0	0	0	0	0	0	0	0
- 8	0	160	120	150	230	480	600	600	600	350	130	120	120	115	50	0	0	0	0	0	0	0	0	0
- 9	0	90	120	125	190	435	600	600	600	270	130	120	130	110	50	0	0	0	0	0	0	0	0	0
-10	0	50	110	125	160	410	595	560	520	210	130	130	120	110	50	0	0	0	0	0	0	0	0	0
-11	0	10	110	120	130	290	520	520	490	150	130	130	120	110	25	0	0	0	0	0	0	0	0	0
-12	0	0	100	120	130	130	410	490	210	130	130	130	120	110	0	0	0	0	0	0	0	0	0	0
-13	0	0	80	120	130	130	130	150	130	130	130	130	120	110	0	0	0	0	0	0	0	0	0	0
-14	0	0	50	115	130	130	130	130	130	130	130	130	120	100	0	0	0	0	0	0	0	0	0	0
-15	0	0	0	110	125	130	130	130	130	130	130	130	115	50	0	0	0	0	0	0	0	0	0	0
-16	0	0	0	100	125	130	130	130	130	130	130	125	115	25	0	0	0	0	0	0	0	0	0	0
-17	0	0	0	50	120	125	130	130	130	130	130	120	90	0	0	0	0	0	0	0	0	0	0	0
-18	0	0	0	0	110	120	130	130	130	130	130	115	25	0	0	0	0	0	0	0	0	0	0	0
-19	0	0	0	0	90	130	130	130	130	130	130	90	0	0	0	0	0	0	0	0	0	0	0	0
-20	0	0	0	0	50	100	120	120	120	120	100	0	0	0	0	0	0	0	0	0	0	0	0	0
-21	0	0	0	0	0	75	100	110	110	90	0	0	0	0	0	0	0	0	0	0	0	0	0	0
-22	0	0	0	0	0	25	50	50	50	0	0	0	0	0	0	0	0	0	0	0	0	0	0	0

TABLE II

SHEARING MODULUS OF ELASTICITY OF CORE SAMPLES

(Taken from reports by Prof. Converse)

Depth of sample in feet	Soil Description	G in psi.
Well X-96		
1529	Siltstone, soft, micaceous	120,000
1978	Shale, not laminated, with streaks of fine sand and fossils	200,000
2270	Clay-shale, soft and fractured very micaceous	110,000
2391	Siltstone, laminated, lenses of cohesionless fine sand	120,000
2391	Oil-sand, medium to fine grained, micaceous	120,000
Well W-12		
1050	Soft siltstone	38,000
1560	Soft sandy siltstone	114,000
1580	Soft sandy siltstone	62,000
1890	Hard siltstone	120,000
2080	Soft sandy siltstone	92,000
Well J-22		
890	Soft siltstone	20,000
1460	Soft very sandy siltstone	112,000
1500	Soft sandy siltstone	110,000
2540	Hard siltstone	162,000
Well W-52		
1030	Soft siltstone	39,000
1570	Soft sandy siltstone	78,000
1590	Mixture of hard and sandy siltstone	96,000
1880	Soft and hard siltstone	82,000
2090	Hard silty-shale	150,000
2740	Hard siltstone	113,000
Well A-37		
880	Soft siltstone	43,000
1480	Soft sandy siltstone	104,000
1780	Hard siltstone	98,000
2280	Hard sandy siltstone	113,000
2625	Soft sandy siltstone	121,000
Well Y-105		
1000	Soft siltstone	40,000
1550	Soft sandy siltstone	50,000
1680	Soft sandy siltstone	86,000
2360	Soft sandy siltstone	107,000

TABLE III

MAXIMUM SHEARING RESISTANCE OF CORE SAMPLES

Depth of sample in feet	Soil Description	Max. Shear Res. in psi.
Well X-96		
1535.5	Laminated shale	320
1536.5	Laminated shale	350
1637	Silty shale	340
1779	Shale	300
1971	Laminated shale	560
2260	Shale	510
Well W-12		
1050	Soft siltstone	190
1560	Soft sandy siltstone	365
1580	Soft sandy siltstone, sand inclusions	375
1590	Soft sandy siltstone, sand inclusions	420
1700	Soft sandy siltstone, sand inclusions	420
1710	Soft sandy siltstone	370
1890	Hard siltstone	425
Well J-22		
890	Soft siltstone	160
1470	Soft sandy siltstone	275
1485	Soft sandy siltstone, sand inclusions	330
1500	Soft sandy siltstone	305
1600	Soft sandy siltstone, sand inclusions	350
1620	Soft sandy siltstone and hard siltstone mixture	320
1720	Hard siltstone	240
Well W-52		
1040	Soft siltstone	240
1570	Soft sandy siltstone	365
1590	Soft sandy siltstone, very sandy	410
1700	Soft sandy siltstone, very sandy	350
1880	Hard sandy siltstone	410
2090	Hard siltstone	510
2450	Hard siltstone, fine sand inclusions	650
2620	Hard siltstone, fine sand inclusions	630
2740	Hard siltstone	700
Well A-37		
865	Soft siltstone	190
880	Soft siltstone	210
1490	Soft sandy siltstone, fine sand inclusions	345
1610	Soft siltstone	400
1780	Hard siltstone, fine sand inclusions	320

TABLE III
(Continued)

Depth of sample in feet	Soil Description	Max. Shear Res. in psi.
Well A-37		
2060	Hard siltstone	570
2290	Hard sandy siltstone, fine sand inclusions	560
2410	Hard sandy siltstone, fine sand inclusions	600
2620	Hard sandy siltstone, fine sand inclusions	650
2730	Hard siltstone, fine sand inclusions	750
Well Y-105		
995	Soft siltstone	230
1550	Soft sandy siltstone	335
1560	Soft sandy siltstone	325
1565	Soft sandy siltstone, fine sand inclusions	360
1570	Soft sandy siltstone	350
1680	Soft sandy siltstone	370
2360	Soft sandy siltstone, fine sand inclusions	485
2610	Hard sandy siltstone, fine sand inclusions	770
2700	Hard sandy siltstone, fine sand inclusions	960

TABLE IV

Product of Pressure Drop and Oil Sand Thickness
Original ΔPxT for 1945

q ↓ / a →	-6	-5	-4	-3	-2	-1	0	+1	+2	+3	+4	+5	+6	+7	+8	+9
+18	0	0	0	0	0	0	0	0	14	21	28	14	0	0	0	0
+17	0	0	0	0	0	0	0	0	36	50	50	57	14	0	0	0
+16	0	0	0	0	0	0	0	21	57	71	71	64	28	14	0	0
+15	0	0	0	0	0	0	21	43	78	78	78	71	43	21	0	0
+14	0	0	0	0	0	0	64	71	85	95	95	71	50	28	2	0
+13	0	0	0	0	0	0	71	82	85	85	85	78	57	13	6	0
+12	0	0	0	0	0	21	71	85	85	85	85	78	41	18	11	0
+11	0	0	0	0	0	57	78	85	85	85	85	68	28	21	13	0
+10	0	0	0	0	36	71	78	85	85	85	78	32	31	23	16	0
+ 9	0	0	0	14	71	78	84	94	87	60	53	38	32	26	18	0
+ 8	0	0	0	36	71	89	130	186	133	75	60	52	38	0	0	0
+ 7	0	0	0	71	93	218	254	145	120	84	75	59	0	0	0	0
+ 6	0	0	14	105	241	262	162	167	152	85	83	6	0	0	0	0
+ 5	0	0	33	223	255	304	296	209	155	35	19	12	3	0	0	0
+ 4	0	0	113	237	308	304	304	286	184	43	32	19	8	0	8	0
+ 3	0	8	204	302	314	311	265	237	207	149	40	28	39	44	26	0
+ 2	0	8	241	287	311	289	262	252	211	178	73	60	56	51	41	0
+ 1	0	22	152	274	319	297	263	271	162	106	66	73	66	56	41	0
0	0	35	81	176	289	297	313	250	207	130	71	81	61	61	21	0
- 1	0	25	102	158	248	301	300	291	234	130	61	61	61	61	21	0
- 2	0	8	36	45	221	306	320	319	306	61	67	76	73	70	21	0
- 3	0	0	34	51	182	272	269	92	92	85	67	76	73	70	21	0
- 4	0	0	0	29	143	215	85	98	92	85	67	76	73	70	21	0
- 5	0	0	0	10	105	111	62	84	92	85	67	76	73	70	21	0
- 6	0	0	0	4	89	78	59	77	92	92	73	73	73	70	0	0
- 7	0	0	0	0	2	84	56	69	92	92	79	73	73	0	0	0
- 8	0	0	0	0	0	92	47	62	80	92	0	0	0	0	0	0
- 9	0	0	0	0	0	2	48	64	69	0	0	0	0	0	0	0
-10	0	0	0	0	0	0	17	0	0	0	0	0	0	0	0	0

TABLE V

Original ΔPxT for 1947

b ↑	a → -6	-5	-4	-3	-2	-1	0	+1	+2	+3	+4	+5	+6	+7	+8	+9
+18	0	0	0	0	0	0	0	0	18	27	36	18	0	0	0	0
+17	0	0	0	0	0	0	0	0	46	64	64	73	0	0	0	0
+16	0	0	0	0	0	0	0	27	73	91	91	82	34	0	0	0
+15	0	0	0	0	0	0	0	55	100	100	100	91	55	0	0	0
+14	0	0	0	0	0	0	27	91	109	109	109	91	64	36	0	0
+13	0	0	0	0	0	0	82	109	109	109	109	100	73	46	14	0
+12	0	0	0	0	0	27	91	109	109	109	109	100	47	22	16	0
+11	0	0	0	0	0	73	100	109	109	109	109	80	35	27	20	0
+10	0	0	0	0	45	91	100	109	109	109	90	37	36	32	23	0
+ 9	0	0	0	18	90	100	110	125	115	69	61	44	37	36	27	0
+ 8	0	0	0	45	90	116	195	233	145	85	68	60	44	29	14	0
+ 7	0	0	0	103	119	285	323	315	328	188	85	68	32	18	14	0
+ 6	0	0	17	132	312	314	304	357	357	298	92	57	41	20	15	0
+ 5	0	0	42	288	312	356	354	351	353	101	73	65	49	27	15	0
+ 4	0	0	156	301	359	355	354	299	258	104	89	73	57	36	17	0
+ 3	0	16	278	357	364	362	364	335	309	198	89	81	65	63	57	0
+ 2	0	31	284	343	361	396	384	352	301	277	97	79	74	69	59	0
+ 1	0	21	229	324	418	401	381	360	277	178	86	91	81	71	61	0
0	0	31	201	363	418	413	406	318	319	219	91	101	81	51	21	0
- 1	0	20	241	310	411	371	369	371	359	257	81	81	81	51	16	0
- 2	0	17	216	94	293	391	390	398	391	81	89	101	97	59	16	0
- 3	0	12	82	116	284	395	353	105	114	113	89	101	97	66	15	0
- 4	0	24	40	77	272	356	144	137	116	113	89	101	97	70	15	0
- 5	0	0	0	41	219	130	92	101	116	113	89	101	97	70	11	0
- 6	0	0	0	36	0	39	92	101	116	122	97	97	97	74	0	0
- 7	0	0	0	0	2	50	84	98	116	122	105	97	0	0	0	0
- 8	0	0	0	0	0	75	131	92	110	122	0	0	0	0	0	0
- 9	0	0	0	0	0	62	132	86	104	0	0	0	0	0	0	0
-10	0	0	0	0	0	15	32	0	0	0	0	0	0	0	0	0

TABLE VI

Original Δ PxT for 1949

q \ a	-6	-5	-4	-3	-2	-1	0	+1	+2	+3	+4	+5	+6	+7	+8	+9
+18	0	0	0	0	0	0	0	0	20	30	40	20	0	0	0	0
+17	0	0	0	0	0	0	0	0	51	71	70	81	20	0	0	0
+16	0	0	0	0	0	0	0	30	81	101	101	91	40	16	0	0
+15	0	0	0	0	0	0	0	61	111	111	111	101	61	30	0	0
+14	0	0	0	0	0	0	30	101	121	121	121	101	71	40	12	0
+13	0	0	0	0	0	0	91	121	121	121	121	111	81	51	16	0
+12	0	0	0	0	0	30	101	121	121	121	121	111	81	26	16	0
+11	0	0	0	0	0	80	111	121	121	121	121	89	41	31	21	8
+10	0	0	0	0	51	101	111	121	121	121	103	41	41	36	21	8
+ 9	0	0	0	20	101	111	127	153	137	77	69	52	41	41	21	12
+ 8	0	0	0	51	101	135	240	286	201	95	77	69	52	41	18	13
+ 7	0	0	0	120	143	333	380	278	416	229	95	77	36	24	18	12
+ 6	0	0	18	167	366	380	360	424	429	382	103	64	46	24	18	12
+ 5	0	0	43	343	370	415	415	415	285	119	82	73	55	36	18	12
+ 4	0	0	188	360	418	415	415	374	384	132	100	82	64	46	21	14
+ 3	0	16	315	421	427	424	399	392	389	331	100	91	73	76	76	0
+ 2	0	24	358	394	421	393	399	387	354	351	97	91	91	81	76	0
+ 1	0	25	347	373	380	393	393	387	385	254	81	101	96	91	76	0
0	0	41	292	365	374	389	486	442	456	325	81	101	81	81	71	0
- 1	0	33	293	355	363	445	481	512	509	342	81	81	81	81	71	0
- 2	0	29	233	83	396	514	500	547	491	81	89	101	97	93	71	0
- 3	0	21	82	98	386	508	443	101	107	113	89	101	97	93	71	0
- 4	0	18	50	70	332	431	76	120	119	113	89	101	97	93	61	0
- 5	0	2	18	26	272	74	124	174	169	114	89	101	97	93	41	0
- 6	0	0	0	16	255	102	165	196	185	134	97	97	97	93	21	0
- 7	0	0	0	0	1	135	162	138	195	142	105	97	49	47	21	0
- 8	0	0	0	0	0	123	180	173	192	141	53	53	49	47	21	0
- 9	0	0	0	0	0	108	173	159	162	97	53	53	49	45	21	0
-10	0	0	0	0	0	38	122	151	154	77	40	40	37	34	11	0
-11	0	0	0	0	0	28	117	134	138	33	1	0	0	0	0	0
-12	0	0	0	0	0	0	66	90	20	0	0	0	0	0	0	0

TABLE VII

Original ΔPxT for 1950

b \ a	-6	-5	-4	-3	-2	-1	0	+1	+2	+3	+4	+5	+6	+7	+8	+9
+18	0	0	0	0	0	0	0	0	0	30	40	20	0	0	0	0
+17	0	0	0	0	0	0	0	0	51	71	71	81	20	0	0	0
+16	0	0	0	0	0	0	0	24	81	101	111	91	40	20	0	0
+15	0	0	0	0	0	0	0	61	111	111	111	101	61	30	0	0
+14	0	0	0	0	0	0	24	101	121	121	121	101	71	40	20	0
+13	0	0	0	0	0	0	82	121	121	121	121	111	81	51	31	0
+12	0	0	0	0	0	27	111	121	121	121	121	111	81	38	31	0
+11	0	0	0	0	0	81	111	121	121	121	121	111	41	41	36	12
+10	0	0	0	0	41	111	111	121	121	121	103	43	43	41	41	13
+ 9	0	0	0	16	101	111	128	155	137	82	69	52	43	43	41	14
+ 8	0	0	0	41	101	137	264	304	230	100	82	69	52	43	20	12
+ 7	0	0	0	101	159	266	383	394	435	395	100	77	36	26	21	13
+ 6	0	0	16	185	381	408	388	443	448	403	109	67	46	27	24	14
+ 5	0	0	46	368	386	450	450	450	443	121	91	77	58	36	27	14
+ 4	0	0	207	381	459	450	450	475	450	150	111	91	71	48	23	15
+ 3	0	16	335	459	468	459	492	493	485	377	111	101	81	81	81	0
+ 2	0	28	385	437	462	497	492	487	442	417	115	91	91	91	81	0
+ 1	0	31	378	423	483	477	477	487	430	325	86	101	101	91	81	0
0	0	41	364	453	464	473	455	522	486	354	86	96	86	86	81	0
- 1	0	57	319	436	464	564	565	539	503	365	86	86	86	86	81	0
- 2	0	50	279	120	474	566	565	561	506	61	95	108	103	99	81	0
- 3	0	36	98	112	465	543	505	131	129	120	95	108	103	99	76	0
- 4	0	66	98	103	444	533	157	155	148	120	95	108	103	99	76	0
- 5	0	50	66	94	406	170	200	237	219	130	95	108	103	99	71	0
- 6	0	25	34	86	408	202	232	233	246	167	103	103	103	99	36	0
- 7	0	0	0	55	78	223	228	225	262	189	112	103	91	87	33	0
- 8	0	0	72	60	77	197	232	225	243	196	86	92	85	82	31	0
- 9	0	0	72	51	64	163	224	203	206	135	79	79	73	67	28	0
-10	0	0	0	26	43	107	162	182	195	102	73	73	67	62	26	0
-11	0	0	0	0	0	64	141	161	169	60	40	40	25	12	0	0
-12	0	0	0	0	0	0	102	122	51	27	0	0	0	0	0	0
-13	0	0	0	0	0	0	0	5	0	0	0	0	0	0	0	0

TABLE VIII

Original $\Delta P_x T$ for 1951

b \ a	-6	-5	-4	-3	-2	-1	0	+1	+2	+3	+4	+5	+6	+7	+8	+9
+18	0	0	0	0	0	0	0	0	20	30	40	20	0	0	0	0
+17	0	0	0	0	0	0	0	0	51	70	71	81	20	0	0	0
+16	0	0	0	0	0	0	0	30	81	101	101	91	40	20	0	0
+15	0	0	0	0	0	0	0	61	111	111	111	101	61	30	0	0
+14	0	0	0	0	0	0	30	101	121	121	121	101	71	40	20	0
+13	0	0	0	0	0	0	91	121	121	121	121	111	81	51	34	0
+12	0	0	0	0	0	30	101	121	121	121	121	111	81	40	37	0
+11	0	0	0	0	0	81	111	121	121	121	121	111	42	41	39	14
+10	0	0	0	0	51	101	111	121	121	121	102	42	42	41	41	15
+ 9	0	0	0	20	101	111	112	125	121	77	68	50	42	42	41	15
+ 8	0	0	0	51	101	120	227	283	184	96	77	68	51	42	26	16
+ 7	0	0	0	101	154	340	391	379	423	293	95	77	34	27	26	16
+ 6	0	0	20	163	378	391	371	471	470	409	104	66	47	27	26	16
+ 5	0	0	49	348	384	464	466	466	439	106	86	76	56	37	26	16
+ 4	0	0	212	381	471	463	469	493	487	163	108	86	66	46	27	16
+ 3	0	16	332	471	482	476	556	535	500	471	109	97	76	91	91	0
+ 2	0	29	394	361	480	577	571	515	484	468	121	94	96	96	91	0
+ 1	0	43	387	446	531	556	539	504	384	361	91	95	101	101	91	0
0	0	71	372	557	564	551	482	552	556	371	87	96	101	102	96	0
- 1	0	49	523	551	587	560	561	579	562	373	111	111	109	102	96	0
- 2	0	43	493	132	476	586	585	588	560	111	122	139	128	117	95	0
- 3	0	31	109	156	482	593	550	173	159	155	122	138	127	117	94	0
- 4	0	86	98	161	459	536	213	225	193	141	117	133	127	116	93	0
- 5	0	43	61	152	432	239	306	386	328	157	111	130	124	115	92	0
- 6	0	24	32	116	317	273	377	407	380	209	119	121	121	110	46	0
- 7	0	8	18	89	118	291	352	360	389	241	125	115	121	116	49	0
- 8	0	0	67	74	88	257	326	344	344	239	122	125	115	110	47	0
- 9	0	0	52	58	70	224	346	275	293	181	101	102	95	89	41	0
-10	0	0	29	39	50	87	220	248	262	122	79	79	76	70	31	0
-11	0	0	12	19	31	75	161	190	202	62	47	40	37	34	8	0
-12	0	0	6	0	0	1	77	144	17	14	14	1	0	1	0	0
-13	0	0	0	0	0	0	0	5	0	0	0	0	0	0	0	0

TABLE IX

Estimated ΔPxT for 1952

b \ a	-6	-5	-4	-3	-2	-1	0	+1	+2	+3	+4	+5	+6	+7	+8	+9
+18	0	0	0	0	0	0	0	0	0	30	40	2	0	0	0	0
+17	0	0	0	0	0	0	0	0	55	78	78	89	22	0	0	0
+16	0	0	0	0	0	0	0	30	89	111	111	100	44	20	0	0
+15	0	0	0	0	0	0	0	67	122	122	122	111	67	33	0	0
+14	0	0	0	0	0	0	30	111	133	133	133	111	78	44	22	0
+13	0	0	0	0	0	0	100	133	133	133	133	122	89	56	51	0
+12	0	0	0	0	0	30	122	133	133	133	133	122	89	51	51	0
+11	0	0	0	0	0	88	122	133	133	133	133	122	51	51	51	20
+10	0	0	0	0	51	111	122	133	133	133	121	51	51	51	51	20
+ 9	0	0	0	0	111	122	140	169	151	91	81	61	51	51	51	20
+ 8	0	0	0	53	111	149	289	334	235	111	91	81	61	56	33	20
+ 7	0	0	0	111	176	371	423	422	480	339	111	91	44	33	33	20
+ 6	0	0	1	203	407	423	414	479	495	448	121	78	56	33	33	20
+ 5	0	0	56	393	412	479	479	479	489	147	100	89	67	44	33	20
+ 4	0	0	241	412	490	479	479	481	470	179	122	100	78	56	33	20
+ 3	0	20	379	486	499	500	558	529	491	423	111	106	89	111	111	0
+ 2	0	40	433	461	499	575	549	536	481	457	115	111	111	111	111	0
+ 1	0	43	426	436	593	577	559	530	484	407	111	111	111	111	111	0
0	0	71	427	577	590	585	591	561	583	413	111	111	111	111	111	0
- 1	0	77	482	541	590	583	592	579	578	419	111	111	111	111	111	0
- 2	0	67	462	162	548	630	610	591	566	111	122	139	133	128	111	0
- 3	0	48	136	168	543	630	550	186	167	155	122	139	133	128	111	0
- 4	0	66	90	175	514	608	209	224	197	155	122	139	133	128	111	0
- 5	0	50	66	174	465	248	236	229	322	167	122	139	133	128	111	0
- 6	0	26	50	150	369	265	281	263	339	228	127	133	133	128	56	0
- 7	0	0	18	89	124	296	284	263	353	277	131	127	127	122	53	0
- 8	0	0	61	79	99	263	305	320	353	280	131	131	121	116	51	0
- 9	0	0	55	64	78	232	305	341	374	210	112	105	97	89	41	0
-10	0	0	40	58	71	152	254	277	313	142	86	79	73	67	31	0
-11	0	0	34	43	53	89	197	222	233	69	53	53	37	34	8	0
-12	0	0	6	0	0	27	138	166	37	40	1	1	0	0	0	0
-13	0	0	0	0	0	0	1	2	1	0	0	0	0	0	0	0

TABLE X

Original ΔPxT for Proposed Ultimate

(Pumping up to but not beyond the stipulated line)

q \ a	-6	-5	-4	-3	-2	-1	0	+1	+2	+3	+4	+5	+6	+7	+8	+9
+18	0	0	0	0	0	0	0	0	0	34	45	0	0	0	0	0
+17	0	0	0	0	0	0	0	0	21	79	79	0	23	0	0	0
+16	0	0	0	0	0	0	0	34	90	113	113	102	45	0	0	0
+15	0	0	0	0	0	0	0	68	124	124	124	113	68	23	0	0
+14	0	0	0	0	0	0	34	113	136	136	136	113	79	34	23	0
+13	0	0	0	0	0	0	102	136	136	136	136	124	90	45	57	0
+12	0	0	0	0	0	34	113	136	136	136	136	124	90	57	57	0
+11	0	0	0	0	0	90	124	136	136	136	136	124	57	57	57	2
+10	0	0	0	0	57	113	124	136	136	136	136	57	57	57	57	18
+ 9	0	0	0	20	113	124	136	178	157	102	90	68	57	57	57	20
+ 8	0	0	0	57	113	156	348	225	311	123	102	90	68	57	34	20
+ 7	0	0	0	113	215	473	548	559	623	430	124	102	45	57	34	20
+ 6	0	0	22	246	531	548	465	638	644	586	136	79	57	34	34	20
+ 5	0	0	57	509	537	626	626	627	638	150	102	90	68	34	34	4
+ 4	0	0	296	537	639	626	626	761	768	207	124	102	79	45	34	4
+ 3	0	20	502	650	648	637	788	783	777	695	124	113	90	57	113	0
+ 2	0	45	616	627	648	788	788	777	746	699	136	113	113	113	113	0
+ 1	0	67	605	616	783	777	777	777	616	491	112	113	113	113	113	0
0	0	111	553	735	767	777	707	695	696	503	112	112	111	111	111	0
- 1	0	89	688	714	767	696	700	695	696	474	111	111	111	111	111	0
- 2	0	78	688	182	680	728	700	695	675	117	122	139	133	128	111	0
- 3	0	56	178	295	681	728	690	289	240	155	122	139	133	128	111	0
- 4	0	178	178	322	671	728	373	373	296	155	122	139	133	128	111	0
- 5	0	178	178	338	660	324	569	653	531	179	122	139	133	128	111	0
- 6	0	178	178	338	676	569	765	765	671	280	133	133	133	128	56	0
- 7	0	114	178	192	280	653	765	765	755	369	144	133	133	128	48	0
- 8	0	0	73	146	254	597	765	765	765	415	144	144	133	122	26	0
- 9	0	0	0	51	138	536	765	765	765	340	144	144	73	0	0	0
-10	0	0	0	0	0	143	760	657	680	256	144	92	0	0	0	0
-11	0	0	0	0	0	0	86	510	570	172	144	79	0	0	0	0
-12	0	0	0	0	0	0	0	18	20	118	131	14	0	0	0	0

TABLE XI

Original ΔPxT for Proposed Ultimate
(Pumping beyond the stipulated line)

	-5	-4	-3	-2	-1	0	+1	+2	+3	+4	+5	+6	+7	+8	+9
+18	0	0	0	0	0	0	0	0	34	45	0	0	0	0	0
+17	0	0	0	0	0	0	0	21	79	79	0	23	0	0	0
+16	0	0	0	0	0	0	34	90	113	113	102	45	23	0	0
+15	0	0	0	0	0	0	68	124	124	124	113	68	34	0	0
+14	0	0	0	0	0	34	113	136	136	136	113	79	45	23	0
+13	0	0	0	0	0	102	136	136	136	136	124	90	57	57	0
+12	0	0	0	0	34	113	136	136	136	136	124	90	57	57	0
+11	0	0	0	0	90	124	136	136	136	136	124	57	57	57	2
+10	0	0	0	57	113	124	136	136	136	136	57	57	57	57	18
+ 9	0	0	20	113	124	136	178	157	102	90	68	57	57	57	20
+ 8	0	0	57	113	156	348	225	311	123	102	90	68	57	34	20
+ 7	0	0	113	215	473	548	559	623	430	124	102	45	34	34	20
+ 6	0	22	246	531	548	465	638	644	586	136	79	57	34	34	20
+ 5	0	0	57	509	537	626	626	627	638	150	102	90	68	45	34	4
+ 4	0	0	296	537	639	626	626	761	768	207	124	102	79	57	34	4
+ 3	0	20	502	650	648	637	788	783	777	695	124	113	90	113	113	0
+ 2	0	45	616	627	648	788	788	772	746	699	136	113	113	113	113	0
+ 1	0	69	605	616	783	777	777	772	616	491	112	113	113	113	113	0
0	0	111	553	735	767	777	767	695	696	503	112	112	111	111	111	0
- 1	0	89	688	714	767	696	700	695	696	474	110	111	111	111	111	0
- 2	0	78	688	183	680	728	700	695	675	117	122	139	133	128	111	0
- 3	0	56	178	295	681	728	690	289	240	155	122	139	133	128	111	0
- 4	0	178	178	322	671	728	373	373	296	155	122	139	133	128	111	0
- 5	0	178	178	338	660	324	569	653	531	179	122	139	133	128	111	0
- 6	0	178	178	338	676	569	765	765	671	280	133	133	133	128	56	0
- 7	0	178	178	192	284	653	765	765	755	369	144	133	133	128	55	0
- 8	0	178	133	165	254	597	765	765	765	415	144	144	133	128	55	0
- 9	0	100	133	139	208	536	765	765	765	340	144	144	133	122	0	0
-10	0	56	122	139	176	370	760	722	680	256	144	144	133	122	0	0
-11	0	11	122	133	144	361	680	680	648	172	144	144	133	122	0	0
-12	0	0	111	133	144	144	536	648	256	144	144	144	133	122	0	0
-13	0	0	89	133	144	144	144	172	144	144	144	144	133	122	0	0
-14	0	0	55	128	144	144	144	144	144	144	144	144	133	111	0	0
-15	0	0	0	122	139	144	144	144	144	144	144	144	128	56	0	0
-16	0	0	0	111	139	144	144	144	144	144	144	139	128	28	0	0
-17	0	0	0	56	133	139	144	144	144	144	133	100	0	0	0	0
-18	0	0	0	0	122	133	144	144	144	144	128	28	0	0	0	0
-19	0	0	0	0	100	133	133	144	144	133	100	0	0	0	0	0
-20	0	0	0	0	56	111	133	133	133	133	111	0	0	0	0	0
-21	0	0	0	0	0	83	111	122	122	100	0	0	0	0	0	0
-22	0	0	0	0	0	28	55	55	56	0	0	0	0	0	0	0

TABLE XII

Revised ΔPxT for 1947

q ↓ \ a →	-6	-5	-4	-3	-2	-1	0	+1	+2	+3	+4	+5	+6	+7	+8	+9
+18	0	0	0	0	0	0	0	0	18	18	18	5	0	0	0	0
+17	0	0	0	0	0	0	0	0	36	36	36	23	9	0	0	0
+16	0	0	0	0	0	0	0	14	50	50	55	36	18	4	0	0
+15	0	0	0	0	0	0	0	32	64	64	59	46	27	14	0	0
+14	0	0	0	0	0	0	18	55	68	68	64	46	32	18	2	0
+13	0	0	0	0	0	0	32	68	68	68	68	50	32	23	3	0
+12	0	0	0	0	0	14	46	68	68	68	68	50	24	7	3	0
+11	0	0	0	0	0	23	46	68	68	68	68	37	10	8	4	0
+10	0	0	0	0	14	32	46	64	68	68	26	19	14	9	4	0
+ 9	0	0	0	0	27	46	64	75	75	39	30	22	15	14	5	0
+ 8	0	0	0	22	45	70	149	165	106	46	38	30	22	11	7	0
+ 7	0	0	0	59	90	253	291	279	225	123	42	34	28	18	10	0
+ 6	0	0	13	101	274	286	284	276	253	200	46	57	41	23	12	0
+ 5	0	0	25	259	290	287	296	285	143	65	73	61	49	27	12	0
+ 4	0	0	103	279	294	305	304	211	171	102	85	73	57	36	17	0
+ 3	0	8	208	285	314	308	304	282	239	127	89	81	65	63	57	0
+ 2	0	19	192	308	327	247	289	294	250	192	81	79	74	69	59	0
+ 1	0	11	156	282	267	286	294	300	277	178	86	91	81	71	61	0
0	0	31	138	158	251	294	401	318	319	219	91	101	81	51	21	0
- 1	0	20	61	96	227	371	369	371	359	256	81	81	81	51	16	0
- 2	0	17	59	87	293	391	390	398	391	81	89	101	97	59	16	0
- 3	0	12	82	104	284	295	253	105	114	113	89	101	97	66	15	0
- 4	0	24	40	62	272	356	116	121	116	113	89	101	97	70	15	0
- 5	0	0	0	19	219	88	92	101	116	113	89	101	97	70	11	0
- 6	0	0	0	12	75	39	92	101	116	122	97	97	97	74	0	0
- 7	0	0	0	0	1	50	84	98	116	122	105	97	0	0	0	0
- 8	0	0	0	0	0	75	131	92	110	122	0	0	0	0	0	0
- 9	0	0	0	0	0	62	132	86	104	0	0	0	0	0	0	0
-10	0	0	0	0	0	15	32	0	0	0	0	0	0	0	0	0

TABLE XIII

Revised ΔPxT for 1949

q	a: -6	-5	-4	-3	-2	-1	0	+1	+2	+3	+4	+5	+6	+7	+8	+9
+18	0	0	0	0	0	0	0	0	20	20	20	5	0	0	0	0
+17	0	0	0	0	0	0	0	0	40	40	40	25	10	0	0	0
+16	0	0	0	0	0	0	0	15	56	56	61	40	20	4	0	0
+15	0	0	0	0	0	0	0	35	71	71	66	51	30	15	0	0
+14	0	0	0	0	0	0	20	61	76	76	71	51	35	20	3	0
+13	0	0	0	0	0	0	35	76	76	76	76	56	36	25	3	0
+12	0	0	0	0	0	15	51	76	76	76	76	56	40	7	3	0
+11	0	0	0	0	0	25	51	76	76	76	76	41	12	9	4	0
+10	0	0	0	0	15	35	51	71	76	76	30	20	16	11	4	0
+ 9	0	0	0	0	30	51	61	98	92	43	34	26	16	16	6	0
+ 8	0	0	0	25	51	85	190	210	157	52	43	34	26	16	9	0
+ 7	0	0	0	72	108	298	344	337	294	154	47	39	32	24	12	0
+ 6	0	0	14	133	323	344	337	332	312	266	52	64	46	28	15	0
+ 5	0	0	26	311	344	337	350	341	184	78	82	68	55	36	15	0
+ 4	0	0	130	337	346	358	358	267	234	122	96	82	64	46	21	0
+ 3	0	8	238	341	371	363	339	332	299	177	100	91	73	76	76	0
+ 2	0	15	246	358	384	288	339	327	294	237	81	91	91	81	76	0
+ 1	0	12	242	326	295	333	333	327	385	254	81	101	96	91	76	0
0	0	41	201	185	268	329	486	442	456	325	81	101	81	81	71	0
- 1	0	33	93	121	249	445	481	512	509	342	81	81	81	81	71	0
- 2	0	29	93	83	396	514	500	547	491	81	89	101	97	93	71	0
- 3	0	21	82	98	386	508	443	101	107	113	89	101	97	93	71	0
- 4	0	18	50	62	332	431	79	120	119	113	89	101	97	93	61	0
- 5	0	1	18	26	272	74	124	174	169	114	89	101	97	93	41	0
- 6	0	0	0	16	255	102	165	196	185	134	97	97	97	93	21	0
- 7	0	0	0	0	1	135	162	188	195	142	105	97	49	47	21	0
- 8	0	0	0	0	0	123	180	173	192	141	53	53	49	47	21	0
- 9	0	0	0	0	0	108	173	159	162	97	53	53	49	45	21	0
-10	0	0	0	0	0	38	122	151	154	77	40	40	37	34	11	0
-11	0	0	0	0	0	28	117	134	138	33	1	0	0	0	0	0
-12	0	0	0	0	0	0	66	90	20	0	0	0	0	0	0	0

TABLE XIV

Revised $\Delta P_x T$ for 1950

q	a: -6	-5	-4	-3	-2	-1	0	+1	+2	+3	+4	+5	+6	+7	+8	+9
+18	0	0	0	0	0	0	0	0	0	20	20	5	0	0	0	0
+17	0	0	0	0	0	0	0	0	40	40	40	25	10	0	0	0
+16	0	0	0	0	0	0	0	12	56	56	61	40	20	5	0	0
+15	0	0	0	0	0	0	0	35	71	71	66	51	30	15	0	0
+14	0	0	0	0	0	0	16	61	76	76	71	51	35	20	5	0
+13	0	0	0	0	0	0	32	76	76	76	76	56	35	25	6	0
+12	0	0	0	0	0	14	51	76	76	76	76	56	40	14	6	0
+11	0	0	0	0	0	25	51	75	76	76	76	51	12	12	7	0
+10	0	0	0	0	12	35	51	71	76	76	30	22	17	12	8	0
+ 9	0	0	0	0	30	51	78	100	92	46	34	26	17	17	8	0
+ 8	0	0	0	20	51	86	214	226	187	55	46	34	26	17	10	0
+ 7	0	0	0	51	118	231	348	353	308	203	50	39	32	26	14	0
+ 6	0	0	16	149	338	373	365	348	326	277	55	67	46	32	20	0
+ 5	0	0	12	333	360	365	380	370	344	80	91	72	58	36	23	0
+ 4	0	0	27	357	379	389	389	340	275	132	106	91	71	48	23	0
+ 3	0	8	145	371	407	394	412	413	362	195	111	101	81	81	81	0
+ 2	0	18	253	398	422	347	412	402	442	275	96	91	91	91	81	0
+ 1	0	15	263	370	377	397	397	402	430	325	86	101	101	91	81	0
0	0	41	242	213	328	393	455	522	486	354	86	96	86	86	81	0
- 1	0	57	99	124	312	564	565	539	503	365	86	86	86	86	81	0
- 2	0	50	99	120	474	566	565	561	506	61	95	108	103	99	81	0
- 3	0	36	98	112	465	543	505	131	129	120	95	108	103	99	76	0
- 4	0	66	98	103	444	533	157	155	148	120	95	108	103	99	76	0
- 5	0	50	66	94	406	170	200	237	219	130	95	108	103	99	71	0
- 6	0	25	34	86	408	202	232	233	246	167	103	103	103	99	36	0
- 7	0	0	0	55	78	223	228	225	262	189	112	103	91	87	33	0
- 8	0	0	72	60	77	197	232	225	243	196	86	92	85	82	31	0
- 9	0	0	72	51	64	163	224	203	206	135	79	79	73	67	28	0
-10	0	0	0	26	43	107	162	182	195	102	73	73	67	62	26	0
-11	0	0	0	0	0	64	141	161	169	60	40	40	25	12	0	0
-12	0	0	0	0	0	0	74	122	51	27	0	0	0	0	0	0
-13	0	0	0	0	0	0	0	5	0	0	0	0	0	0	0	0

TABLE XV

Revised ΔPxT for 1951

b \ a	-6	-5	-4	-3	-2	-1	0	+1	+2	+3	+4	+5	+6	+7	+8	+9
+18	0	0	0	0	0	0	0	0	20	20	20	5	0	0	0	0
+17	0	0	0	0	0	0	0	0	40	40	40	25	10	0	0	0
+16	0	0	0	0	0	0	0	15	56	57	61	40	20	5	0	0
+15	0	0	0	0	0	0	0	35	71	71	66	51	30	15	0	0
+14	0	0	0	0	0	0	20	61	76	76	71	51	35	20	5	0
+13	0	0	0	0	0	0	35	76	76	76	76	56	35	25	7	0
+12	0	0	0	0	0	15	51	76	76	76	76	56	40	12	7	0
+11	0	0	0	0	0	25	51	76	76	76	76	51	12	12	8	0
+10	0	0	0	0	15	35	51	71	76	76	30	21	17	12	8	0
+ 9	0	0	0	0	30	51	62	70	76	43	34	25	17	17	8	0
+ 8	0	0	0	25	51	70	177	204	144	52	43	34	25	17	13	0
+ 7	0	0	0	51	107	305	355	339	288	199	47	38	30	27	17	0
+ 6	0	0	15	127	333	355	348	366	335	275	52	66	47	32	22	0
+ 5	0	0	30	313	359	374	391	381	337	66	86	71	56	37	22	0
+ 4	0	0	145	355	387	400	405	338	265	129	103	86	66	46	27	0
+ 3	0	8	247	378	420	407	456	439	362	226	109	97	76	91	91	0
+ 2	0	18	264	421	439	416	469	417	391	299	101	94	96	96	91	0
+ 1	0	21	265	391	411	456	436	406	384	361	91	95	101	101	99	0
0	0	71	245	239	392	451	482	552	556	371	87	96	101	102	96	0
- 1	0	49	93	122	382	560	561	579	562	373	111	111	109	102	96	0
- 2	0	43	93	132	476	586	585	588	560	111	122	139	128	117	95	0
- 3	0	31	109	156	482	593	550	173	159	155	122	138	127	117	94	0
- 4	0	86	98	161	459	536	213	225	193	141	117	133	127	116	93	0
- 5	0	43	61	152	432	239	306	386	328	157	111	130	124	115	92	0
- 6	0	24	32	116	317	273	377	407	380	209	119	121	121	110	46	0
- 7	0	8	18	89	118	291	352	360	389	241	125	115	121	116	49	0
- 8	0	0	67	74	88	257	326	344	344	239	122	125	115	110	47	0
- 9	0	0	52	58	70	224	346	275	293	181	101	102	95	89	41	0
-10	0	0	29	39	50	87	220	248	262	122	79	79	76	70	31	0
-11	0	0	12	19	31	75	161	190	202	62	47	40	37	34	8	0
-12	0	0	6	0	0	1	77	144	17	14	14	1	0	1	0	0
-13	0	0	0	0	0	0	0	5	0	0	0	0	0	0	0	0

TABLE XVI

Revised ΔPxT for Proposed Ultimate

(Pumping up to but not beyond the stipulated line)

b \ a	-6	-5	-4	-3	-2	-1	0	+1	+2	+3	+4	+5	+6	+7	+8	+9
+18	0	0	0	0	0	0	0	0	0	23	23	5	0	0	0	0
+17	0	0	0	0	0	0	0	0	16	45	45	28	11	0	0	0
+16	0	0	0	0	0	0	0	17	62	62	68	45	22	6	0	0
+15	0	0	0	0	0	0	0	40	79	79	74	57	34	6	0	0
+14	0	0	0	0	0	0	22	68	85	85	79	57	40	17	6	0
+13	0	0	0	0	0	0	40	85	85	85	85	62	40	23	11	0
+12	0	0	0	0	0	17	57	85	85	85	85	62	45	28	11	0
+11	0	0	0	0	0	28	57	85	85	85	85	57	17	17	11	0
+10	0	0	0	0	17	40	57	79	85	85	40	28	23	17	11	0
+ 9	0	0	0	0	34	57	80	116	106	57	45	34	23	17	11	0
+ 8	0	0	0	28	57	99	292	318	263	67	57	45	34	23	17	0
+ 7	0	0	0	57	151	433	508	508	441	299	62	51	40	23	23	0
+ 6	0	0	17	207	475	508	454	501	467	404	68	79	57	34	28	0
+ 5	0	0	34	466	508	507	528	515	494	100	102	85	68	40	28	0
+ 4	0	0	213	508	528	542	542	537	418	153	119	102	79	45	34	0
+ 3	0	10	384	525	565	547	648	643	567	303	124	113	90	57	113	0
+ 2	0	28	426	572	593	574	648	632	606	433	113	113	113	113	113	0
+ 1	0	33	426	541	609	637	637	632	616	491	112	113	113	113	113	0
0	0	111	357	315	529	637	707	695	696	503	112	112	111	111	111	0
- 1	0	89	128	294	501	696	700	695	696	474	111	111	111	111	111	0
- 2	0	78	128	182	680	728	700	695	675	117	122	139	133	128	111	0
- 3	0	56	178	295	681	728	690	289	240	155	122	139	133	128	111	0
- 4	0	177	178	322	671	728	373	373	296	155	122	139	133	128	111	0
- 5	0	178	178	338	660	324	569	653	531	179	122	139	133	128	111	0
- 6	0	178	178	338	676	569	765	765	671	280	133	133	133	128	56	0
- 7	0	114	178	192	280	653	765	765	755	369	144	133	133	128	48	0
- 8	0	0	73	146	254	597	765	765	765	415	144	144	133	122	26	0
- 9	0	0	0	51	138	536	765	765	765	340	144	144	73	0	0	0
-10	0	0	0	0	0	143	760	657	680	256	144	92	0	0	0	0
-11	0	0	0	0	0	0	86	510	570	172	144	79	0	0	0	0
-12	0	0	0	0	0	0	0	18	20	118	131	14	0	0	0	0

APPENDIX I

The problem proposed in Section II of this report is to determine the motion and stress condition within a semi-infinite, uniform, isotropic elastic medium when a tension center or a vertical pincer acts at a specified distance below the free surface.

The coordinates used in the subsequent analysis are shown in Fig. A-1. Because of circular symmetry, cylindrical coordinates r and z are used. The free surface is taken to be the plane z = 0, and z is considered positive below the surface (i.e. inside the elastic medium). The motion of any point whose original coordinates are r and z is described by the horizontal (radial) component and the vertical component, u and w respectively. Radial motion is measured positive inward, and vertical motion is positive downward. Shear stress in a horizontal plane is denoted by the symbol τ. The problem of a "tension center" in an infinite medium is quite simple and the problem of a "vertical pincer" is of moderate complexity. However in both cases the introduction of the free boundary seriously complicates the problem.

THE TENSION CENTER

The simplest approach to this problem is to consider first an infinite medium with a tension center at z = +h and to attempt to determine a system of applied forces at the surface z = 0 and in the region $z < 0$ (image forces) which renders the net normal stress and horizontal shear stress zero over the surface z = 0. Since this is the proper boundary condition for a free surface, we could imagine the medium cut at this point giving in effect a free surface. The second, more difficult phase of the problem is to then determine the deflections and stresses in the region $z \geq 0$ due to the original tension center and the added system of forces.

Consider an infinite uniform isotropic medium with two equal tension centers located on the z-axis at $z = \pm h$ as shown in Fig. A-2. By symmetry, the horizontal shear on the boundary z = 0 is zero, but there is a normal tension which is twice as great as the normal tension σ_o due to one tension center alone. This normal tension is a function of r only. The semi-infinite medium of Fig. A-1 would have identical deflection and stress conditions if the normal tension $2\sigma_o$ were applied at the surface z = 0. Furthermore, the deflections and stresses for the semi-infinite medium (with normal tension $2\sigma_o$) could therefore be obtained by superposing the solutions for the two tension centers. To completely free the boundary it is necessary now to apply a normal pressure $(2\sigma_o)$ over the surface z = 0 thus giving the stress conditions of a free surface. The solution for a normal force acting at the free surface of a semi-infinite medium is well known.[4] Nevertheless the motion and stresses due to the normal pressure distribution can be found from this solution only by integration of the solution multiplied by the stress function $(2\sigma_o)$ over the entire free surface. This can be accomplished using two-dimensional Fourier integrals. These were used for one method of

derivation. There is however a simpler method which will be given below. In any case, deflections and stresses are obtained by superposition (addition) of solutions for (1) a tension center at z = +h in an infinite medium, (2) a tension center at z = -h in an infinite medium and (3) a surface distribution of normal pressure ($2\sigma_o$) on the free surface (z = 0) of a semi-infinite medium.

The solution for a tension center in an infinite medium, with origin at the tension center is:[5]

$$(1) \qquad v = -\frac{C}{2G}\,\frac{1}{R^2}$$

where v is the radial displacement at a distance R from the origin, G is the shear modulus of the medium and C is a constant proportional to the "strength" of the tension center. If a is the radius of the tension center and (t_i) the tension at its surface, then $C = \frac{1}{2}\, t_i a^3$. If the tension center is located on the z-axis at z = +h, then the radial and vertical components of deflection are seen in Fig. A-1 to be:

$$(2a) \qquad w_1 = -v\cos\theta = +\frac{C}{2G}\,\frac{(h-z)}{[r^2+(h-z)^2]^{3/2}}$$

$$(2b) \qquad u_1 = -v\sin\theta = +\frac{C}{2G}\,\frac{r}{[r^2+(h-z)^2]^{3/2}}$$

The shear stress can be most readily calculated from the relation:

$$(2c) \qquad \tau_1 = G\left[\frac{\partial w_1}{\partial r} - \frac{\partial u_1}{\partial z}\right] = \frac{-3C\,r\,(h-z)}{[r^2+(h-z)^2]^{5/2}}$$

The normal tension on the plane z = 0 is:

$$(2d) \qquad \sigma_o = C\left[\frac{3h^2}{(r^2+h^2)^{5/2}} - \frac{1}{(r^2+h^2)^{3/2}}\right]$$

Similar results are obtained for a tension center at z = -h by substituting (-h) for (h) in the above equations.

$$(3a) \qquad w_2 = -\frac{C}{2G}\,\frac{(h+z)}{[r^2+(h+z)^2]^{3/2}}$$

$$(3b) \qquad u_2 = +\frac{C}{2G}\,\frac{r}{[r^2+(h+z)^2]^{3/2}}$$

$$(3c) \qquad \tau_2 = \frac{+3C\,r\,(h+z)}{[r^2+(h-z)^2]^{5/2}}$$

Terezawa has obtained a general solution for the motion and stress conditions in a semi-infinite medium under the action of a normal pressure

distribution which is symmetrical.[6] This general solution is frequently unusable because of difficulty in evaluating the integrals. However, for the symmetrical distribution ($2\sigma_o$) it is possible to evaluate all the necessary integrals, and thus obtain a solution more easily than by use of the method mentioned earlier. Those portions of the solution which are of interest here are:

$$(4a)\quad w = -\frac{z}{2G}\int_0^\infty Z(k)\, e^{-kz}\, J_o(kr)\, dk - \frac{(1-\nu)}{G}\int_0^\infty Z(k)\, e^{-kz}\, J_o(kr)\frac{dk}{k}$$

$$(4b)\quad u = +\frac{z}{2G}\int_0^\infty Z(k)\, e^{-kz}\, J_1(kr)\, dk - \frac{(1-2\nu)}{2G}\int_0^\infty Z(k)\, e^{-kz}\, J_1(kr)\,\frac{dk}{k}$$

$$(4c)\quad \tau = z\int_0^\infty Z(k)\, e^{-kz}\, k\, J_1(kr)\, dk$$

where

$$(5)\quad Z(k) = -k\int_0^\infty 2r\ \sigma_o(r)\ J_o(kr)\, dr$$

To evaluate the integrals in (4) and (5), two well known definite integrals are useful:

$$(6)\quad \int_0^\infty J_o(kr)\,\frac{hr}{(h^2+r^2)^{3/2}}\, dr = e^{-kh}$$

$$(7)\quad \int_0^\infty k^n\, e^{-kh}\, J_m(kr)\, dk = \frac{(n-m)!}{(h^2+r^2)^{\frac{n+1}{2}}}\ P_n^m\left[\frac{h}{(h^2+r^2)^{1/2}}\right] \quad n \geqslant m$$

The normal pressure $\sigma_o(r)$ was given in equ. 2:

$$\sigma_o(r) = +C\left[\frac{3h^2}{(r^2+h^2)^{5/2}} - \frac{1}{(r^2+h^2)^{3/2}}\right]$$

so that equation (5) becomes

$$(8)\quad Z(k) = 2Ck\int_0^\infty\left[\frac{r}{(r^2+h^2)^{3/2}} - \frac{3h^2 r}{(r^2+h^2)^{5/2}}\right] J_o(kr)\, dr$$

Differentiation of (6) with respect to h yields

$$(9)\quad \int_0^\infty J_o(kr)\left[\frac{r}{(h^2+r^2)^{3/2}} - \frac{3h^2 r}{(h^2+r^2)^{5/2}}\right] dr = -ke^{-kh}$$

Thus

$$(10)\quad Z(k) = -2Ck^2\, e^{-kh}$$

If this value of Z(k) is inserted in equation (4), all integrals can be evaluated

using equation (7). The final results are:

$$(11a)\quad w_3 = \frac{C}{G}\left\{\frac{3z\,(h+z)^2}{[r^2+(h+z)^2]^{5/2}} - \frac{[z-2(1-\nu)\,(h+z)]}{[r^2+(h+z)^2]^{3/2}}\right\}$$

$$(11b)\quad u_3 = \frac{-C}{G}\left\{\frac{3\,r\,z\,(h+z)}{[r^2+(h+z)^2]^{5/2}} - \frac{(1-2\nu)\,r}{[r^2+(h+z)^2]^{3/2}}\right\}$$

$$(11c)\quad \tau_3 = +6\,C\,rz\left\{\frac{5(h+z)^2}{[r^2+(h+z)^2]^{7/2}} - \frac{1}{[r^2+(h+z)^2]^{5/2}}\right\}$$

Combining equation (2), (3), and (11) the final solution of the problem is:

$$(12a)\quad w = w_1 + w_2 + w_3 = \frac{C}{2G}\left\{\frac{(h-z)}{[r^2+(h-z)^2]^{3/2}} + \frac{(3-4\nu)(h+z)-2z}{[r^2+(h+z)^2]^{3/2}} + \frac{6z\,(h+z)^2}{[r^2+(h+z)^2]^{5/2}}\right\}$$

$$(12b)\quad u = u_1 + u_2 + u_3 = \frac{+C}{2G}\left\{\frac{+r}{[r^2+(h-z)^2]^{3/2}} + \frac{(3-4\nu)\,r}{[r^2+(h+z)^2]^{3/2}} - \frac{6zr\,(h+z)}{[r^2+(h+z)^2]^{5/2}}\right\}$$

$$(12c)\quad \tau = \tau_1 + \tau_2 + \tau_3 = -3C\left\{\frac{r\,(h-z)}{[r^2+(h-z)^2]^{5/2}} - \frac{r\,(h+3z)}{[r^2+(h+z)^2]^{5/2}} + \frac{10\,rz\,(h+z)^2}{[r^2+(h+z)^2]^{7/2}}\right\}$$

THE VERTICAL PINCER

The coordinates used in the solution of this problem are the same as for the tension center. The model to be used is again a semi-infinite medium with free surface at z = 0. The force system consists of a pair of equal and opposite forces F acting along the z axis. One of these located at z = +h acts in the positive z direction, the other at z = h+Δz acts in the negative direction. For mathematical convenience it is desirable to let $\Delta z \longrightarrow 0$ but at the same time keep the product FΔz finite and constant. At any appreciable distance from the points of force application, this solution will be indistinguishable from that for finite (but small) Δz. As in other problems involving discrete forces, the solution should give rise to physically impossible results near the point z = +h, but if such a solution is integrated over a region to give the effect of a pressure distribution, then the discrepancies disappear and a valid solution results. Suppose the desired vertical motion is given by w, and the vertical motion due to a unit force at z = +h is w_1. Then,

$$(13)\quad w = \lim_{\Delta z \to 0} F\left[w_1(h) - w_1(h + \Delta z)\right]$$

$$= \lim_{\Delta z \to 0} (F\Delta z)\ \frac{(w_1(h) - w_1(h + \Delta z)}{\Delta z}$$

$$= -M \frac{\partial w_1}{\partial h}$$

where M is the constant value of $F\Delta z$. Thus the solution for a "pincers" can be obtained by differentiation of the solution for a unit force acting along the z-axis. The solution for a single force can be obtained in the same manner as for a tension center. In principle, the method of solution is identical, but in detail it is somewhat more difficult.

If a force F_1 acts in the positive direction at $z = +h$ and an equal force F_2 acts in the negative direction at $z = -h$, by symmetry the horizontal shear at $z = 0$ is zero, but again there is a normal tension $2\sigma_1$, where σ_1 is the normal tension due to one force alone. The boundary $z = 0$ is again freed by application of a normal pressure $(2\sigma_1)$ at $z = 0$. The final solution is a superposition of solutions for (1) a positive force F_1 acting along the z axis at $z = +h$ in an infinite medium, (2) a negative force F_2 acting along the z axis at $z = -h$ in an infinite medium, and (3) a surface distribution of normal pressure $(2\sigma_1)$ acting on the free surface $z = 0$ of a semi-infinite medium.

The solution for a single force in an infinite medium (where the force acts in the positive z-direction at $z = +h$, $r = 0$ is:[7]

$$(14a)\quad w_1 = \frac{B}{2G}\left\{\frac{4(1-\nu)}{\left[r^2 + (h-z)^2\right]^{1/2}} - \frac{r^2}{\left[r^2 + (h-z)^2\right]^{3/2}}\right\}$$

$$(14b)\quad u_1 = +\frac{B}{2G}\left\{\frac{r(h-z)}{\left[r^2 + (h-z)^2\right]^{3/2}}\right\}$$

$$(14c)\quad \tau_1 = -B\left\{(1-2\nu)\frac{r}{\left[r^2 + (h-z)^2\right]^{3/2}} + \frac{3r(h-z)^2}{\left[r^2 + (h-z)^2\right]^{5/2}}\right\}$$

$$(14d)\quad \sigma_1 = +B\left\{(1-2\nu)\frac{h}{\left[r^2 + h^2\right]^{3/2}} + \frac{3h^3}{\left[r^2 + h^2\right]^{5/2}}\right.$$

$$\text{where } B = \frac{P}{8\pi(1-\nu)}$$

For a force at $z = -h$, $r = 0$ acting in the negative direction, the solution is obtained from Eqn. (14) by substituting (-P) for (P) and (-h) for (h)

$$(15a)\quad u_{z_2} = -\frac{B}{2G}\left\{\frac{4(1-\nu)}{\left[r^2 + (h+z)^2\right]^{1/2}} - \frac{r^2}{\left[r^2 + (h+z)^2\right]^{3/2}}\right\}$$

$$(15b)\quad u_{r_2} = +\frac{B}{2G}\left\{\frac{r\,(h+z)}{\left[r^2+(h+z)^2\right]^{3/2}}\right\}$$

$$(15c)\quad \tau_2 = +B\left\{\frac{(1-2\nu)\quad r}{\left[r^2+(h+z)^2\right]^{3/2}} + \frac{3\,r(h+z)^2}{\left[r^2+(h+z)^2\right]^{5/2}}\right\}$$

Terezawa's solution is again used, with

$$2\sigma_1(r) = +2B\left\{\frac{(1-2\nu)\,h}{(r^2+h^2)^{3/2}} + \frac{3\,h^3}{(r^2+h^2)^{5/2}}\right\}$$

Equation (5) becomes

$$Z(k) = -k\int_0^\infty 2\,r\,B\left\{(1-2\nu)\,\frac{h}{(r^2+h^2)^{3/2}} + \frac{3\,h^3}{(r^2+h^2)^{5/2}}\right\}J_o(kr)\,dr$$

$$= -2k\,B\int_0^\infty\left\{\frac{2(1-\nu)\,rh}{(r^2+h^2)^{3/2}} - h\left[\frac{r}{(r^2+h^2)^{3/2}} - \frac{3\,h^2\,r}{(r^2+h^2)^{5/2}}\right]\right\}J_o(kr)\,dr$$

which can be evaluated using equations (6) and (9):

$$(16)\qquad Z(k) = -2kB\left[\,2(1-\nu) + kh\right]e^{-kh}$$

The integrals in equation (4) can be evaluated using equation (7) except for the integral:

$$\int_0^\infty e^{-k(h+z)}\,J_1(kr)\,dk$$

This can be evaluated by integration by parts, with the result

$$(17)\quad \int_0^\infty e^{-k(h+z)}\,J_1(kr)\,dk = \frac{r}{\left[r^2+(h+z)^2\right]^{1/2}\left\{(h+z)+\left[r^2+(h+z)^2\right]^{1/2}\right\}}$$

If this is used with equation (7) to evaluate the integrals in Eqn. (4), the results are:

$$(18a)\quad w_3 = \frac{B}{G}\left\{\frac{3zh\,(h+z)^2}{\left[r^2+(h+z)^2\right]^{5/2}} + \frac{2(1-\nu)(h+z)^2 - zh}{\left[r^2+(h+z)^2\right]^{3/2}} + \frac{4(1-\nu)^2}{\left[r^2+(h+z)^2\right]^{1/2}}\right\}$$

$$(18b)\quad u_3 = \frac{-B}{G}\left\{\frac{3\,rzh\,(h+z)}{\left[r^2+(h+z)^2\right]^{5/2}} + \frac{2(1-\nu)rz - (1-2\nu)hr}{\left[r^2+(h+z)^2\right]^{3/2}}\right.$$

$$\left. - \frac{2\,(1-\nu)\,(1-2\nu)\,r}{\left[r^2+(h+z)^2\right]^{1/2}\left\{(h+z)+\left[r^2+(h+z)^2\right]^{1/2}\right\}}\right\}$$

$$(18c)\quad \tau_3 = -2Bz\left\{\frac{15rh\,(h+z)^2}{\left[r^2+(h+z)^2\right]^{7/2}} + \frac{3(1-2\nu)\,r(h+z)}{\left[r^2+(h+z)^2\right]^{5/2}}\right\}$$

where $B = \frac{P}{8\pi(1-\nu)}$

The total solution, too long to reproduce here is

(19a) $w_o = w_1 + w_2 + w_3$

(19b) $u_o = u_1 + u_2 + u_3$

(19c) $\tau_o = \tau_1 + \tau_2 + \tau_3$

The final result for a double force or vertical pincer is obtained by differentiating this result with respect to h

(20) $w = -\frac{M}{P}\frac{\partial w_o}{\partial h}$,

$u = -\frac{M}{P}\frac{\partial u_o}{\partial h}$, etc.

Thus

(21a) $$w = +\frac{M}{8\pi G(1-\nu)}\left\{+\frac{2(1-\nu)(h-z)}{[r^2+(h-z)^2]^{3/2}} - \frac{3/2\, r^2(h-z)}{[r^2+(h-z)^2]^{5/2}}\right.$$
$$-\frac{2(1-\nu)(h+z)}{[r^2+(h+z)^2]^{3/2}} + \frac{3/2\, r^2(h+z)}{[r^2+(h+z)^2]^{5/2}}$$
$$-\frac{4\nu(1-\nu)(h+z) - 2z}{[r^2+(h+z)^2]^{3/2}} - \frac{3z(4h+z)(h+z) - 6(1-\nu)(h+z)^3}{[r^2+(h+z)^2]^{5/2}}$$
$$\left.+\frac{15\, zh(h+z)^3}{[r^2+(h+z)^2]^{7/2}}\right\}$$

(21b) $$u = -\frac{M}{8\pi G(1-\nu)}\left\{\frac{r}{[r^2+(h-z)^2]^{3/2}} - \frac{3r(h-z)^2}{[r^2+(h-z)^2]^{5/2}}\right.$$
$$+\frac{r}{[r^2+(h+z)^2]^{3/2}} - \frac{3r(h+z)^2}{[r^2+(h+z)^2]^{5/2}}$$
$$-\frac{(1-2\nu)^2 r}{[r^2+(h+z)^2]^{3/2}}$$
$$\left.-\frac{3r[(1-2\nu)(h^2-z^2)+hz]}{[r^2+(h+z)^2]^{5/2}} + \frac{15\, r\, z\, h\,(h+z)^2}{[r^2+(h+z)^2]^{7/2}}\right\}$$

$$(21c)\quad \tau = + \frac{M}{8\pi(1-\nu)} \left\{ + \frac{3(1+2\nu)\, r\,(h-z)}{[r^2 + (h-z)^2]^{5/2}} - \frac{15 r\,(h-z)^3}{[r^2 + (h-z)^2]^{7/2}} \right.$$

$$- \frac{3\,(1+2\nu)\, r\,(h+z)}{[r^2 + (h+z)^2]^{5/2}} + \frac{15 r\,(h+z)^3}{[r^2 + (h+z)^2]^{7/2}}$$

$$+ \frac{30\,[\,3rzh\,(h+z) - (1-2\nu)\, rz(h+z)^2]}{[r^2 + (h+z)^2]^{7/2}}$$

$$\left. + \frac{6(1-2\nu)\, r\, z}{[r^2 + (h+z)^2]^{5/2}} - \frac{210\, rzh\,(h+z)^3}{[r^2 + (h+z)^2]^{9/2}} \right\}$$

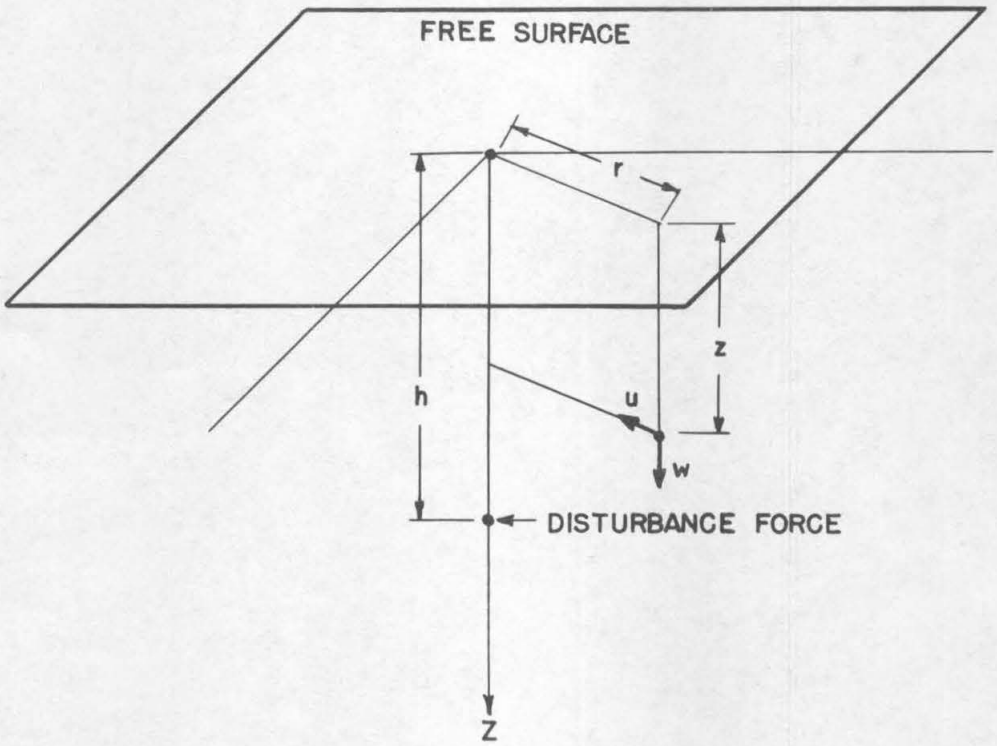

FIG. A-1 COORDINATE SYSTEM FOR SEMI-INFINITE ELASTIC MEDIUM.

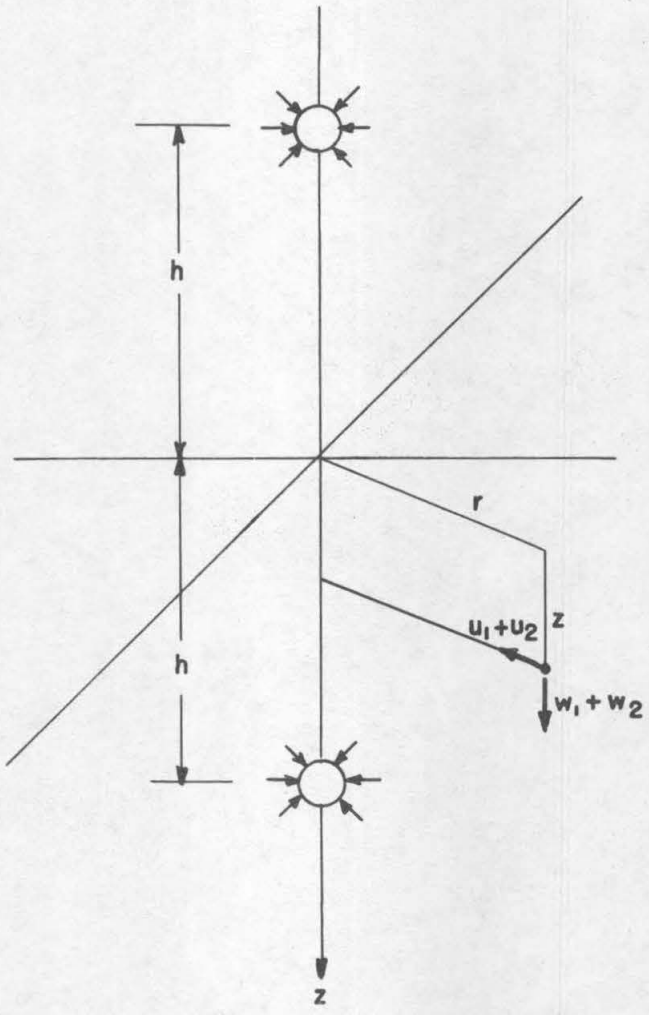

FIG. A-2 TENSION CENTER AND ITS "IMAGE" IN AN INFINITE ELASTIC MEDIUM.

APPENDIX II

CALCULATION OF VERTICAL SUBSIDENCE

If a medium is perfectly elastic, the effect of a number of forces can be found by addition of the separate effects. When the forces are uniformly distributed over a surface this addition is best accomplished by an integration. For calculation of vertical motion, the function to be integrated is the product of a subsidence function (w_o), multiplied by the "disturbance force" function. The subsidence function gives the subsidence at the point in question due to a unit disturbance at a general point. The "disturbance force" function is evaluated at this same general point, and the integration is carried out by allowing the point to cover the entire surface.

This can be expressed concisely if we use the following notation. Let the point at which subsidence is to be determined be described by the coordinates (x_o, y_o), and let the general point be denoted by coordinates (x_1, y_1). The strength of the "disturbance force" per unit area is a function of (x_1, y_1) only and can be written $F(x_1, y_1)$. The vertical subsidence at (x_o, y_o) due to a unit force at (x_1, y_1) is a function only of the horizontal distance between the two points, the depth of the disturbance force (z_1), and the vertical coordinate (z_o) of the point (x_o, y_o, z_o). This can be written

$$w_o \left(\sqrt{(x_1 - x_o)^2 + (y_1 - y_o)^2}, z_1, z_o \right).$$

For a given integration, z_1 and z_o are generally fixed, so that the simpler notation

$$w_o \left(\sqrt{(x_1 - x_o)^2 + (y_1 - y_o)^2} \right)$$

will be used. The total subsidence can be written:

$$w(x_o, y_o) = \int w_o \left(\sqrt{(x_1 - x_o)^2 + (y_1 - y_o)^2} \right) F(x_1, y_1)\, dA(x_1, y_1)$$

Such an integral cannot be evaluated analytically because of the empirical nature of the function ($\Delta P \times T$). It is therefore necessary to resort to numerical integration for an approximation to the integral. The deflection is then found by evaluating the double summation:

$$w(x_o, y_o) = \sum_{i=1}^{N} \sum_{j=1}^{M} w_o \left(\sqrt{(x_i - x_o)^2 + (y_i - y_o)^2} \right) F(x_i, y_j)\, \Delta A_{ij}$$

Similar equations are used for horizontal motion and horizontal shear stress, except that the contribution from each point (x_i, y_j) must first be resolved into components parallel to the coordinate axes, and each set of components summed separately. These sums are then combined to give the total motion or stress.

It was found that surface motion could be calculated with satisfactory accuracy if the points (x_i, y_j) were spaced 2000 ft. apart and the areas $\Delta A(x_i, y_j)$ thus taken to be 4×10^6 ft.^{2} in extent. However subsurface motion and shear stress all required spacing of about 500 ft. in order to obtain acceptable accuracy. Since the oil-bearing sands extend 30,000 ft. and 10,000 feet along the major and minor axes respectively, each integration required the summation of many hundreds of products, and it was necessary that this be carried out at all points in the field. It was immediately apparent that such an ambitious schedule of calculation required the application of some type of digital computer in an elaborate computing program. It then became possible to carry out a calculation of surface subsidence over the entire field in less than a day while a horizontal motion or shear stress survey could be accomplished in 2 or 3 days.

It has been suggested that the strength of the "force model" (that is tension center or vertical pincer) depends primarily upon the pressure drop within the oil bearing sands and upon the thickness of the oil bearing sands. As has been discussed in the text, the strength should not be taken proportional to the product of pressure drop and sand thickness, but should possibly be modified in a manner dependent upon the compaction. For the general study to correlate the time histories of pumping schedule and the development of the subsidence bowl however this complication was omitted. It was considered that the strength of the stress center depends directly on the product of pressure drop and sand thickness. Symbolically this will be represented by ΔPxT. The actual quantity used in the subsidence equations depends upon whether one is using tension centers or vertical pincers. However this quantity is proportional to ΔPxT. The constant of proportionality can be readily evaluated for the vertical pincer model. The subsidence formulas for this model involved a "disturbance force" $M = F\Delta h$. The quantity (Δh) is clearly analagous to the sand thickness (T) and the force (F) to the pressure drop (ΔP) multiplied by the area associated with the point in question. Thus in the subsidence equations, M should be set equal to the following function:

$$M = F\Delta h = (\Delta PxT)(\Delta A_{ij})$$

and for example the vertical surface motion is obtained using Eqn. 21 of Appendix I and evaluating the summation:

$$w(x_o, y_o) = \frac{5}{8\pi Gh^2} \sum_{i=1}^{N} \sum_{j=1}^{M} (\Delta PxT)_{ij} \, \Delta A_{ij} \left\{ \frac{1}{\left[\left(\frac{r_{ij}}{h}\right)^2 + 1\right]^{3/2}} \right.$$

$$\left. \left[\frac{6}{5} \frac{1}{\left(\frac{r_{ij}}{h}\right)^2 + 1} - \frac{1}{5} \right] \right\}$$

where

$$r_{ij} = \sqrt{(x_i - x_o)^2 + (y_i - y_o)^2}$$

Similar equations hold for other displacements and the shear stress.

For the tension center a somewhat more elaborate argument is required. The subsidence equations contain a "force" constant C which depends upon the size of the tension center and the magnitude of the tension:

$$C = 1/2\ a^3 t_i$$

where (a) is the radius and (t_i) the tension stress. The simplest conversion to a rectangular parallelopiped (of surface area ΔA_{ij} and thickness T) involves competely filling the volume with tension centers of various sizes and summing the effects of these. The result is the conversion

$$C = 1/2\ a^3 t_i = \frac{3}{8\pi} \quad (\Delta P x T)(\Delta A_{ij})$$

This result holds even if several strata are involved, provided they are sufficiently close together so that their effect can be approximated by a "disturbance force" at one depth. Using equation 12 of Appendix I, the vertical subsidence for this model now can be written:

$$w(x_o, y_o) = \frac{9}{16\pi G\ h^2} \sum_{i=1}^{N} \sum_{j=1}^{M} (\Delta P x T)_{ij} \Delta A_{ij} \frac{1}{\left[\left(\frac{r_{ij}}{h}\right)^2 + 1\right]^{3/2}}$$

and again similar formulas hold for the other quantities of interest.